الجمهورية الجزائرية الديمقراطية الشعبية
République Algérienne Démocratique et Populaire
وزارة التعليم العالي والبحث العلمي
Ministère de l'enseignement supérieur et de la recherche scientifique

Université Mohamed Khider – Biskra
Faculté des Sciences Exactes et des
Sciences de la Nature et de la Vie
Département : Sciences de la Matière

Ref :

جامعة محمد خيضر بسكرة
كلية العلوم الدقيقة وعلوم الطبيعة والحياة
قسم: علوم المادة
المرجع: .....

Thèse présentée en vue de l'obtention
du diplôme de

Doctorat en sciences : Chimie

Spécialité : Chimie bioorganique et théorique

Etude théorique des réactions de transfert d'hydrogène catalysées aux métaux de transition

Présentée par :

MEFTAH Yazid

Soutenue publiquement le : / / 2016

Devant la commission d'Examen

M. MEGHEZZI. A	Prof	Université de Biskra	Président
M. BOUMEDJANE. Y	MC/A	Université de Biskra	Directeur de thèse
M. BOUTARFAIA. A	Prof	Université d'Ouargla	Examinateur
M^{me}. BERREDJEM. M	Prof	Université d'Annaba	Examinateur
M. MESSAOUDI. A	MC/A	Université de Batna	Examinateur

ACKNOWLEDGEMENTS

First of all, I would like to thank my research advisor, Dr. Youcef BOUMEDJANE. I have been working with him since Oct. 2011. Dr. Youcef BOUMEDJANE is a very kind and knowledgeable person. He has guided me step by step in the research process and is an ideal advisor that I can imagine. I also thank him for supporting me as a research assistant most of time (including summers) in the past five years.

I am grateful for the Faculty of exact and Natural Sciences, at biskra University for their financial support.

Thanks to the « Université de Lyon, CNRS, Ecole Normale Supérieure de Lyon, 46 Allée d'Italie, 69364 Lyon, Cedex 07, France and Pole de modélisation numérique (PSMN) in Ecole Normale Supérieure de Lyon for offering the computing facilities and helpful discussion with the scientists.

I would like to thank past and current group members in Prof. Philippe sautet's group. At the early stage of my research, I got a lot of help from Dr. Françoise delbecq Dr. Carine Michel, Dr. Paul fleurat lessard. I had many useful discussions with them.

I appreciate Prof. MEGHEZZI Ahmed, Prof. Boutarfaia ahmed, Prof. Berredjem malika and Dr. Messaoudi abdelatif to be in my dissertation committee to read and help to improve this dissertation.

At last, I would like to thank my parents, relatives and friends.

Finally, I owe my deepest gratitude to my wife, Samira. She always stood by me, encouraging me all the way.

ABBREVIATIONS

Symbol	*Definition*
DFT	*density functional theory*
ee	*enantiomeric excess*
EX	*exchange correlation functionals*
G	*free energy*
ΔG	*difference in free energy*
ATH	*Asymmetric transfer hydrogenation*
Ar	*aryl group*
Cp*	*pentamethylcyclopentadiene*
Me	*methyl group*
Ph	*phenyl group*
BINAP	*2,2'-bis(diphenylphosphino)-1,1'-binaphthyl*
TolBINAP	*2,2'-bis(di-4-tolylphosphino)-1,1'-binaphthyl*
XylBINAP	*2,2'-bis(diphenylphosphino)-1,1'-binaphthyl*
DPEN	*1,2-diphenylethylenediamine*
DMDPEN	*N,N-dimethyl-1,2-diphenylethylenediamine*
DMAPEN	*2-dimethylamino-1-phenylethylamine*
INT	*intermediate*
TS	*transition state*
ESI	*Electrospray ionisation*

ABSTRACT

Firstly, the effects of several functionals in the prediction of the geometrical parameters of four diastereomeric half-sandwich Ru (II) cationic complexes containing amino amide ligands were investigated. Four Ruthenium complexes were used to evaluate the performance of fifteen density functionals. The standard 6-31G (d,p) basis set was used for all light elements, while pseudo potential LANL2DZ was used for the Ruthenium atom. The best bond lengths, bond angles and bond dihedrals were obtained using (PBE-GD3BJ), (TPSS-GD3BJ) and (BP86-GD3BJ) functionals respectively. The energy difference of the two diastereomeric half-sandwich Ru (II) cationic complexes ($Ru_{(S)}$) and ($Ru_{(R)}$) containing the phenyl alanine amide ligand has been calculated using the fifteen density functionals in other side the enantioselectivity in ATH of acetophenone catalyzed by Ru(II) complexes containing amino amide ligands were also investigated by defferents functionals,The best overall performance is observed for (PBE-GD3BJ) , because this functional gives good results both for the geometry and the energetics and is not too costly in terms of computation time. For the solvent system, we have chosen PCM.

Secondly The origin of enantioselectivity in the reaction of chiral Ru amino amide complexes in asymmetric transfer hydrogenation of acetophenone was investigated with DFT calculation. The roles of the chirality of the ruthenium in Ru amino amide complexes was analyzed by considering foor tested cases: 1) Ru(*S*)C(*S*) phenyl alanine amide , 2) Ru(*R*)C(*S*) phenyl alanine amide, 3) Ru*(S)C(S)* proline amide and, 4) Ru*(R)*C*(S) proline amide*. We succeeded in reproducing the experimentally observed enantioselectivity for the foor studied Ru amino amide complexes, For each of these, the full free energy profile for the reaction is calculated according to the concerted hydrogen transfer mechanism. Our results indicated that high enantioselectivity explained by stabilizing CH–π interaction exists between the phenyl group of acetophenone and the cymene ring of the catalyst. This is in line with the explanations provided by Noyori et al. Hence, ours results show that rotation of p-cymene play a significant role in selectivity. finaly our results showed that important insights can be obtained with such a theoretical approach, particularly the origin of the reaction asymmetry. This can help experimentalists to design new catalysts that will ensure good enantioselectivity.

Finally a proline amide/amine derived amino acid has been experimentally employed as an effective chiral catalytic precursor in the ruthenium-mediated asymmetric reduction of prochiral ketones in water to produce the corresponding secondary alcohols, which provides the products in 80% ee. We show that transition state modeling according to the outer-spher reaction

mechanism at the PBE-GD3BJ/LANL2DZ/6-31G (d,p) level of theory can accurately model enantioselectivity for various proline-catalyzed asymmetric transfer hydrogenation in water.

RESUME

Tout d'abord, nous avons étudié les effets de plusieurs fonctionnelles dans la prédiction des paramètres géométriques de quatre diastéréoisomère demi-sandwich de complexes de Ru (II) ligandé avec l'amino amide. Quatre complexes de ruthénium ont été utilisés pour évaluer la performance de quinze fonctionnelles de densité. La base standard 6-31G (d, p) a été utilisé pour tous les éléments légers, tandis que le pseudo potentiel LANL2DZ a été utilisé pour l'atome de ruthénium. Les meilleures longueurs de liaison, angles de liaison et dièdres ont été obtenus en utilisant les fonctionnelles (PBE-GD3BJ), (TPSS-GD3BJ) et (BP86-GD3BJ) respectivement. La différence d'énergie des deux diastéréoisomère demi-sandwich de complexes de Ru (II) (Ru (*S*)) et (Ru (*R*)) ligandé avec l'amino amide a été calculé en utilisant les quinze fonctionnelles de densité, finalement l'énantiosélectivité dans l'ATH de l'acétophénone catalysée par le complexe de Ru (II) ligandé avec l'amino amide ont également été étudiés par defferents fonctionnels, la meilleure performance globale est observée pour (PBE-GD3BJ), parce que cette fonction donne de bons résultats à la fois pour la géométrie et de l'énergétique et ne soit pas trop coûteuse en termes de temps de calcul. Pour le système de solvant, nous avons choisi PCM.

L'origine de l'énantiosélectivité dans la réaction de transfert asymétrique d'hydrogène (ATH) de l'acétophénone catalysé par des complexes chiraux de Ruthénium ligandé par des amino-amides a été étudiée à l'aide de calculs DFT en utilisant la fonctionnelle PBE avec la dispersion GD3BJ et la base LANL2DZ pour le Ruthénium et 6-31G (d,p) pour les autre éléments . Le rôle de la chiralité du ruthénium dans les complexes de Ru-amino amide a été analysé en considérant quatre cas testés: 1) $Ru_{(S)}$ $C_{(S)}$ phényl alanine amide, 2) $Ru_{(R)}$ $C_{(S)}$ phényl alanine amide , 3) $Ru_{(S)}$ $C_{(S)}$ proline amide et 4) $Ru_{(R)}$ $C_{(S)}$ proline amide. Nous avons réussi à reproduire l'énantiosélectivité observée expérimentalement pour ces quatre complexes pour lesquels le profil de l'énergie libre totale de la réaction a été calculé. Nos résultats ont montré que l'énantiosélectivité élevée est due à l'interaction (CH-π) qui existe entre le groupe phényle de l'acétophénone et le cymène du catalyseur. Ceci est en accord avec les explications fournies par Noyori et collaborateur. Par conséquent, on peut conclure que la rotation de p-cymène joue un rôle important dans la sélectivité. Nos résultats ont montré les progrès importants de cette approche théorique, en particulier pour déterminer l'origine de l'asymétrie de la réaction, ce qui peut aider les expérimentateurs à synthétiser de nouveaux catalyseurs qui assureront une bonne énantiosélectivité.

Finalement, un dérivé de l'acide aminé proline (amide / amine) a été expérimentalement employé

comme catalyseur chiral efficace dans la réduction asymétrique de cétones prochirales catalysée par le complexe de ruthénium dans l'eau pour produire les alcools secondaires correspondants, qui fournit les produits avec 80% d'excès enantiomérique. Nous montrons que la modélisation moleculaire de l'état de transition à l'aide de la fonctionnel de densité, selon le mécanisme concerté au niveau de calcule PBE-GD3BJ / LANL2DZ / 6-31G (d, p) peut prédire l'énantiosélectivité expérimentale pour le transfert d'hydrogène asymétrique catalysée par diverses proline (amide/amine).

ملخص

في البداية, قمنا بدراسة تأثير عدة طرق نظرية للتنبؤ بالبنية الفراغية لأربعة معقدات الروتينيوم Ru(II) المتساندة مع الاميد الاميني. استعملنا الأربع معقدات لتقييم أداء خمسة عشرة طريقة نظرية، استعملنا القاعدة 6 -31G (d ،p) لجميع العناصر الخفيفة في حين تم استخدام القاعدة LANL2DZ للروتينيوم أحسن النتائج بالنسبة لطول الروابط و الزوايا تحصلنا عليها باستعمال الطرق النظرية(PBE-GD3BJ) ,(BP86-GD3BJ) , (TPSS-GD3BJ) علي التوالي.

فرق الطاقة بين معقدي الروتينيوم Ru (*S*), Ru(II) و Ru (*R*) حسب بواسطة الخمسة عشرة طريقة نظرية , و أخيرا قمنا بحساب الانتقائية في تفاعل الإرجاع للكيتونات المحفز بمعقدات الروتينيوم المتساندة مع الاميد الاميني , لوحظت نتائج جيدة مع الطريقة (PBE-GD3BJ)سواءا لحساب البعد الفراغي أو الطاقة و ليست مكلفة من حيث الوقت في الحساب , بالنسبة لنظام المذيبات اخترنا PCM.

أصل الانتقائية في تفاعل الإرجاع للكيتون الحلقي المحفز عن طريق معقدات الروتينيوم المتساندة مع الاميد الاميني قد درست بواسطة نظرية PBE ونظرية التداخل GD3BJ والقاعدة LANL2DZبالنسبة للريتنيوم و 6-31G (d ،p) بالنسبة لبقية العناصر الخفيفة.

وقمنا أيضا بدراسة اللاتناظر لعنصر الروتينيوم حيث قمنا بتجربة أربع احتمالات 1) فينيل الأنين أميد (*S*) C (*S*) Ru(*S*) , 2) فينيل الأنين أميد (*S*) C (*R*) Ru , 3) برولين أميد (*S*) C (*S*) Ru , 4) برولين أميد (*S*) C (*R*) Ru ، نجحنا في إيجاد الانتقائية الملاحظة تجريبيا عن طريق الحساب النظري و قمنا بحساب الانطالبي الحرة لكل مراحل التفاعل. نتائجنا بينت ان الانتقائية المرتفعة ناتجة عن التجاذب بين حلقة الكيتون و حلقة المحفز، كما قام بتفسيرها العالم نويوري ،من جهة أخرى بإمكاننا استنتاج أن دوران حلقة المحفز تلعب دورا هاما في الانتقائية، نتائجنا بينت اهمية الطرق النظرية لتفسير انتقائية التفاعلات الكيميائية و بذلك يمكنها مساعدة التجريبيين لاصطناع محفزات جديدة .

و أخيرا، معقد الروتينيوم المتساند مع برولين أميد أو برولين أمين استعمل تجريبيا في الإرجاع اللامتناظر للكيتونات في وسط مائي للحصول على الكحولات المرافقة مع انتقائية تصل إلى 80%، أثبتنا أن محاكاة الحالة الانتقالية وفقا للآلية التفاعلية الحلقية بواسطة مستوى الحساب (PBE-GD3BJ) / LANL2DZ / 6-31G (d ،p)يمكنها التنبؤ بالانتقائية التجريبية.

List of Tables

List of Figures

List of Schemes

Table of Contents

Chapter 1

General Introduction

1.1 Introduction

Most of the molecules that make up plants and animals are chiral, and usually only one form of the chiral molecule occurs in a given species. All but one of the 20 amino acids that make up naturally occurring proteins are chiral, and all of them are classified as being left handed. Chiral molecules can show their different handedness in many ways, including the way they affect human beings. One enantiomeric form of a compound called limonene is primarily responsible for the odor of oranges, and the other enantiomer, for the odor of lemons (Figure 1.1).

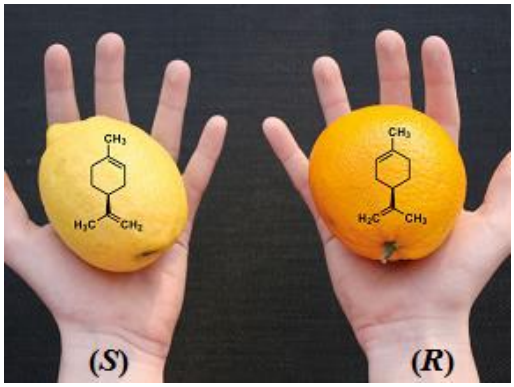

Figure 1.1. Enantiomeric forms of limonene

The activity of drugs containing stereocenters can similarly vary between enantiomers, sometimes with serious or even tragic consequences. For several years before 1963 the drug thalidomide was used to alleviate the symptoms of morning sickness in pregnant women. In 1963 it was discovered that thalidomide was the cause of horrible birth defects in many children born subsequent to the use of the drug. Even later, evidence began to appear indicating that whereas one of the thalidomide enantiomers (the right-handed molecule) has the intended effect of curing morning sickness, the other enantiomer, which was also present in the drug (in an equal amount), may be the cause of the birth defects. (Figure 1.2).

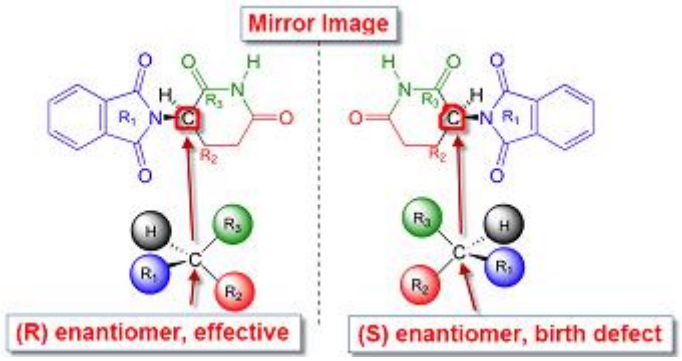

Figure 1.2. Enantiomeric forms of thalidomide

In 1992, the U. S. Food and drug administration (FDA) released long-awaited guidelines for the marketing of chiral drugs. The decision about whether to sell a chiral drug in the racemic mixture of the enantiomerically pure form has been left to the drug's manufacturer, although is subject to FDA approval. with the regulations in place,drug companies have been faced with major scientific, technical, and economic choices.they must decide whether to market a drug as an easier-to-synthesize racemic mixture or to tackle the more costly and difficult synthesis of the pure active enantiomer.which will give them the competitive edge?

Enormous effort has been devoted to the development of methods that are enantioselective in contrast to classical organic synthesis in which racemic mixtures are obtained. With an increasing demand for enantiomerically pure compounds, asymmetric synthesis has today become an important field of organic chemistry.

Enantiomerically pure compounds can be obtained in three different ways:

i) By derivatization of a chiral natural product, such as amino acids, hydroxyl acids, terpenes, sugars and alkaloids [1].

ii) By resolution of a racemate with a chiral resolving agent [2].

iii) Or by asymmetric synthesis, in which an achiral substance is converted into a chiral one.

Asymmetric synthesis involves the conversion of a prochiral starting material, in a chiral environment, in such a way that the reaction product contains unequal amounts of the two enantiomers or diastereomers. The chirality is introduced by using a chiral reagent, chiral auxiliary or by asymmetric catalysis. The aim of asymmetric synthesis is to find efficient and cheap methods that selectively produce one of the two enantiomers.

QM methods like density functional theory (DFT) [3], have been used as a powerful tool in the study of reaction mechanisms [4,5].These methods have been successfully used to study and to clarify the mechanism of several metal-catalyzed reactions used in organic synthesis like σ-bond activation [6], hydrogenation of carbon dioxide [7], olefin polymerization [8], isomerization of double and triple C-C bonds [9], oxygen transfer reactions [10], benzannulation [11] and coupling reactions (Heck [12], Suzuki [13] and Stille [14] reactions).

The work in this thesis is based on experiment findings and uses computational techniques to firstly investigate the asymmetric transfer hydrogenation of ketones catalysed by ruthenium (II) amino amide complexes, the step controlling the stereochemical outcome of the reaction is

identified. The value of $\Delta G^{\ddagger}$ for this step is then computed with a QM method considering the real system and the origin of enantioselectivity is rationalized. This strategy has been successfully applied in the study of several catalytic systems used in asymmetric hydrogenation [15, 16], olefin dihydroxylation [17, 18], hydroformylation [19, 20] and hydrosylylation [21].

1.2 Structure of the thesis

The manuscript of this thesis is divided into two parts: The first part entitled bibliography contains two chapters:

The chapter 2 delineates the experimental and computational background relevant to the field (asymmetric transfer hydrogenation ATH).

The third chapter is devoted to the computational theories and methodology.

The second part contains three chapters (three applications):

In The chapter 4, we investigated The effects of several functionals in the prediction of the geometrical parameters and energetics of four diastereomeric half-sandwich Ru (II) cationic complexes containing amino amide ligands, the enantioselectivity in ATH of acetophenone catalyzed by Ru (II) complexes containing amino amide ligands were also investigated by defferents functional, In order to adopt the best method of calculation for this thesis.

Chapter 5 presents the Theoretical Study of Asymmetric Transfer Hydrogenation of Ketones Catalyzed by phenylalanine amide or proline amide Ruthenium Complexes.

Finally an efficient computational method has been identified which uses Density Functional Theory to predict the enantioselectivity showed in Asymmetric transfer hydrogenation reaction of prochiral ketones in water promoted by chiral proline (amide/amine) ruthenium (II) complexes. This application published in **"Journal of Pharmaceutical Research, Biological and Chemical Sciences (RJPBCS)"**

These are followed in Chapter 7 by general conclusions.

" Cotrary to what is sometimes supposed, the theoretical chemist is not a mathematician, thinking mathematically, but a chemist, thinking chemically"

C. A Coulson, valence (Oxford University. Press, 1952), preface, on v.

1.3 References

[1] S. Hanessian, In Total Synthesis of Natural Products: The Chiron Approach, *Pergamon Press,Oxford, U. K*. **1983**.

[2] S. H. Wilen, A. Collet, J. Jacques, *Tetrahedron*, **1977**, 33, 2725.

[3] Koch, W.; Holthausen, M. C. A Chemist's Guide to Density Functional Theory; *Wiley-VCH:* Weinheim, **2001**.

[4] Torrent, M.; Sola, M.; Frenking, G. *Chem. Rev*. **2000**, 100, 439.

[5] Ziegler, T.; Autschbach, J. *Chem. Rev*. **2005**, 105, 2695.

[6] Musaev, D. G.; Morokuma, K. In Theoretical Aspects of Transition Metal Catalysis; Frenking, G. Ed.*; Springer*: Berlin, **2005**; p. 1.

[7] Sakaki, S.; Musashi, Y. In Computational Modeling of Homogeneous Catalysis; Maseras, F.; Lled´os, A. Eds.; Kluwer: Dordrecht, **2002**; p.79.

[8] Michalak, A.; Ziegler, T. In Theoretical Aspects of Transition Metal Catalysis; Frenking, G. Ed.; *Springer:* Berlin, **2005**; p. 145.

[9] Clot, E.; Eisenstein, O. In Computational Modeling of Homogeneous Catalysis; Maseras, F.; Lledos, A. Eds.; Kluwer: Dordrecht, **2002**; p.137.

[10] Deubel, D. V.; Loschen, C.; Frenking, G. In Theoretical Aspects of Transition Metal Catalysis; Frenking, G. Ed.; *Springer*: Berlin, **2005**; p. 109.

[11] Sol`a, M.; Duran, M.; Torrent, M. In Computational Modeling of Homogeneous Catalysis; Maseras, F.; Lled´os, A. Eds.; Kluwer: Dordrecht, **2002**; p. 269.

[12] Sundermann, A.; Uzan, O.; Martin, J. M. L. *Chem. Eur. J*. **2001**, 7, 1703.

[13] Braga, A. A. C.; Morgon, N. H.; Ujaque, G.; F., M. *J. Am. Chem. Soc.* **2005**, 127, 9298.

[14] Alvarez, R.; Faza, O. N.; L´opez, C. S.; de Lera, A. R. *Org. Lett*. **2006**, 8, 35.

[15] Landis, C. R.; Hilfenhaus, P.; Feldgus, S. *J. Am. Chem. Soc*. **1999**, 121, 8741.

[16] Feldgus, S.; Landis, C. R. *J. Am. Chem. Soc*. **2000**, 122, 12714.

[17] Dapprich, S.; Ujaque, G.; Maseras, F.; Lled´os, A.; Musaev, D. G.; Morokuma, K. *J. Am. Chem. Soc.* **1996**, 118, 11660.

[18] Ujaque, G.; Maseras, F.; Lled´os, A. *J. Am. Chem. Soc*. **1999**, 121, 1317.

[19] Matsubara, T.; Koga, N.; Ding, Y.; Musaev, D. G.; Morokuma, K. *Organometallics* **1997**, 16, 1065.

[20] Carbo, J. J.; Maseras, F.; Bo, C.; van Leeuwen, P. W. N. M. *J. Am. Chem. Soc*. **2001**, 123, 7630

[21] Magistrato, A.; Woo, T. K.; *Organometallics* **2004**, 23, 3218.

Chapter 2

Asymmetric Transfer Hydrogenation (ATH) of ketones

2.1. Catalysis

Catalysis is generally defined as a process by which a small amount of material, e.g. the catalyst, increases the rate of a chemical reaction without being consumed it self [1]. Catalysts can be divided into three types:

i) Heterogeneous, the catalyst (usually a solid) and the reactants are in separate phases.

ii) Homogeneous, the catalyst exists in solution with the reaction mixture.

iii) Enzymatic, has features of both homogenous and heterogeneous catalysis.

Heterogeneous catalysts are commonly used for the production of chemicals such as acetic acid, ammonia, gasoline and methanol. These catalysts can be used at high temperature with high turn over numbers and frequencies. The product and the catalyst can easily be separated [2].

Enzymes are ideal catalysts, optimized by nature over several generations. These macromolecules can promote highly chemo- and enantioselective organic reactions and the diversity of transformations being discovered is rapidly increasing [3]. Homogenous catalysts are associated with high selectivities, mild reaction conditions, easier modification of the reaction parameters and the possibility for mechanistic studies. Product separation and recycling of the catalyst may be problematic.

Transition metals have been explored extensively as catalysts due to their unique ability to enable chemical transformations [4]. An important breakthrough for homogenous catalysis was published by Wilkinson in 1965 when he discovered a catalyst, $RhCl(PPh_3)_3$, that reduced alkenes, alkynes and other unsaturated molecules at 25 ^oC with a hydrogen pressure of 1 bar. Mechanistic studies by Wilkinson, Halpern's group and others, revealed that $RhCl(PPh_3)_2$ was the actual catalyst and a catalytic cycle could be proposed [5].

2.2. Asymmetric catalysis

The discovery of Wilkinson's catalyst provoked an increasing awareness of the possibility to hydrogenate unsaturated hydrocarbons under mild conditions and in particular opened up the field of asymmetric catalysis. Replacement of the two coordinated phosphines with a chiral diphoshine creates an asymmetric catalyst that might be able to selectively catalyze the hydrogenation of a prochiral unsaturated substrate to give only one of the two enantiomers.

Contributions by Kagan and Dang [6]. in 1972 and Knowles [7]. The same year, showed that chiral bidentate phosphines coordinated to rhodium could reduce Z-*N*-acetamidocinnamic acids enantioselectively. These compounds serve as precursors for amino acid derivatives. Knowles at Monsanto introduced the first commercial application of asymmetric transition metal

catalysis in 1974; the enantioselective production of *L*-DOPA promoted by a chiral rhodium based catalyst [8]. As shown in Scheme 1, the hydrogenation can be performed with a substrate to catalyst molar ratio of 20000:1 with 3 bar of hydrogen pressure at 50 ^{o}C and yields the product in 95% ee and 90% yield. The product is then recrystallized to 100% ee. The catalyst can be recycled and it has been stated that 0.5 kg of catalyst yields 1000 kg of *L*-DOPA.

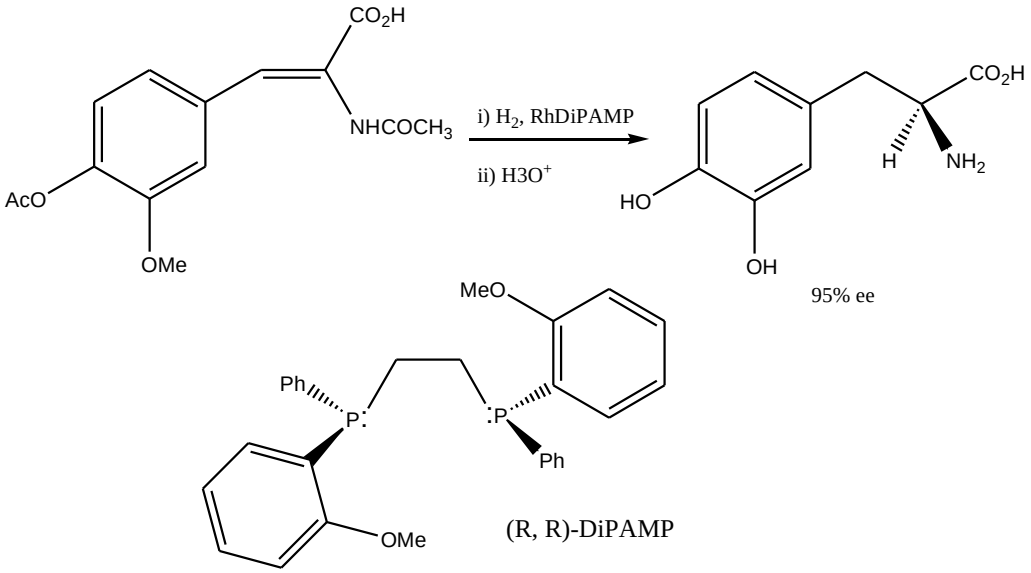

Scheme 2.1. Knowles catalytic asymmetric synthesis of *L*-DOPA

In the last decades, a great number of new catalytic asymmetric reactions have been discovered. A good example is the Sharpless epoxidation of allylic alcohols that was published at the beginning of the 80's (Scheme 2.2) [9].

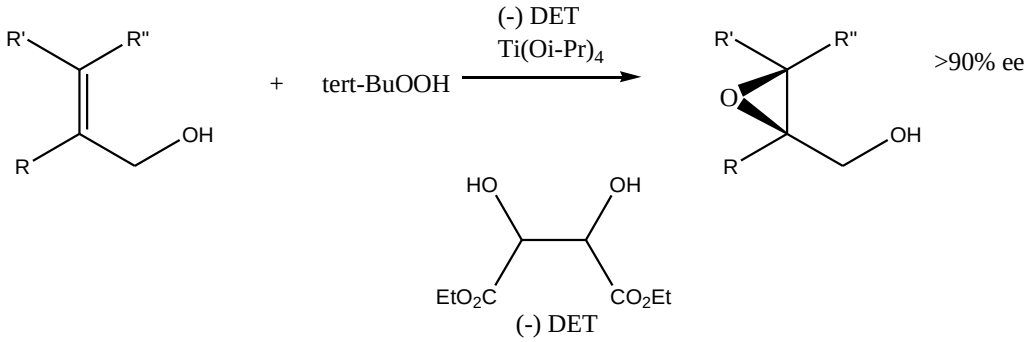

Scheme 2.2. Sharpless asymmetric epoxidation of allylic alcohols

The reaction has a wide scope and is characterized by simplicity, high selectivity and versatility. The obtained epoxides are useful intermediates in asymmetric synthesis.

Another important work is Noyori's enantioselective hydrogenation of unsaturated carbon-carbon bonds and ketones [10]. A ruthenium catalyst constructed of a chiral diamine and a chiral diphosphine, [$RuCl_2$((*S*)-xylbinap)((*S*)-daipen)] and *t*-BuOK as co-catalyst, reduces acetophenone with a substrate to catalyst molar ratio of 100 000:1 under 8 atmosphere of hydrogen gas in 99% enantiomeric excess as shown in Scheme 2.3.

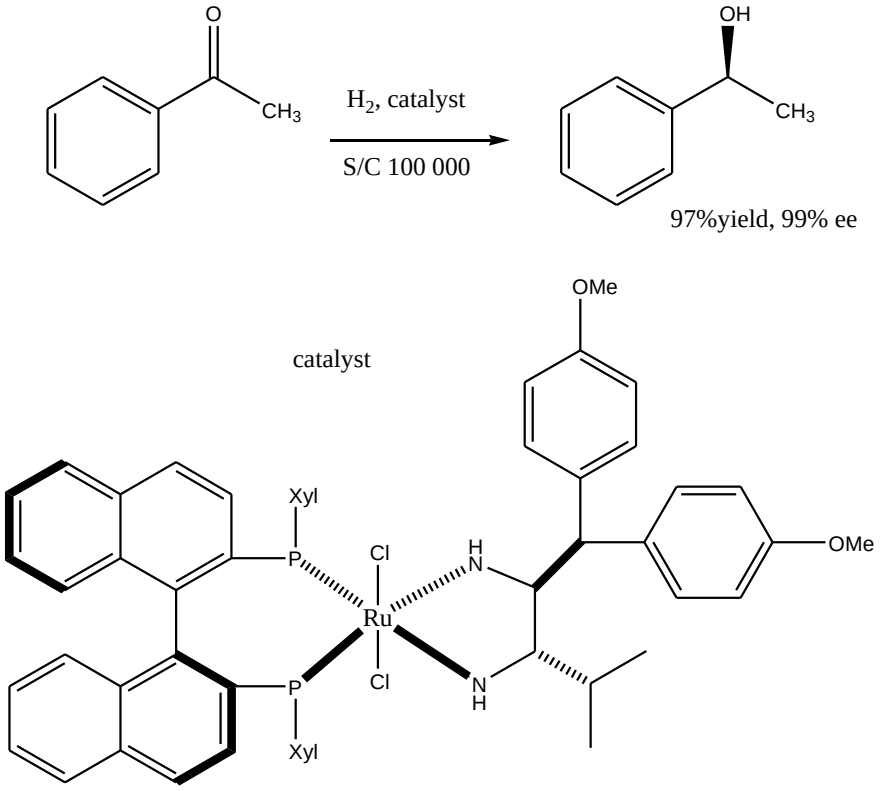

Scheme 2.3. Noyori's asymmetric hydrogenation of aromatic ketones

These and other discoveries have shown the synthetic value of enantioselective catalysis [11]. and have contributed to an ever-increasing list of applications in fine chemical production [12]. In 2001, K. Barry Sharpless, Ryoji Noyori and William Knowles shared the Nobel Prize in chemistry for their pioneering work in asymmetric catalysis and for the important commercial applications derived from their work.

2.3. Transition Metal Catalysed Asymmetric Transfer Hydrogenation of Ketones

2.3.1. A Short History of Asymmetric Transfer Hydrogenation

The asymmetric transfer hydrogenation (ATH) of ketones is one of the most convenient and extensively studied transformations in organic chemistry. The benefits, including excellent selectivity, operationally simplicity and wide substrate scopes, have led to their broad applications to the synthesis of secondary chiral alcohols and related natural products.

To date, several categories of substrate, including aromatic/aliphatic ketones, imines and compounds with activated C=C bonds such as α,β-unsaturated ketones, cyanoolefins and dicyanoolefins have all been found to be active substrates for ATH reactions [12].

Different types of catalyst complexes have been prepared and screened (Scheme 2.4). At first, chiral diphosphine ligands, and bipyridine based ligands, were developed and applied to transfer hydrogenation in 2-propanol at elevated temperatures. However, only poor enantioselectivities and reactivities were found.

When complex 3-[$HRu(CO)_2$] was used the reaction had to be carried out at 120 °C; after 111 h the resulting (S)-1-phenylethanol (S)-2 was obtained with only 35% yield and 4% ee [13]. When 4-[$RuBr_2$] complex was applied the same product chiral 1-phenylethanol 2 was formed in 80% yield and 52% ee [14].

No success was achieved when a bipyridine based ligand 5 was used in ATH of acetophenone 1 [15]. Instead of bipyridine ligand, improvement was achieved by using a chiral bioxazole ligand. Plaftz reported by using 6-[$Ir(cod)Cl_2$] complex, in which case the enantioselectivity of formation of chiral 1-phenylethanol reached 58% ee and it was isolated in good yield (89%) [16].

Diphosphine-diamine 7 and diphosphine-diimine 8 ligands were combined with the same metal core; [$Ru(DMSO)Cl_2$], to form catalytic complexes by the Noyori group. Interestingly, when the two complexes were tested under the same reaction conditions the results were totally different. The enantioselectivity and reactivity of the diphosphinediamine [$Ru(DMSO)Cl_2$] (7-[$Ru(DMSO)Cl_2$]) complex was remarkable. The reduction of acetophenone 1 proceeded from room temperature to 45 °C with only 0.5 mol% of [$Ru(DMSO)Cl_2$] and both excellent yield (80%) and ee (52%) were achieved. When a 8-[$Ru(DMSO)Cl_2$] catalyst was tested there was almost no conversion and also the ee was poor (18%). The authors claimed that catalyst 8-[$Ru(DMSO)Cl_2$] is less effective because of the lack of NH functionality [17].

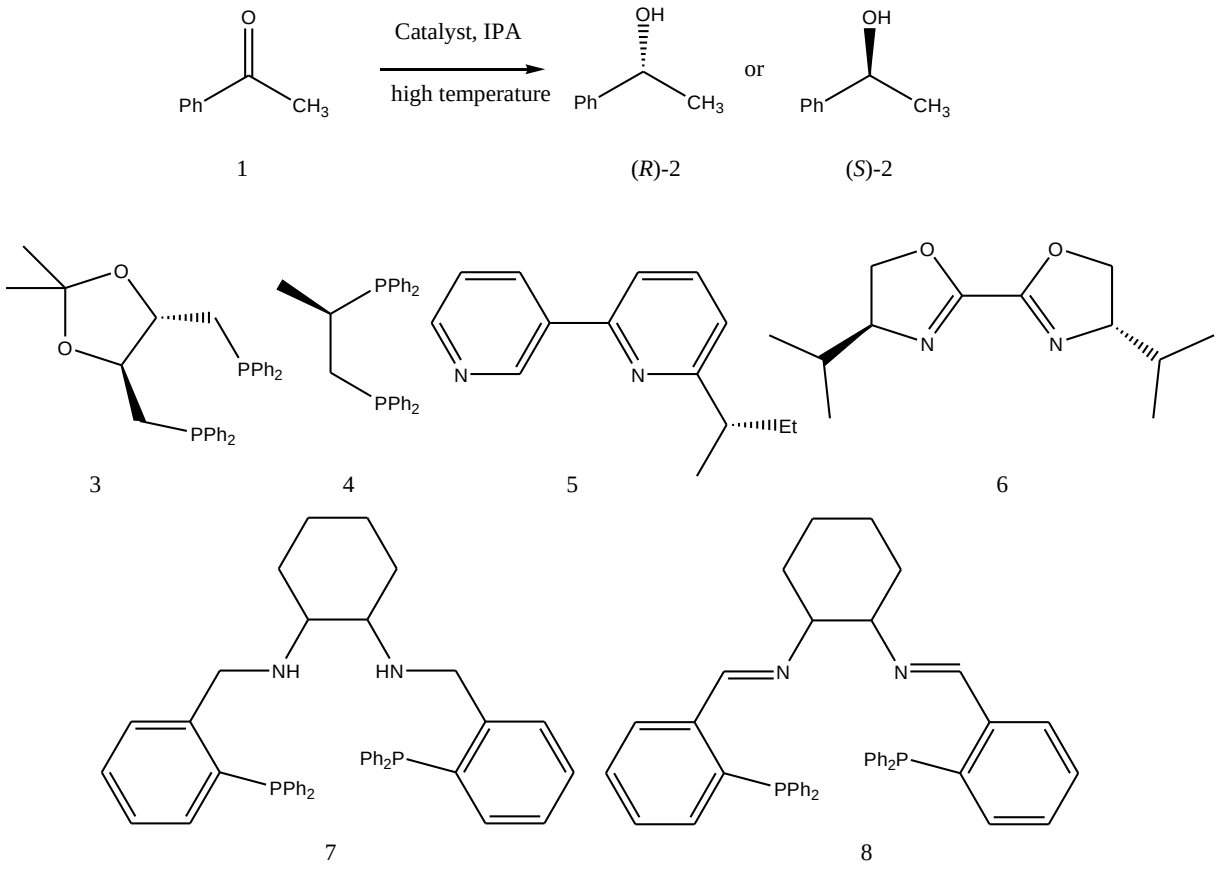

Scheme 2.4. ATH with different ligands

2.3.2. Ligands with NH Functionality

Ligands that incorporate NH functionality have attracted significant attention. In 1995, Noyori's group reported a ruthenium catalyst [$RuCl_2$(mesitylene)]-(S,S)-TsDPEN 9 for asymmetric transfer hydrogenation of prochiral aromatic ketones at low catalyst loadings (S/C=200-500). This reduction could be carried out at room temperature in 2-propanol in a very efficient manner. Excellent ee values (up to 98%) and yields (up to 98%) were obtained by this catalyst. The authors also elaborated the reason why they used [$RuCl_2$(arene)]$_2$ to form the catalyst complex. The special function of the arene which is coordinated with Ru are as follows: (1) arene ligands automatically occupy three adjacent coordination sites of Ru in an octahedral coordination environment, leaving three sites with a fac relationship for other functions; (2) arene ligands are relatively weak electron donors which may provide a unique reactivity on the metallic centre; (3) ready modification of the substitutions of the arene is possible.

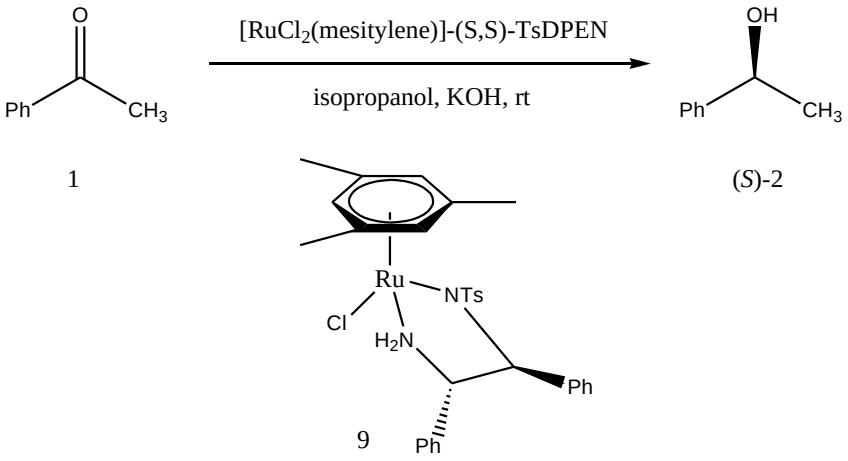

Scheme 2.5. ATH by TsDPEN ligand

After extensive investigation the conclusions were: (1) high enantioselectivity was obtained only when an appropriate arene and chiral ligand were combined; (2) the presence of a primary or secondary amine end in the amino alcohols/diamine ligands is crucial for the catalytic activity[18].

In addition to TsDPEN 10, other amine ligands such as TsDACH 11 and β-amino alcohols 12-14 (Scheme 2.6) have been combined with $[RuCl_2(arene)]_2$ (usually the arenes are benzene, p-cymene, mesitylene and hexamethylbenzene) and excellent results were achieved in the transfer hydrogenation of aromatic ketones [19].

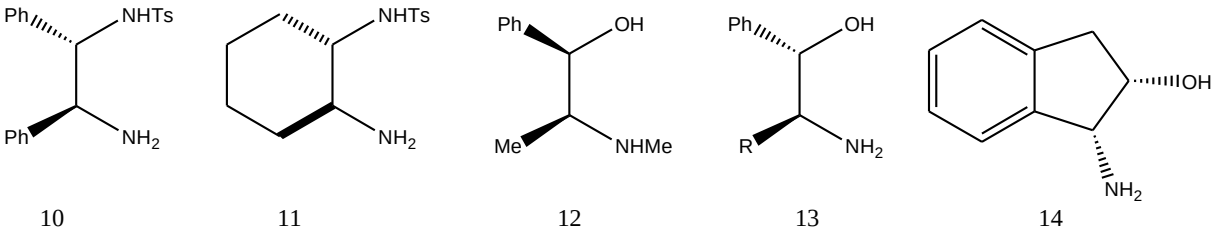

Scheme 2.6. Different structures of ligands with NH functionality

2.4 Prediction of enantiomeric excess (ee)

Figure 2.1 shows the reaction coordinate diagram of an asymmetric reaction generating equal amounts of (*R*)- and (*S*)- configurations in products that are racemate with an *ee* of 0%. Figure 2.2 shows the reaction coordinate diagram of an asymmetric reaction generating different amounts of (*R*)- and (*S*)-configurations of enantiomers, in which the activation energy favours

the (*S*)-product. Enantioselectivity is the preferential formation of molecules of one chirality (enantiomer) over the other and is usually measured as the enantiomeric excess (*ee*):

$$ee = \frac{|R| - |S|}{|R| - |S|}\% \quad 2.1$$

where *R* and *S* are stereochemical descriptors defined in the Cahn-Ingold-Prelog (CIP) system [20]. [*R*] denotes the number of moles of one enantiomer and [*S*] indicates that of the other enantiomer. Enantioselective reactions are usually under kinetic control at a certain temperature and and therefore the final [*S*]/[*R*] ratio is given as follows:

$$\frac{[S]}{[R]} = e^{-\Delta\Delta G_{S-R}/N_A k_B T} \quad 2.2$$

where ΔΔG is the difference in free energies of activation for the (*S*)- and (*R*)-products respectively; *NA* is the Avogadro constant; *kB* is. the Boltzmann constant.

The Curtin-Hammett principle [21]. Postulates that in a reaction having a pair of reactive intermediates which interconvert rapidly, with each going irreversibly to a different

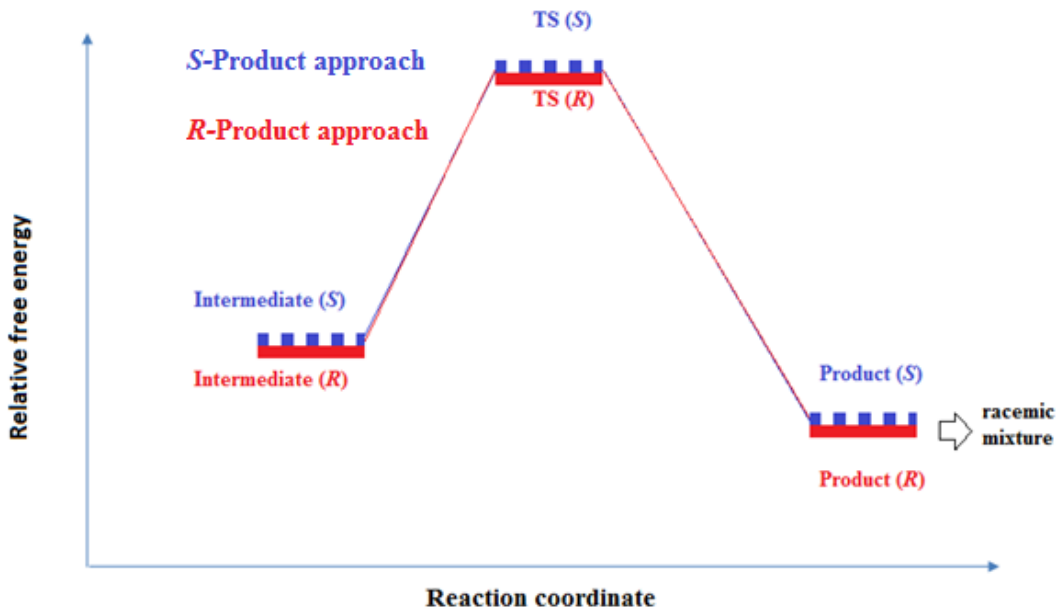

Figure 2.1. A typical asymmetric reaction generating (*R*)- and (*S*)- configuration of products racemic mixture [22].

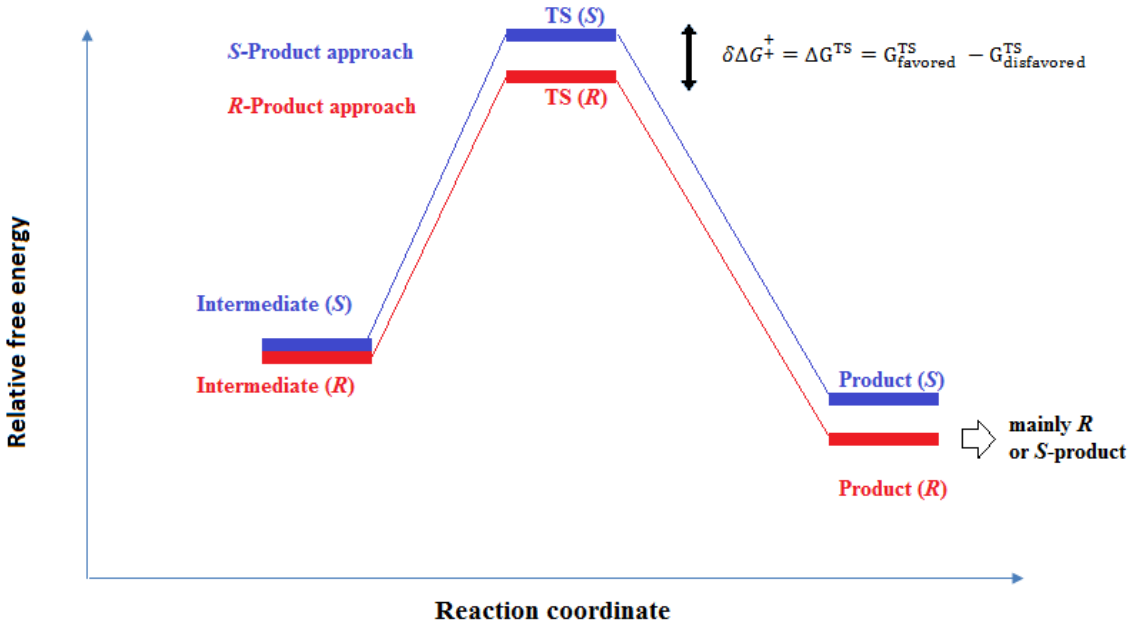

Figure 2.2. A typical asymmetric reaction generating (*R*)- and (*S*)- configuration of products — non-racemic mixture [22].

product, the product ratio will depend only on the difference in the free energy of the transition state associated with each product, and will be independent of the difference in the free energy of the intermediates. Thus, once we have obtained the free energy, we can predict the value of the *ee* based as follows:

$$\%ee_{theory}(\Delta\Delta G) = \frac{1 - e^{\frac{-\Delta\Delta G_{S-R}}{N_A k_B T}}}{1 + e^{\frac{-\Delta\Delta G_{S-R}}{N_A k_B T}}} \times 100 \quad 2.3$$

2.5. Computational studies

2.5.1 Introduction

A large number of catalytic methods involving Ru-based catalysts have been successfully developed to achieve selectivity and efficiency in the hydrogenation of a large family of organic substrates. One of the most important transformations in synthetic organic chemistry is the enantioselective reduction of C=O [23-26]. The design of chiral Ru (II) complexes has become amajor area of research because of their ability to promote the formation of alcohols with high enantiomeric purity starting from prochiral ketones [27–30]. Many cases have been extensively investigated using both experimental and computational methods in order to cast light on the

mechanistic details of the hydrogen transfer. Most of the computational investigations were aimed at identifying the preferred pathway among several possibilities [31–33]. Particular attention has been dedicated to the rationalization of the chemo- and stereoselective outcome induced by chiral catalysts [34–36]. The Ru-catalyzed hydrogenation reaction thus represents an excellent example of cooperation between experimental and theoretical investigations.

For many years, the preferred mechanism has been the center of debate, mainly because of the large number of parameters affecting the pathway. Moreover, these parameters show a synergistic influence on the mechanism and stereoselectivity, and in many cases, it was possible to distinguish the major contributions only by employing a computational approach. In particular, metal-catalyzed transfer hydrogenations are described by three different activation modes (Fig. 2.3):

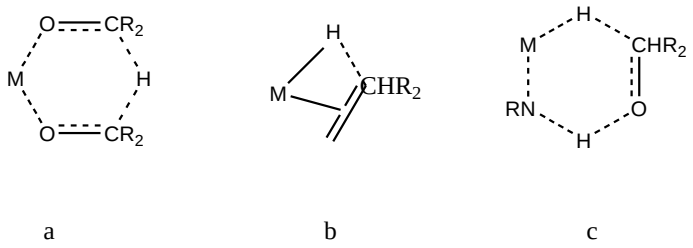

a b c

Figure 2.3. General activation modes for carbonyl hydrogenations

(a) direct transfer of a hydrogen involving both donor and acceptor covalently interacting with the metal (the metal hydride complex is not involved in this mechanism), (b) migratory insertion of a π-coordinated substrate into a metal–hydrogen bond, and (c) an outer sphere mechanism (OSM) where both donor and acceptor never interact directly with the metal but only through hydrogen bonds (the catalyst provides both the proton and the hydride).

the most relevant investigations employing different computational approaches including DFT-based methods are reviewed. During the past 20 years, these methods have been extensively employed to address which mechanism(s) reported in Fig. 2.3 is (are) correct for the Ru-catalyzed hydrogen transfer by comparing calculated PESs for representative models. Such models were selected on the basis of experimental evidence, unclear catalytic behaviors, and computational time. Computational approaches have seen progressive improvements, because more complex and realistic models have been considered thanks to more efficient technology, and also because earlier studies highlighted new factors which play important roles in these reactions. A significant example is the role that the solvent plays in the hydrogen transfer.

2.5.2 Hydrogenation of a Carbonyl Group

The reduction of the C=O functional group has been extensively investigated with computational tools. It is important to highlight that in the case of a mild hydrogen such as a primary or secondary alcohol, the thermodynamic balance is very close to thermoneutral, limiting the intermediates that need to be considered along the reaction pathway. Consequently, earlier computational investigations performed by attention to the extremely stable intermediates that could be classified as catalyst reservoirs of Ru (II). For some Ru (II) catalysts, which do not involve arene ligands as stabilizers, the suggested mechanism for the carbonyl reduction is a migratory insertion of the C=O into the Ru–H bond, as depicted in Fig. 2.3, mode b [23]. Although direct hydrogen transfer as depicted in mode a (Fig. 2.3) could not be excluded, the generally accepted mechanism for this catalyst is shown in Scheme 2.7. The key to this mechanism is the ability of Ru (or other metals) to form an alkoxide complex, rearrange to form the metal hydride, and complex the ketone. One of the principle factors studied for the inner sphere mechanism (ISM) is the kinetics of the reaction with respect to the base concentration. In this mechanistic view, the base is believed to increase the concentration of the alkoxide, facilitating the overall reaction.

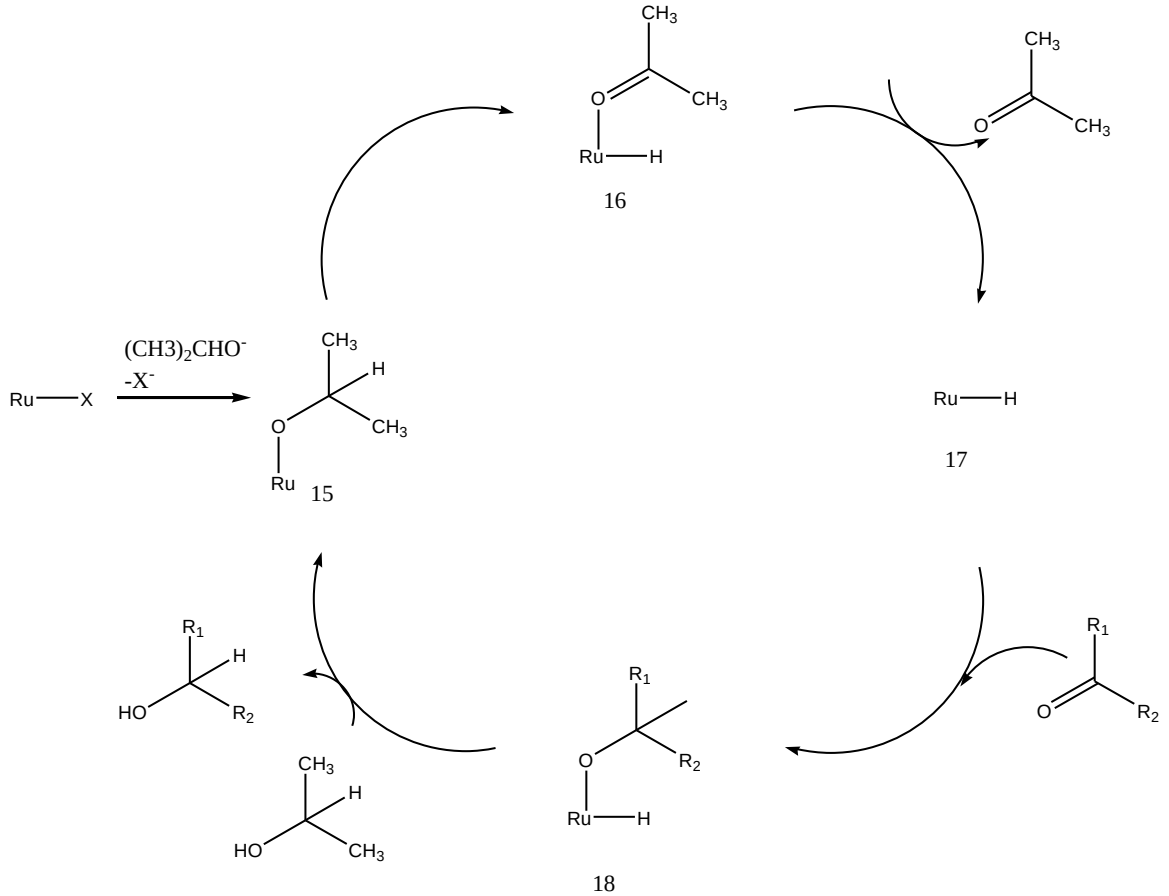

Scheme 2.7. Proposed catalytic cycle for ruthenium-catalyzed transfer hydrogenation

In the case where η^6 coordinated arenes stabilize the Ru catalyst with primary or secondary amine ligands, the experimental observations stimulated the investigation of a new mechanism. Alonso and coworkers [31] performed a computational investigation using the B3PW91 functional and different basis sets in order to compare the direct insertion (Scheme 2.8), the migratory insertion (Scheme 2.9), and the concerted hydrogen transfer (Scheme 2.10) mechanism for the reduction of the C=O bond. The Ru catalyst has been modeled and simplified with the small 2-aminoethanol ligand and benzene as the arene. The authors were not able to describe the entire PES for all three proposed mechanisms, but they obtained a well-defined energetic picture which highlights a preferred pathway.

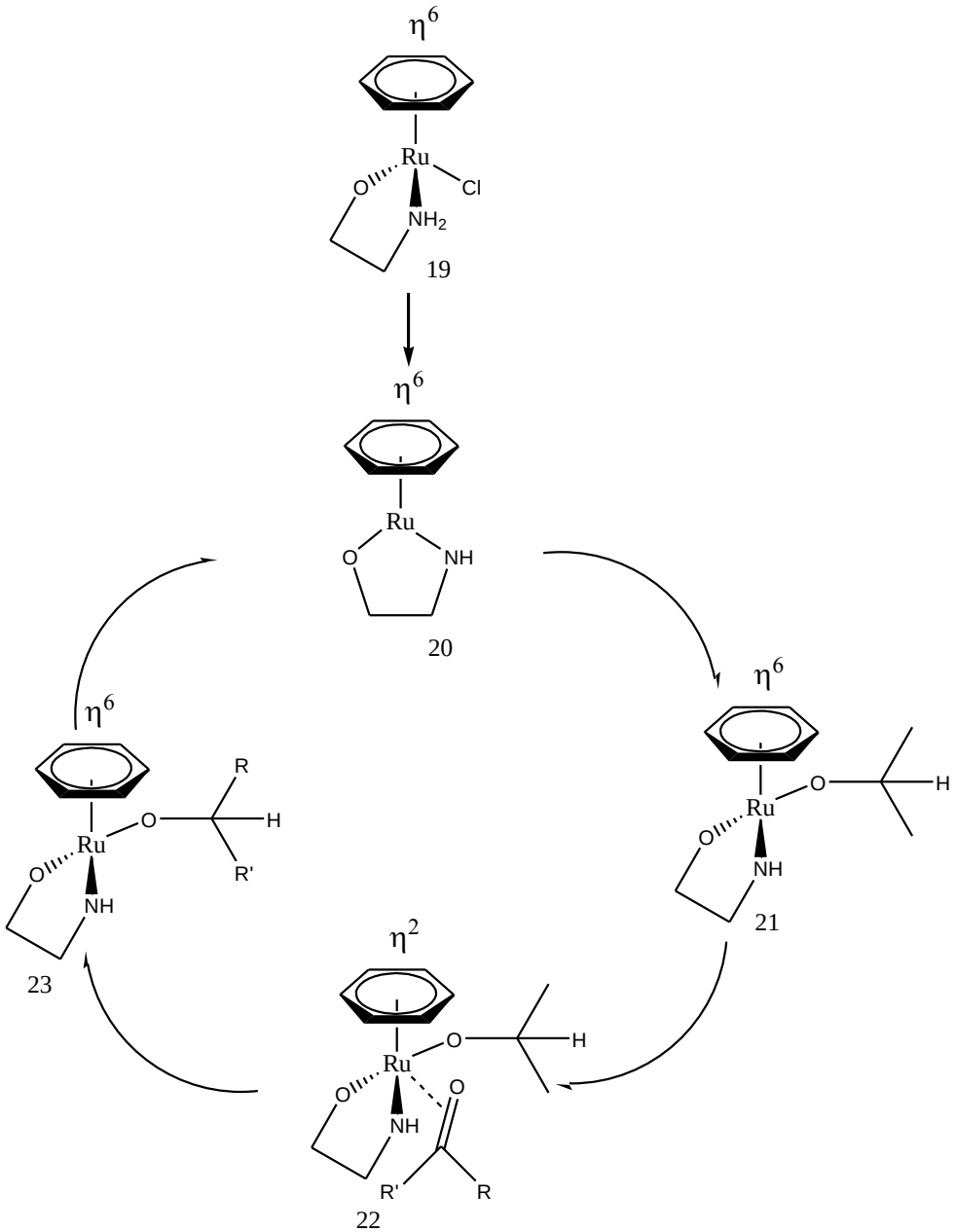

Scheme 2.8. Direct insertion mechanism for Ru (II)-catalyzed hydrogenation

In the direct transfer mechanism, precursor 19 undergoes elimination of HCl, forming the 16e_complex 20 (Scheme 2.8). The preformed alkoxide reacts with 20 generating stable alkoxide complex 21. The ketone substrate interacts via π-coordination, leading to complex 22 after partial decoordination of the arene ligand. Complex 22 is in equilibrium with the analogous 23 through TS22–23 via hydride transfer. The concerted mechanism (Scheme 2.9) is described by the formation of precursor 20 which is transformed into active catalyst 24 via an outer sphere interaction with the hydrogen donor. Hydride 24 reduces the incoming ketone, which interacts with the catalyst via the outer sphere as well.

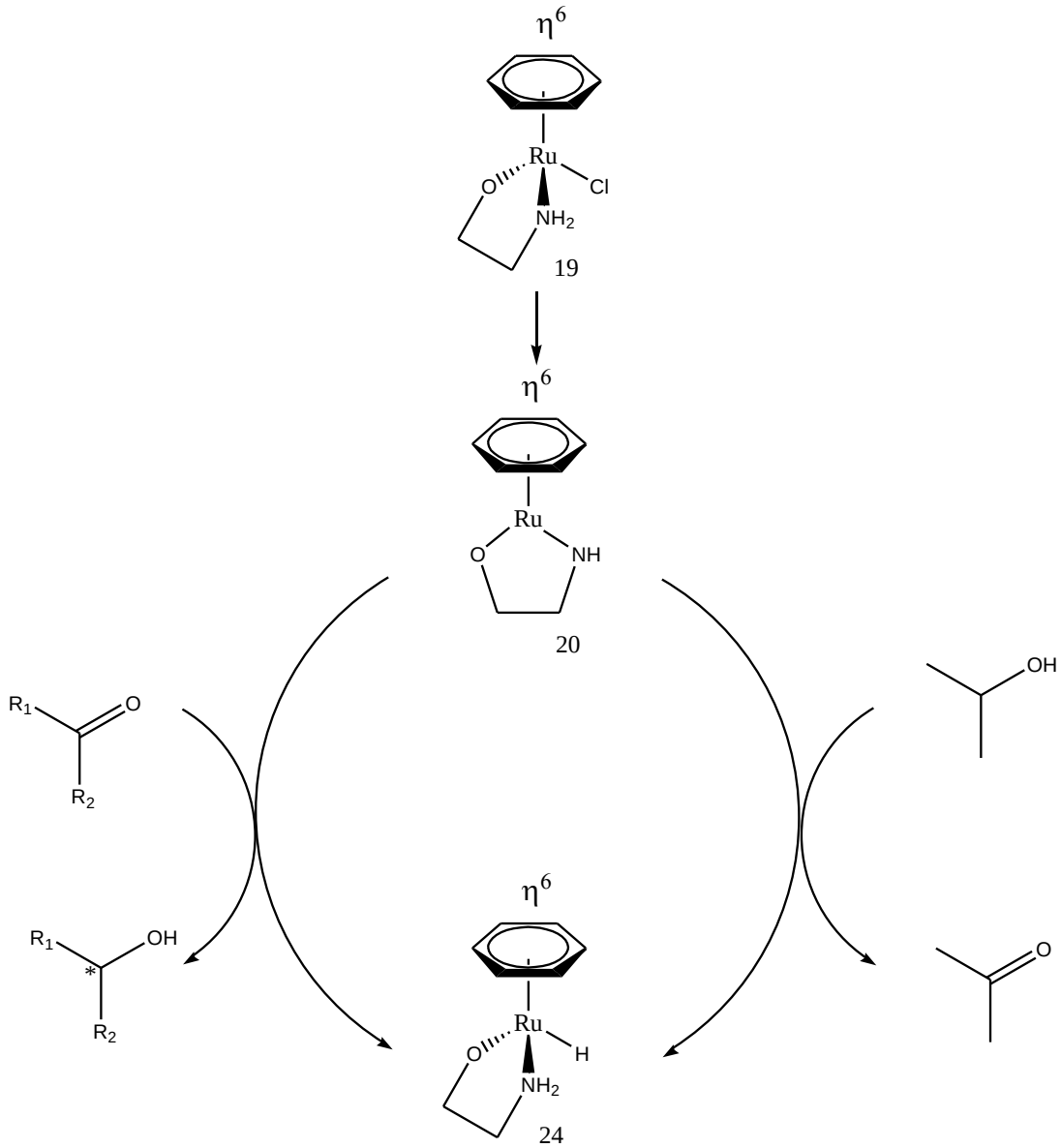

Scheme 2.9. Concerted hydrogen transfer mechanism for Ru (II)-catalyzed hydrogenation

Finally, the "migratory insertion" shares the same intermediates seen in the direct transfer until the generation of complex 21 (Scheme 2.10). Partial slippage of the arene ligand ensures the nucleophilic interaction between the forming hydride and the Ru in complex 25. At this stage, the first hydrogen transfer takes place via an ISM generating hydride complex 26. TS25–26 is characterized by a four-membered ring including Ru–H–C–O. Complex 26 is in equilibrium with active catalyst 24 via decoordination of the ketone formed from the hydrogen donor and coordination of the arene back to the η^6 configuration. The incoming ketone interacts with the catalyst via π-coordination, and the second hydrogen transfer takes place through the similar TS27–28.

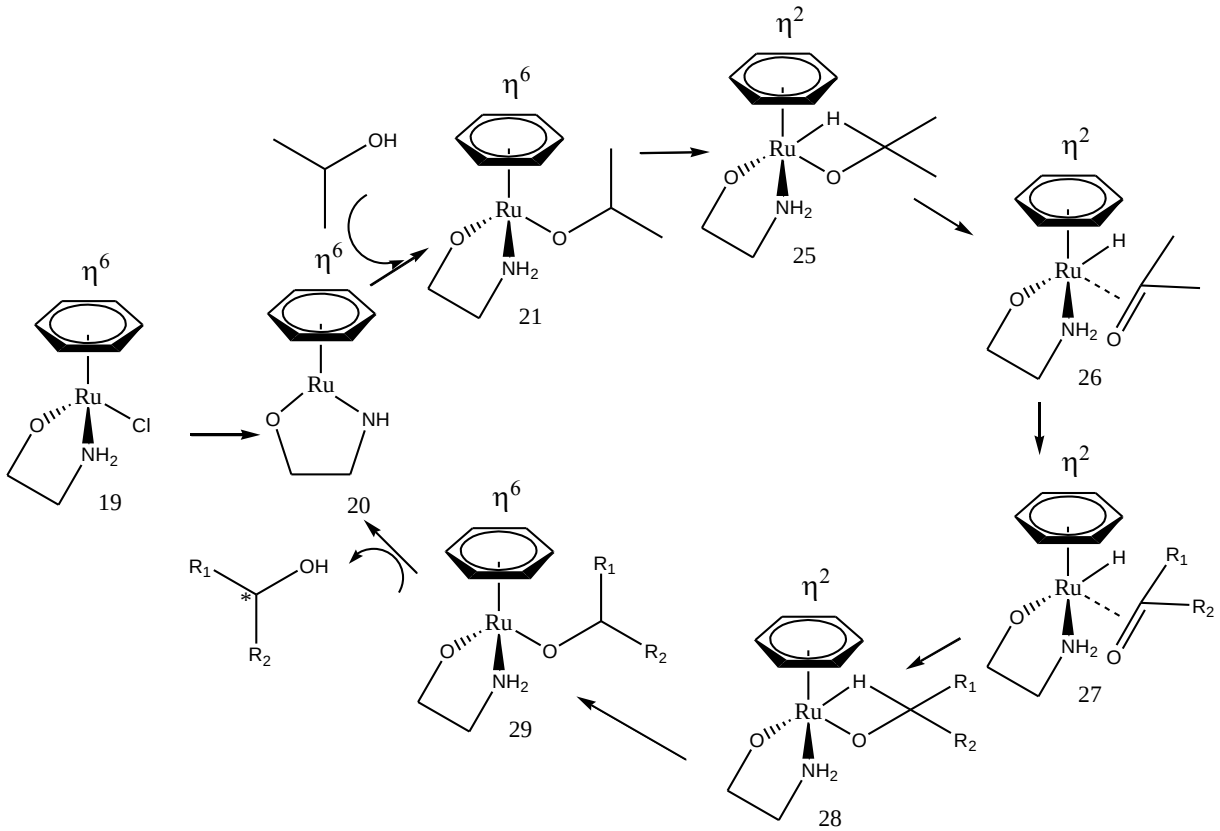

Scheme 2.10 Migratory insertion mechanism for Ru (II) catalyzed hydrogenation

The transition states optimized at the B3PW91/LANL2DZ ECP level of theory and relative energies calculated at the B3PW91/6-311 + G** level for all atoms except for Ru where a SDD basis set augmented by f polarization functions have been used to show that TS20–24 is lower in energy by 7.1 kcal/mol with respect to TS25–26 and 17.9 kcal/mol with respect to TS22–23. This mechanism, initially proposed by Noyori [91], is also referred to as the OSM as neither the ketone nor the alcohol interacts directly with Ru during the process. TS20–24 is characterized by a synchronous transfer of a proton from the nitrogen and a hydride from the Ru. The presence of a NH or NH_2 group in the ligand is crucial for the catalytic activity as reported by Noyori and coworkers. These computational results support this finding.

2.5.3 Conclusions

The main contributions of computational chemistry to the understanding of the mechanisms of ruthenium-catalyzed hydrogenation reactions of ketones are summarized. These studies provided atomistic-level detail into the rate- and stereoselectivity-determining steps for a class of reactions that is widely used in organic synthesis at both the laboratory and the industrial scale.

2.6. References

[1] R. Noyori, In Asymmetric Catalysis in Organic Synthesis, Wiley, New York, **1994**.

[2] B Cornill, A. Herrmann, *In Applied Homogenous Catalysis with Organometallic Compounds* vol 1,Ed B Cornill, A. Herrmann VCH, Weinheim, **1996**.

[3] R. B. Silverman, *The Organic Chemistry of Enzyme Catalyzed Reactions*, Academic Press, San Diego, **2000**.

[4] a)M. Schlosser, *In Organometallics in Synthesis*,Wiley, Chichester, UK, 1994. b) L. S. Hegedus, *Transition Metals in the Synthesis of Complex Organic Molecules*, University Science Books, Mill Valley, CA, **1994**.

[5] a) H. Arai, J. Halpern, *J. Chem. Soc. Dalton T.* **1971**, 1571. b) J. Halpern, C. S. Wong, *J. Chem. Soc. Chem. Comm*. **1973**, 629. c) J. Halpern, *Inorg. Chim. Acta*, **1981**, *50*, 11. d) C. A. Tolman, P. A. Meakin, D.L. Lindner, J. P. Jesson, *J. Am. Chem. Soc*. 96, 2762. e) J. A. Osborn, F. J. Jardine, F. J. Young, G. Wilkinson, *J. Chem. Soc*. **1966**, 1711.

[6] Dang, T. P., Kagan, H. B., *J. Am. Chem. Soc.* **1972**, 94, 6429.

[7] Knowles, W. S., Sabacky, M. J., Vineyard, B. D., *J. Chem. Soc. Chem. Comm*. **1972**, 10.

[8] W. S. Knowles, *Acc. Chem. Res*. **1983**, 16, 106.

[9] a) T. Katsuki. B. K. Sharpless, *J. Am. Chem. Soc.* **1980**, 102, 5974. b) R. A. Johnson, K. B. Sharpless, *In Catalytic Asymmetric Synthesis*, I. Ojima, Ed., VCH, New York, **1993**, 103.

[10] a) T. Ohkuma, M. Koizumi, H. Doucet, T. Pham, M. Kozawa, K. Murata, E. Katayama, T. Yokozawa, T. Ikariya, R. Noyori, *J. Am. Chem. Soc.* **1998**, 120, 13529. b) T. Ohkuma, D. Ishii, H.Takeno, R. Noyori, *J. Am. Chem. Soc*. **2000**, 122, 6510. c) R. Noyori, Ohkuma, T., *Angew. Chem. Int. Ed*. **2001**, 40, 40.

[11] a)E. N. Jacobsen, A. Pfaltz, H. Yamamoto,Eds, *Comprehensive Asymmetric Catalysis*, Springer,Berlin, **1999**. b) I. Ojiima Ed., *In Catalytic Asymmetric Synthesis*, Wiley-VCH, New York, **2000**.

[12] a) H. U. Blaser, M. Studer, *Chirality*, **1999**, 11, 459. b) A. N. Collins, G. N. Sheldrake, J. Crosby, *Chirality in Industry*, J. Wiley, West Sussex, **1996**.

[13] a) X. Li, L. Li,Y. Tang, L. Zhong, L. Cun, J. Zhu, J. Liao, J. Deng, *J. Org. Chem*., **2010**, 75, 2981-2988. b) D. Xue, Y. Chen, X. Cui, Q. Wang, J. Zhu, J. Deng, *J. Org. Chem*., **2005**, 70, 3584-3591. c) R. Noyori, S. Hashiguchi, *Acc. Chem. Res*., **1997**, 30, 97-102.

[14] M. Bianchi, U. Matteoli, G. Menchi, P. Frediani, S. Pratesi, F. Piacenti, C. Botteghi, *J. Organomet. Chem.*, **1980**, 198, 73-80.

[15] J. P. Genêt, V. Ratovelomonana-Vidal, C. Pinel, *Synlett.*, **1993**, 7, 478-480.

[16] C. Botteghi, G. Chelucci, G. Chessa, G. Delogu, S. Gladiali, F. Soccolini, *J. Organomet.Chem.*, **1986**, 304, 217-225.

[17] D. Müller, G. Umbricht, B. Weber, A. Pfaltz, *Helv. Chim. Acta*, **1991**, 74, 232-240.

[18] J. X. Gao, T. Ikariya, R. Noyori, *Organomet*, **1996**, 15, 1087-1089.

[19] S. Hashiguchi, A. Fujii, J. Takehara, T. Ikariya, R. Noyori, *J. Am. Chem. Soc.*, **1995**, 117, 7562-7563.

[20] a) V. Prelog and G. Helmchen, Basic principles of the CIP-system and proposals for a revision. *Angewandte Chemie International Edition* **1982**, 21, 567; b) R. S. Cahn, C. Ingold and V. Prelog, Specification of molecular chirality. *Angewandte Chemie International Edition* **1966**, 5, 385.

[21] A. D. McNaught and A. Wilkinson. IUPAC. Compendium of chemical terminology. Oxford, *Blackwell Scientific Publications* **1997**.

[22] F. Maseras and D. Balcells, Computational approaches to asymmetric synthesis. *New Journal of Chemistry* **2007**, 31, 333.

[23] Clapham SE, Hadzovic A, Morris RH **(2004)** *Coord Chem Rev* 248:2201

[24] Sandoval CA, Ohkuma T, Muniz K, Noyori R **(2003)** *J Am Chem Soc* 125:13490

[25] Noyori R, Ohkuma T **(2001)** *Angew Chem Int Ed* 40:40

[26] Wu XF, Vinci D, Ikariya T, Xiao JL **(2005)** *Chem Commun* 4447

[27] Hashiguchi S, Fujii A, Takehara J, Ikariya T, Noyori R **(1995)** *J Am Chem Soc* 117:7562

[28] Takehara J, Hashiguchi S, Fujii A, Inoue S, Ikariya T, Noyori R **(1996)** *Chem Commun* 233

[29] Hashiguchi S, Fujii A, Haack KJ, Matsumura K, Ikariya T, Noyori R **(1997)** *Angew Chem Int Ed* 36:288 (in English)

[30] Alonso DA, Brandt P, Nordin SJM, Andersson PG **(1999)** *J Am Chem Soc* 121:9580

[31] Yamakawa M, Ito H, Noyori R **(2000)** *J Am Chem Soc* 122:1466

[32] Petra DGI, Reek JNH, Handgraaf JW, Meijer EJ, Dierkes P, Kamer PCJ, Brussee J, Schoemaker HE, van Leeuwen PWNM **(2000)** *Chem Eur J* 6:2818

[33] Handgraaf JW, Reek JNH, Meijer EJ **(2003)** *Organometallics* 22:3150

[34] Brandt P, Roth P, Andersson PG **(2004)** *J Org Chem* 69:4885

[35] Rossin A, Kovacs G, Ujaque G, Lledos A, Joo F **(2006)** *Organometallics* 25:5010

Chapter 3
Computational Methodology

By fusing chemical, physical and mathematical principles, computational modelling is capable of characterising, interpreting and predicting the structures and properties of molecules and materials at the atomic level, and has become an important and commonly used tool in contemporary scientific research. In this thesis, density functional theory (DFT) has been applied in order to understand the mechanisms of organometallic hydrogenations catalysed by ruthenium (II). In this chapter, basic electronic structure theory is summarised briefly before introducing DFT, exchange-correlation functionals, pseudopotential methods, techniques for geometry optimisation and locating transition state structures.

3.1. Electronic structure theory

Electronic structure theory describes electrons in atoms and molecules in terms of quantum mechanics, which postulates that the physical and chemical properties of a system may be obtained by solving the Schrödinger equation. Quantum mechanics explains the wave-particle duality of matter; solution of the Schrödinger equation yields the wavefunction of a system, Ψ. The particle probability density is given by $\Psi^*(\vec{x})\Psi(\vec{x})$ at coordinate $\vec{x}$. The time-dependent Schrödinger equation $i\hbar\frac{\partial\Psi}{\partial r} = \hat{H}\Psi$ gives the time evolution behaviour of the wavefunction. Ignoring relativistic effects, the theory is exact. In most applications, including those in the thesis, the time-independent Schrödinger equation is used:

$$\hat{H}\Psi = E\Psi \quad 3.1$$

where $\hat{H}$ is the Hamiltonian operator corresponding to the kinetic and potential energies,and *E* is the total energy of the system.For a polyatomic system constituting *Nn* nuclei and *Ne* electrons, the many-body time-independent Schrödinger equation in the non-relativistic regime can be written as:

$$\hat{H}\Psi(\vec{r}_1, \vec{r}_2, \dots, \vec{r}_{Ne}, \vec{R}_1, \vec{R}_2, \dots, \vec{R}_{Nn}) = E\Psi(\vec{r}_1, \vec{r}_2, \dots, \vec{r}_{Ne}, \vec{R}_1, \vec{R}_2, \dots, \vec{R}_{Nn}) \quad 3.2$$

Where $\vec{r_i}$ stands for the coordinate of the *i*th electron and $\overrightarrow{R_i}$ stands for that of the *i*th nucleus. The non-relativistic Hamiltonian operator is the sum of the kinetic and potential operators of all the particles in the system and can be expressed as follows:

$$\hat{\mathrm{H}} = -\sum_{i=1}^{N} \frac{\hbar^2}{2m_e} \nabla_{\vec{r}_i}^2 + \frac{1}{2} \sum_{i1 \neq i2=1} \frac{1}{4\Pi\varepsilon 0} \frac{e^2}{|\vec{r}_{i1} - \vec{r}_{i2}|}$$

$$- \sum_{k=1}^{M} \frac{\hbar^2}{2M_k} \nabla_{\vec{R}_k}^2 + \frac{1}{2} \sum_{k1 \neq k2=1} \frac{1}{4\Pi\varepsilon 0} \frac{Z_{k1} Z_{k2} e^2}{|\vec{R}_{k1} - \vec{R}_{k2}|} - \sum_{k=1}^{M} \sum_{i=1}^{N} \frac{1}{4\Pi\varepsilon 0} \frac{Z_k e^2}{|\vec{R}_k - \vec{r}_i|}$$

$$= T_e(\vec{r}) + V_{ee}(\vec{r}) + T_n(\vec{R}) + V_{nn}(\vec{R}) + V_{en}(\vec{r}, \vec{R}) \quad 3.3$$

The first two terms correspond to the electronic kinetic energy and potential energy operators for electron-electron repulsion. The third and fourth terms represent the same physical quantities for the nuclei. The fifth term is the potential energy operator for the electron-nuclear attraction, which couples the dynamics of the nuclear and electronic systems. However, the Schrödinger equation can only be solved exactly for hydrogen atoms and other one-electron systems, while for larger systems, approximations are needed.

3.1.1. The Born-Oppenheimer approximation

The Born-Oppenheimer approximation exploits the fact that the mass of a nucleus is *ca.* 10^3 times larger than that of an electron, which allows us to address the dynamics of the electronic system separately from that of the nuclear system by viewing the latter as static. As a result, electrons adjust to positions of nuclei instantaneously after any change in nuclear positions. The Hamiltonian for the system composed of both nuclei and electrons is thus simplified as below:

$$\hat{\mathrm{H}}_e = -\sum_{i=1}^{N} \frac{\hbar^2}{2m_e} \nabla_{\vec{r}_i}^2 + \frac{1}{2} \sum_{i1 \neq i2=1} \frac{1}{4\Pi\varepsilon 0} \frac{e^2}{|\vec{r}_{i1} - \vec{r}_{i2}|}$$

$$- \sum_{k=1}^{M} \sum_{i=1}^{N} \frac{1}{4\Pi\varepsilon 0} \frac{Z_k e^2}{|\vec{R}_k - \vec{r}_i|}$$

$$= T_e(\vec{r}) + V_{ee}(\vec{r}) + V_{en}(\vec{r}, \vec{R}) \quad 3.4$$

This gives an electronic Schrödinger equation:

$$\hat{\mathrm{H}}_e\left(\vec{R}\right)\Psi_e\left(\vec{r},\vec{R}\right) = E^e\left(\vec{R}\right)\Psi_e\left(\vec{r},\vec{R}\right) \quad 3.5$$

Where $\vec{R}$ and $\vec{r}$ are the coordinates of the nucleus and electron respectively. E^e is the electronic energy in the field of the nuclei and Ψe is the corresponding electronic wave function.

The above equation shows that both the motion and the energy of the electrons depend on the nuclear coordinates. In determining the lowest energy conformation of the system, the differential of the energy with respect to nuclei coordinates (the force) is used to propagate the nuclei to their new positions. The nuclei are fixed and the electronic problem solved again. This optimisation is carried out iteratively until certain convergence thresholds are reached. As discussed later, second derivatives may also be used in the optimisation process.

Although the Born-Oppenheimer approximation reduces the complexity of the Schrödinger equation, the electron-electron interaction term is complicated. As noted, for most electron systems, there are no analytic solutions. Moreover, the motion of electrons is correlated. According to the Pauli exclusion principle, electrons with parallel spin repel each other more than can be accounted for by Coulomb repulsion. The Hartree-Fock approach seeks to simplify this by introducing a mean field approximation where an external field replaces the effects of all the other electrons. DFT also reduces the dimensionality of the problem by treating the many-body problem in terms of the electron density.

3.2. The Hartree and Hartree-Fock Approximations

In the Hartree equation, the Hamiltonian of a system constituting *N* particles is the sum of one-particle Hamiltonians and the total wavefunction is the product of the wavefunctions of all particles [1]:

$$\widehat{H} = \sum_{i}^{N} \hat{h}\ (i) \quad 3.6$$

$$\Psi(\vec{r}_1\, S_1, \vec{r}_2 S_2, \ldots, \vec{r}_N S_N) = \Psi(\vec{r}_1\, S_1)\,\Psi(\vec{r}_2 S_2), \ldots, \Psi(\vec{r}_N S_N) \quad 3.7$$

Where $\hat{h}$ is the one-particle Hamiltonian and s_i is the spin of the ith electron. Hence, the Schrödinger equation for one particle can be written as below:

$$\left(-\frac{1}{2}\nabla^2 + V_{\vec{r}}\right)\Psi(\vec{r}\,S) = E\Psi(\vec{r}\,S) \quad 3.8$$

The Hartree approximation has a major shortcoming - the many-particle wavefunction of the electrons does not obey the Pauli principle, which prohibits two electrons from occupying the same quantum state. By ignoring this principle, the Hartree approximation in general underestimates the average distance between electrons whilst overestimating the average repulsion between them, thus overestimating the total energy.

To obey the Pauli principle, the many-particle wavefunction must be antisymmetric with respect to the exchange of electrons with the same spin; this can be formulated using the Slater Determinant. This approach was proposed by V. Fock, and is known as the Hartree-Fock approximation [2].

As noted, the electron-electron interaction is described using a mean field theory.

The Hartree-Fock theory provides an inadequate treatment of the correlation between the motions of the electrons within a molecular system, particularly interactions arising between electrons of opposite spin. The major correlation effects arise from pairs of electrons with the same spin, which is termed the exchange interaction, but the motion of electrons of opposite spin remains uncorrelated under the Hartree-Fock theory. Any method which goes beyond the Hartree-Fock theory in attempting to treat this phenomenon properly is known as an electron correlation method or a post-Hartree-Fock method, e.g., the Møller-Plesset (MP) perturbation theory [3].

3.3. Density functional theory (DFT)

3.3.1. Thomas-Fermi theory

DFT is a method based on the concept of using electron density instead of the wavefunction to determine properties of the system. In the late 1920s [4], the Hartree approximation was reformulated in terms of electron density, proposed independently by Thomas and Fermi, and named Thomas-Fermi theory [5,6], which was the first primitive quantum mechanical approach applied to many-body electronic structure calculations of molecular and condensed matter

systems. In this theory, the kinetic energy is locally approximated by that of a non-interacting homogeneous electron gas with the same density.

Later, using the same approximation, Dirac introduced the exchange term into this model [7]. However, a breakthrough was made by P. Hohenberg and W. Kohn in 1964 [8], who showed that the ground-state energy and all other ground-state electronic properties were uniquely defined by the electron density. Basing the energy on the total electron density means that there are fewer degrees of freedom to consider in the DFT method. This approach has become popular because of the favourable compromise between accuracy and computational cost, allowing the treatment of large many-electron systems.

3.3.2. Hohenberg-Kohn theorems

In 1964, Hohenberg and Kohn proposed two theorems that used the density as the basic variable in determining the total energy of an interacting many-body system [9]. The first theorem demonstrated a one-to-one correspondence between the many-body wavefunction $\Psi(\vec{r})$ in the ground state and the electron density $\rho(\vec{r})$ in the ground state. The total energy of a system can be written as a functional of electron density, $\rho(\vec{r})$

$$E[\,\rho(\vec{r})] = \int V_{ext}(\vec{r})dr + F[\rho(\vec{r})] \quad 3.9$$

The first term, $V_{ext}(\vec{r})dr$, arises from the interaction of the electrons with an external potential. In the Born-Oppenheimer approximation, $V_{ext}(\vec{r})$ represents the Coulomb interaction between the electrons and nuclei. The second term, $F[\rho(\vec{r})]$, is the sum of the kinetic energy of the electrons and the potential energy of the electron-electron interactions. However, the exact form is unknown. Because the expression for the Hartree energy as a functional of the density is known, $F[\rho(\vec{r})]$ then could be written as:

$$F[\,\rho(\vec{r})] = E_H[\,\rho(\vec{r})] + E_{unknown}[\,\rho(\vec{r})] \quad 3.10$$

Where $E_H[\,\rho(\vec{r})]$is the Hartree energy and $E_{unknown}[\,\rho(\vec{r})]$ is an unknown universal function of the density independent of the external potential. The total energy can be re-written as:

$$E[\,\rho(\vec{r})] = \int V_{ext}(\vec{r})\rho(\vec{r})dr + E_H[\,\rho(\vec{r})] + E_{unknown}[\,\rho(\vec{r})] \quad 3.11$$

The second Hohenberg-Kohn theorem proved that the exact ground-state energy of the electronic system corresponds to the global minimum of $E[\,\rho(\vec{r})]$, and the electron density $\rho(\vec{r})$ which minimises this functional is the exact ground-state electron density $\rho_0(\vec{r})$.

3.3.3. Kohn-Sham equations

The second landmark in the development of DFT was by W. Kohn and L. J. Sham (1965) [10], who suggested a practical method to obtain the ground-state electron density.Kohn and Sham suggested that $F[\,\rho(\vec{r})]$can be recast as the sum of the three terms:

$$F[\,\rho(\vec{r})] = E_{KE}[\,\rho(\vec{r})] + E_H[\,\rho(\vec{r})] + E_{XC}[\,\rho(\vec{r})] \quad 3.12$$

where $E_{KE}[\,\rho(\vec{r})]$is the kinetic energy, $E_H[\,\rho(\vec{r})]$ is the electron-electron Coulomb energy and $E_{XC}[\,\rho(\vec{r})]$ is the sum of the contributions from the exchange and correlation interactions. The ground-state electron density $\rho(\vec{r})$ is given by:

$$\rho(\vec{r}) = \sum_{i=1}^{n} n_i\,|\varphi_i(\vec{r})|^2 \quad 3.13$$

where n_i is the occupation number of the *i*th state and $|\varphi_i(\vec{r})|$is a Kohn-Sham orbital.
The first term in equation 3.12, $E_{KE}[\,\rho(\vec{r})]$, is defined as the kinetic energy of a system of non interacting electrons with the same density as the real system:

$$E_{KE}[\,\rho(\vec{r})] = \sum_{i=l}^{N} \int \psi_i(\vec{r}) \left(-\frac{\vec{v}^2}{2}\right) \psi_i(\vec{r})dr \quad 3.14$$

Where $\vec{v}_i$is the velocity of the *i*th electron.

The second term, $E_H[\,\rho(\vec{r})]$, is the Hartree energy. In the Hartree approach, this electronic energy arises from the classical interactions between two charge densities when summed over all possible pairwise interactions, giving:

$$E_H[\,\rho(\vec{r})] = \frac{1}{2}\iint \frac{\rho(\overrightarrow{r_1})\rho(\overrightarrow{r_2})}{|\overrightarrow{r_1} - \overrightarrow{r_2}|}\, dr_1 dr_2 \quad 3.15$$

The last term$E_{XC}[\,\rho(\vec{r})]$ has contributions from not only exchange and correlation, but also from the difference between the true kinetic energy of the interacting system and the kinetic energy of the non-interacting system. The following section will introduce some commonly used exchange-correlation functionals.

3.4. Exchange-correlation functionals

In the earlier section we introduced the Kohn-Sham equations which in principle allow an exact treatment of the total electronic energy of an atomic or molecular system.

Our ignorance of the exact exchange and correlation contributions is expressed in the exchange-correlation term, $E_{XC}[\,\rho(\vec{r})]$. Appropriate approximations for $E_{XC}[\,\rho(\vec{r})]$ have been the subject of intense study and development. Indeed, there are now many different types of functionals available that are more or less appropriate for particular systems. In this thesis, we discuss the local density approximation (LDA), the generalised gradient approximation (GGA) and hybrid exchange correlation functionals.

3.4.1. Local Density Approximation (LDA)

The LDA is based on the known exchange-correlation energy of a uniform electron gas. The LDA functional is dependent only on the value of the densityρ $\rho(\vec{r})$ at a specific point in space $\vec{r}$, emphasising the local nature of this approach. In the LDA, the exchange-correlation potential V_{xc} can be separated into exchange and correlation parts. The exchange contribution to ε_X can be obtained analytically [11], giving:

$$\varepsilon_X(\rho) = \frac{3}{4}\left(\frac{3n}{\pi}\right)^{\frac{1}{3}} \quad 3.16$$

while the correlation contribution is obtained through analytic interpolation of accurate values obtained using quantum Monte Carlo calculations by Ceperley and Alder in 1980. The correlation term of the LDA functionals used at the present depends on the parameterisation of these results, one of the most commonly-used of which was proposed by Perdew and Zunger in 1981.

The LDA is strictly applicable to the homogeneous electron gas, but may be useful in solid systems, although the LDA functional usually leads to the underestimation of bond lengths and results in a significant error in the cohesive energy under most circumstances. To improve the accuracy for inhomogeneous systems we consider the gradient of the electron density at each point as well as the density; this approach is called the generalized gradient approximation (GGA).

3.4.2. Generalised Gradient Approximation (GGA)

As noted, the GGA adds a dependence on the gradient of the density. The exchange-correlation energy is now written as:

$$E_{XC}^{GGA}\left[\,\rho(\vec{r})\right] = \int \rho(\vec{r})\varepsilon_{XC}[\rho(\vec{r}), \nabla\rho(\vec{r})]dr \quad 3.17$$

One of the most commonly-used non-empirical GGA functionals is the PBE (Perdew-Burke-Ernzerhof) functional. When using the GGA, many computed properties are improved compared with LDA, such as geometries and the ground-state energy of molecules [12, 13].

3.4.3. Hybrid Functionals

Hybrid functionals include a proportion of exact exchange from the Hartree-Fock theory. The exact exchange energy functional is expressed in terms of the Kohn-Sham orbitals instead of the electron density. Two of the most commonly-used hybrid functionals are B3LYP (Becke, 3-parameter, Lee-Yang-Parr) and PBE0.

The B3LYP hybrid exchange-correlation functional is shown below:

$$E_{XC}^{B3LYP} = E_{XC}^{LDA} + a_0(E_X^{HF} - E_X^{LDA}) + a_x(E_X^{GGA} - E_X^{LDA}) + a_c(E_C^{GGA} - E_C^{LDA}) \quad 3.18$$

Where the three empirical parameters a_0=0.20, a_x=0.72 and a_c =0.81 are determined by fitting to a set of measured atomisation energies. E_X^{HF} is the Hartree-Fock exact exchange energy. E_X^{GGA} and $E_C^{GGA}$are the exchange functional of Becke 88 and the correlation functional of Lee, Yang and Parr respectively. $E_C^{LDA}$is the correlation functional of the VWN local-density approximation.

In 1996, Adamo modified the pure Perdew-Burke-Ernzerhof functional with 25% Hartree-Fock exchange and 75% PBE exchange, which is known as PBE0, given below:

$$E_{XC}^{PBE0} = E_{XC}^{GGA} + \frac{1}{4}(E_X^{HF} - E_X^{GGA}) \quad 3.19$$

PBE0 affords good accuracy for molecular structures and properties as well as energies [14].

3.5. Dispersion in density functional theory (DFT-D)

None of the functionals considered so far incorporates dispersions physics, Thus, it should not be surprising that no conventional DFT can mode dispersion-bound complexes with even qualitative accuracy. This demonstrates a fundamental principle of functional development- a DFT model can only yield meaningful results if the correct physics is built into the model at the outset.

To our knowledge only two attempts have been described in the literature to develop a unified DFT model including the physics of dispersion. One of these is the approach of Sato, Tsuneda, and Hirao, which extends the dispersion model of Andersson , Langreth, and Lundqvist (ALL). The ALL method is based on the dispersion interaction energy between two separated uniform-electron-gas-like regions. For an intermolecular complex, the total dispersion energy has the form

$$E_{disp} = -\frac{6}{(4\pi)^{\frac{3}{2}}} \int_{V1} dr_1 \int_{V2} dr_2 \frac{\rho^{\frac{1}{2}}(r_1)\,\rho^{\frac{1}{2}}(r_2)}{\rho^{\frac{1}{2}}(r_1) + \rho^{\frac{1}{2}}(r_2)} \frac{1}{r_{12}^6} \quad 3.20$$

V_1 and V_2 correspond to the volumes of the constituent monomers. Remarkably, while based on electron-gas physics, the ALL model gives atomic C_6's in fairly good agreement with experiment, with a mean absolute percent error (MAPE) of 15.5% for a set of 45 noble-gas and alkali-atom pairs.

To compute potential-energy-surfaces, the dispersion energy is decomposed into a sum over atomic pair terms for atoms *A* and *B* in V_1 and V_2.

$$E_{disp} = \sum_{A \in V1} \sum_{B \in V2} E_{AB} \quad 3.21$$

With

$$E_{AB} = -\frac{6}{(4\pi)^{\frac{3}{2}}} \int_A dr_1 \int_B dr_2 \frac{\rho^{\frac{1}{2}}(r_1)\, \rho^{\frac{1}{2}}(r_2)}{\rho^{\frac{1}{2}}(r_1) + \rho^{\frac{1}{2}}(r_2)} \frac{1}{r_{12}^6} f_{damp}(r_{12}) \quad 3.22$$

And where the *A* and *B* integrations are performed on numerical atom-centered grids.
The damping function,

$$f_{damp}(r_{12}) = \exp[-(\frac{a_{AB}}{r_{12}})^6] \quad 3.23$$

Prevents unphysical behavior at small r_{12}. The parameter a_{AB} is linearly related to The sum of atomic van der waals radii, R_m, as follows:R

$$a_{AB} = C_1 R_m + C_2 \quad 3.24$$

The constante c_1=0.4290 and c_2=1.8949 au are universal parameters fit to accurate potential-energy curves of noble-gas dimers.
This model has been applied to noble-gas pairs and noble-gas – diatomic complexes, and later to the bezene dimer, but has not been systematically benchmarked. More importantly, since the system must be divided into separated monomers, the ALL dispersion model is not applicable to intramolecular dispersion interactions.

3.6. Basis sets

Although there is no exact analytical solution to the time-independent Schrödinger (equation 3.2) for systems containing more than one electron, approximate solutions can be obtained using standard numerical techniques — building the total wavefunction from a basis set of mathematical functions capable of reproducing critical properties of the system.
An individual molecular orbital can be expressed as:

$$\Phi_i = \sum_{\mu} C_{\mu i} \chi_{\mu}$$

Where χ_{μ} (r) are the basis functions and the $C_{\mu i}$ are the molecular orbital coefficients. Molecular orbitals are therefore expressed as linear combinations of a pre-defined set of one-electron functions commonly centred on the atomic nuclei so they bear some resemblance to atomic orbitals. The basis set can be interpreted as restricting each electron to a particular region of space. Larger basis sets impose fewer restrictions on electrons and more accurately approximate exact molecular orbitals, but more computational resources are required.

3.7. Pseudopotentials

Pseudopotentials, as used in the Hartree-Fock and Kohn-Sham methods, are effective potentials which act upon the valence electrons, and are constructed to represent the potential of the core electrons and nuclei. The idea is derived from the fact that only the valence electrons are involved in the chemical bonding of a system. We are therefore able to simplify the description of the system: the contributions from the nucleus and the core electrons are replaced with an angular dependent pseudopotential formed from the free atom of the corresponding element68, meaning that only the valence states are considered explicitly, reducing computing costs significantly. Inside the core region, the pseudopotential is designed to be much softer than the ionic one. Outside the core region, it is required that the corresponding pseudo wavefunction is close to its all-electron counterpart to maintain the correct behaviour over a broad range of chemical environments.

3.7.1. Pseudopotentials applied in this thesis

LANL (Los Alamos National Laboratory) ECPs: This type of pseudopotential is available for a variety of elements together with the appropriate double zeta valence basis set. The combination of ECP and a valence basis set is thus referred to as LANL2DZ basis. LANL2 ECPs have not been defined for elements H – Ne; the all-electron valence double zeta basis sets developed by Dunning (D95V) are used for these elements instead. The ECP parameters for elements Na – Kr have been derived from atomic wavefunctions obtained in all-electron non-relativistic Hartree-Fock calculations, while relativistic Hartree-Fock calculations have been used for the heavier elements Rb – Bi.

3.8. Optimisation

3.8.1. Minimisation

Optimisations of structures to their minimum energies are also called minimisations. These methods fall into two categories: (a) first-derivative methods such as the steepest descent, giving a quick but rough estimated result, and the conjugate gradients methods, which converge more rapidly than the former; (b) second- derivative methods such as the Newton-Raphson and the quasi-Newton approaches. In addition to the gradient, the curvature of the function is also considered. The second derivative is stored in the Hessian matrix. These methods are generally used when the potential energy surface is harmonic close to the extrema; thus the minimum will be located in a single step using a pure quadratic interpolating function; in more complicated real systems, more steps are required. Both the Newton-Raphson and quasi-Newton approaches require the inverse of the Hessian matrix. The quasi-Newton approach builds up the inverse Hessian in successive geometry steps whereas the Newton-Raphson approach requires the inverse Hessian at every point in a geometry search and therefore consumes more computing time.

3.8.2. Methods of locating transition state structures

3.8.2.1. Constrained optimisation (CO) method

The constrained optimisation (CO) is one of the simplest and most widely-used methods to search for transition states. Reaction pathways and transition states are located with a constrained minimisation technique. We select a pseudo reaction coordinate and fix the distance between the two reactants and minimise the total energy with respect to all remaining degrees of freedom. Through a series of such constrained structure optimisations, with a different reactant separation in each case, we obtain a reaction coordinate diagram. Since the only constraint is the distance between the reactants, the reactants are free to rotate and translate subject to the above constraint. The transition state is identified when the forces on the atoms vanish and the energy is a maximum along the reaction coordinate but a minimum with respect to all remaining degrees of freedom.

3.8.2.2. Synchronous transit-guided quasi-Newton (STQN) method

When searching for transition states, a very accurate estimate of the inverse Hessian is necessary at each step because the potential energy surface around the transition state is usually flatter than it is around a minimum. The synchronous transit-guided quasi-Newton (STQN)

method uses a linear (LST) or quadratic synchronous transit (QST) approach to locate the quadratic region of the transition states and then uses a quasi-Newton or eigenvalue-following algorithm to complete the optimisation. For the LST approach, the highest point is located by drawing a line between the reactant and product minima on the potential energy surface. The QST approach refines this method by starting at the LST maximum and minimising the energy perpendicular to the LST line. In Gaussian, using the QST2 option, we require one optimised reactant and one optimised product, followed by the generation of a guess for the transition state which is midway between the reactant and product in terms of redundant internal coordinates. For more complicated systems, one would provide the reactant, the product and a guess for the transition state and use the QST3 option to perform a transition state optimisation.

3.9. Modelling Solvation

Modelling solvation is one of the most challenging issues in computational chemistry. There are several methods currently used; in this thesis we use the PCM (polarisable continuum model). For the asymmetric hydrogenation of ketones, 2-propanol is used as the solvent .

3.9.1. The Polarisable Continuum Model (PCM)

The PCM, proposed by Tomasi *et al*., is one of the most widely used models to compute a system in a non-aqueous solution, and belongs to the class of self-consistent reaction field (SCRF) methods. These methods all model the solvent as a continuum of uniform dielectric constant ε. The PCM solvation model is available for calculating energies and gradients at the Hartree-Fock and DFT levels of theory. Solvation models based on polarisable continuum dielectrics have been demonstrated to be flexible and accurate, particularly when the solute is situated in a cavity of realistic molecular shape.

Table 3.1. Density functional applied in this thesis.

Functional	Year	Ref	Type *a*
BP86	1986	[16,17]	GGA
B3LYP	1993	[18,19]	global-hybrid GGA
PBE	1996	[15]	GGA
TPSS	2003	[20]	meta-GGA
PBE0	1996	[13,14]	global-hybrid GGA
M06	2008	[24,25]	global-hybrid meta-GGA
M06L	2006	[23]	meta-GGA
WB97X	2008	[21]	RS-hybrid GGA
WB97XD	2008	[22]	RS-hybrid GGA + MM
BP86-GD3BJ	2011	[16,17] [26]	GGA+ MM
B3LYP-GD3BJ	2011	[18,19] [26]	global-hybrid GGA+ MM
PBE-GD3BJ	2011	[15] [26]	GGA + MM
TPSS-GD3BJ	2011	[20] [26]	meta-GGA+ MM
MP2	1934	[3]	(MP) perturbation theory
B2PLYP	2006	[27]	doubly hybrid
B2PLYPD	2006	[28]	doubly hybrid + MM

a "GGA" denotes generalized gradient approximation; "RS" denotes range-separated; "+ MM" denotes the addition of a post-SCF empirical molecular mechanics term.

3.10. References

[1] D. R. Hartree, *Proceedings of the Cambridge Philosophical Society* **1928**, 24, 89.

[2] V. Fock, *A Hadrons and Nuclei* **1930**, 61, 126.

[3] C. Møller and M. S. Plesset, *Physical Review* **1934**, 46, 618.

[4] (a) E. Fermi, A Hadrons and Nuclei **1928**, 48, 73; (b) L. H. Thomas. *Proceedings of the Cambridge Philosophical Society* **1927**,23, 542.

[5] F. A. Hamprecht, A. J. Cohen, D. J. Tozer and N. C. Handy. *AIP* **1998**.

[6] (a) A. D. Becke. *Journal of Chemical Physics* **1996**, 104, 1040; (b) Y. Zhao, B. J. Lynch and D. G. Truhlar. *The Journal of Physical Chemistry A* **2004**, 108, 2715.

[7] P. A. M. Dirac. *Mathematical Proceedings of the Cambridge Philosophical Society* **1930**, 26, 361.

[8] W. Kohn and L. J. Sham. *Physical Review* **1965**, 140, 1133.

[9] P. Hohenberg and W. Kohn. *Physical Review* **1964**, 136, B864.

[10] J. P. Perdew and A. Zunger. *Physical Review B* **1981**, 23, 5048.

[11]. J. VandeVondele and J. Hutter. *Journal of Chemical Physics* **2007**, 127,114105.

[12]. J. P. Perdew, K. Burke and M. Ernzerhof,. *Physical Review Letters* **1996**, 77, 3865.

[13] (a) A. D. Becke. *Journal of Chemical Physics* **1997**, 107, 8554; (b) W.Kohn, A. D. Becke and R. G. Parr. *Journal of Physical Chemistry* **1996**, 100, 12974.

[14] (a) C. Adamo and V. Barone. *Journal of Chemical Physics* **1999**, 110, 6158;

[15] JP Perdew; K Burke; M Ernzerhof. *Phys Rev Lett*., **1996**, 77(18-28),3865.

[16] AD Becke. *Phys Rev A*., **1988**, 38(6), 3098.

[17] JP Perdew. *Phys Rev* B., **1986**, 33(12), 8822.

[18] PJ Stephens; FJ Devlin; CF Chabalowski; MJ Frisch. *J Phys Chem*.,**1994**, 98(45),11623.

[19] C Lee; W Yang; RG Parr.*Phys. Rev. B*., **1988,** 37(2), 785.

[20] J Tao; JP Perdew; VN Staroverov; GE Scuseria; **2003**, *Phys Rev Lett* 91(14), 146401.

[21] JD Chai; M Head-Gordon. *J. Chem. Phys.*, **2008**, 128(8), 084106.

[22] JD Chai; M Head-Gordon. *Phys. Chem. Chem. Phys.*, **2008,** 10(44)**,** 6615-6620.

[23] Y Zhao; DG Truhlar. *J Chem Phys.*, **2006**, 125(19):194101.

[24] Y Zhao; DG Truhlar. *Acc Chem Res*., **2008**, 41(2), 157.

[25] Y Zhao; DG Truhlar. *Theor Chem Acc*., **2008**, 120(1), 215-241.

[26] S Grimme; S Ehrlich; L Goerigk. *J. Comp. Chem*., **2011**, 32(7), 1456-1465.

[27] S Grimme. *J Chem Phys*., **2006**, 124(3), 034108.

[28] S. Grimme, *J. Comp. Chem.*, **2006**, 27(15), 1787-1799.

Chapter 4: Application I

The Choice of Density Functional

4.1. Introduction

Ruthenium complexes have been found to be highly efficient catalysts for asymmetric transfer hydrogenation, a process with important applications in organic and pharmaceutical chemistry [1-4], Intensive theoretical studies have been applied for these complexes to get a better understanding of their catalytic properties [5-8].

Density Functional Theory (DFT) is one of the most widely used quantum chemical method for electronic structure calculations in inorganic and organometallic chemistry. [9–12].It is well known that the performance of the density functional theory depends mainly on the accuracy of the chosen functional. Therefore, the very important thing for a DFT investigation is to choose an appropriate functional for a specific system. The only way to be sure that a functional yield better results is to compare it to previous methods and some reference calculations, Di Tommaso et al showed that The choice of the functional is a critical step in establishing an accurate DFT based approach for computational kinetics [13]. In this work we have investigated the performance of several functionals in the prediction of the geometrical parameters of four diastereomeric half-sandwich Ru(II) cationic complexes containing amino amide ligands (Figure.4.1).

The asymmetric transfer hydrogenation of acetophenone catalyzed by Ru (proline-amide) hydride complex is also computed against different functionals to understand the influence of the functional on the selectivity.

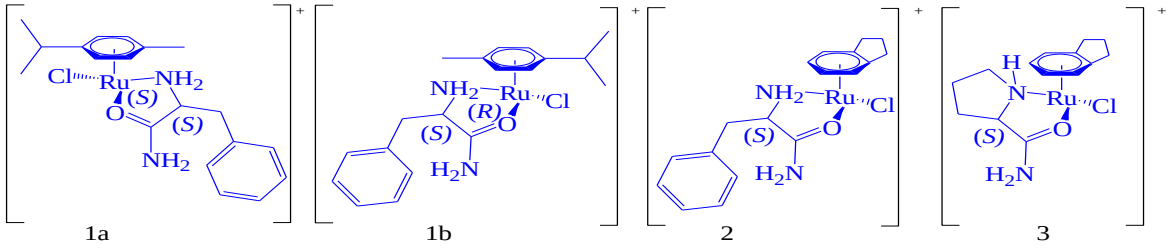

Figure. 4.1. Structures of the selected complexes. Complexes 1a, 1b, 2, and 3 are from Ref. [14]

In this study, we focus on the geometry parameters that are closely related to the Ruthenium atom. Taking complex 1a for example, only the geometry parameters around the central Ru (II) are discussed, including 4 bond lengths, 6 bond angles involving the central Ru (II), and 4 dihedral angles (Figure. 4.2).

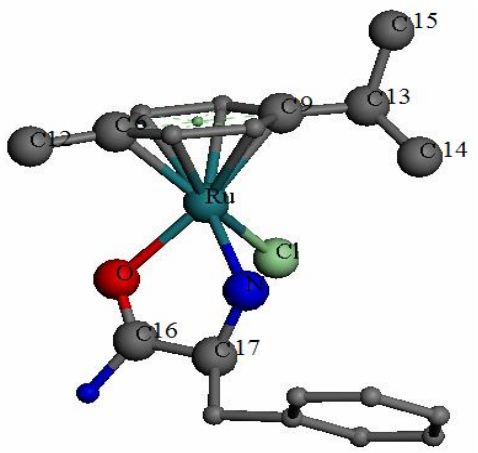

Figure. 4.2. The three-dimensional structure of complex 1a showing the bond lengths, bon angles and dihedral angles involved in the studies. Ru–X bond lengths: Ru–O, Ru–N, Ru–Cl, Ru–CM; X-Ru–X bond angles: ∠Cl-Ru–O, ∠N-Ru–O, ∠N-Ru–Cl, ∠CM-Ru–Cl, ∠CM-Ru–O, ∠CM-Ru–N; X-Ru–C-C dihedral angles :Cl-Ru–C(9)-C(13), N-Ru–C(9)-C(13), O-Ru–C(6)-C(12), O–C(16)-C(17)-N

4.2. Experimental section

4.2.1. Computational details

All calculations have been carried out using Gaussian 09 D01 [15] package. Ground state geometries of all the complexes were fully optimized using the crystal structures as starting geometries with no symmetry or internal coordinate constrains. The set of functionals not including dispersion, namely the standard generalized gradient approximation (GGA) functionals PBE [16] and BP86 [17-18], the hybrid-GGA functional B3LYP [19-20] and the meta-GGA functional TPSS [21] were used. Secondly, to account for dispersion, two types of functionals were used. The first ones are constructed to account for dispersion, namely the hybrid meta-GGA functional wB97X [22] that includes long-range corrections and wB97XD [23] that contains empirical dispersion terms, and also long-range corrections. The meta-GGA M06L [24-25] and the hybrid functional M06 [26] account for noncovalent attractions and dispersion via an extensive parametrization using training sets including non-covalently bound complexes. The second type of functionals includes dispersion by addition of the D3 version of Grimme's dispersion with Beck-Johnson Damping functions [27] to the ones used previously [PBE-GD3BJ, TPSS-GD3BJ, BP86-GD3BJ, B3LYP-GD3BJ]. The second-order Moller-Plesset [MP2] method [28] and the double hybrid functionals [B2PLYP [29], B2PLYPD [30]] were also used,The 6-31G (d,p) [31-32] basis set was used for the C, N, O, Cl and H elements and the LANL2DZ pseudopotential for the ruthenium [33].

4.3. Results and discussion

4.3.1. Geometries

The ground state geometries of the 4 diastereomeric half-sandwich Ru (II) cationic complexes containing amino amide ligands have been optimized using fifteen density functionals PBE, TPSS, BP86, B3LYP, M06, M06L, Wb97x, Wb97xD, PBE-GD3BJ, TPSS-GD3BJ, BP86-GD3BJ, B3LYP-GD3BJ, MP2, B2PLYP and B2PLYPD in combination with the LANL2DZ basis set for Ru(II) and 6-31G(d,p) for other atoms.

The PBE/TZ, wB97XD/TZ, PBE-GD3BJ/TZ and MP2/TZ optimized geometry of the 4 diastereomeric half-sandwich Ru (II) cationic complexes is depicted in figures (4.3- 4.18) and The details of the principal bond lengths, bond angles and dihedral angles together with the crystal structures are given in Tables (4.1- 4.16).

Table 4.1.principal bond lengths,angles and dihedrals of [Ru(*R*)(η^6-p-cymene) Phenyl alanine amide]Cl$^+$complex, and related errors.

Empirical bond length (A)		Calculated bond length (A˚) (methods/error)							
nomenclature	Bond length (A˚)	PBE /TZ	Error	TPSS /TZ	Error	BP86 /TZ	Error	B3LYP /TZ	Error
Ru-CM	1.64	1.677	0.037	1.682	0.042	1.693	0.053	1.729	0.089
Ru-Cl	2.394	2.401	0.007	2.406	0.012	2.408	0.014	2.417	0.023
Ru-N	2.130	2.171	0.041	2.173	0.043	2.176	0.046	2.183	0.053
Ru-O	2.095	2.164	0.069	2.148	0.053	2.156	0.061	2.151	0.056
Empirical bond angle (˚)		Calculated bond angle (˚) (methods/error)							
nomenclature	Bond angle (˚)	PBE /TZ	Error	TPSS /TZ	Error	BP86 /TZ	Error	B3LYP /TZ	Error
Cl-Ru-CM	129.8	128.478	-1.322	128.202	-1.598	128.546	-1.254	128.030	-1.770
N-Ru-CM	134.4	135.469	1.069	135.750	1.35	135.589	1.189	135.894	1.494
O-Ru-CM	126.8	129.779	2.979	129.722	2.922	129.386	2.258	129.779	2.979
Cl-Ru-O	88.2	86.922	-1.278	86.604	-1.596	86.474	-1.726	86.669	-1.531
O-Ru-N	76.5	75.851	-0.649	75.935	-0.547	75.977	-0.523	75.585	-0.915
Cl-Ru-N	82.9	81.815	-1.085	81.573	-1.327	81.773	-1.127	81.783	-1.117
Empirical bond dihedral (˚)		Calculated bond dihedral (˚) (methods/error)							
nomenclature	Bond dihedral (˚)	PBE /TZ	Error	TPSS /TZ	Error	BP86 /TZ	Error	B3LYP /TZ	Error
N-C(16)-C(17)-O	19.7	20.028	0.328	18.669	-1.031	18.262	-1.438	15.531	-4.161
C(12)-C(9)-Ru-O	0	9.288	9.288	10.518	10.518	18.741	18.741	17.111	17.111
C(13)-C(6)-Ru-Cl	-34	-29.120	4.880	-28.525	5.475	-20.497	13.503	-21.671	12.329
C(13)-C(6)-Ru-N	52	54.066	2.066	54.175	2.175	60.633	8.633	60.015	8.015

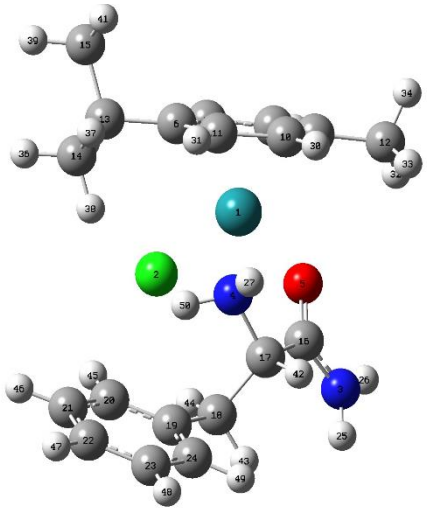

Figure 4.3. The PBE/TZ optimized geometry of [Ru(*R*)(η^6-p-cymene)Phenyl alanine amide]Cl$^+$

Table 4.2.principal bond lengths, angles and dihedrals of [Ru(*S*) (η6-p-cymene) Phenyl alanine amide]Cl^{+}complex, and related errors.

Empirical bond length (A˚)		Calculated bond length (A˚) (methods/error)							
nomenclature	Bond length (A˚)	PBE /TZ	Error	TPSS /TZ	Error	BP86 /TZ	Error	B3LYP /TZ	Error
Ru-CM	1.660	1.680	0.02	1.685	0.025	1.695	0.035	1.731	0.071
Ru-Cl	2.406	2.402	-0.004	2.405	-0.002	2.409	0.003	2.418	0.012
Ru-N	2.140	2.176	0.036	2.175	0.035	2.178	0.038	2.181	0.041
Ru-O	2.146	2.150	0.004	2.133	-0.013	2.139	-0.007	2.148	0.002
Empirical bond angle (˚)		Calculated bond angle (˚) (methods/error)							
nomenclature	Bond angle (˚)	PBE /TZ	Error	TPSS /TZ	Error	BP86 /TZ	Error	B3LYP /TZ	Error
Cl-Ru-CM	127.6	128.440	0.84	128.447	0.847	128.791	1.191	128.496	0.896
N-Ru-CM	132.5	135.079	2.579	135.595	3.095	135.771	3.271	136.887	4.387
O-Ru-CM	132	129.900	-2.1	130.080	-1.92	129.734	-2.266	130.595	-1.405
Cl-Ru-O	86.6	85.540	-1.06	85.152	-1.448	85.061	-1.539	84.622	-1.978
O-Ru-N	76.4	76.861	0.461	77.092	0.692	77.195	0.795	76.278	-0.122
Cl-Ru-N	83.3	81.945	-1.355	81.110	-2.19	80.849	-2.451	79.747	-3.553
Empirical bond dihedral (˚)		Calculated bond dihedral (˚) (methods/error)							
nomenclature	Bond dihedral (˚)	PBE /TZ	Error	TPSS /TZ	Error	BP86 /TZ	Error	B3LYP /TZ	Error
N-C(16)-C(17)-O	0.6	-3.774	-4.374	-1.636	-2.236	0.331	-0.262	25.181	24.581
C(12)-C(6)-Ru-O	2	-14.080	-16.08	-5.401	-7.401	-19.325	-21.325	-16.743	-18.743
C(13)-C(9)-Ru-Cl	38	26.022	-11.978	25.021	-12.979	21.126	-16.874	23.364	-14.663
C(13)-C(9)-Ru-N	-48	-56.608	-8.608	-56.507	-8.507	-59.370	-11.37	-56.698	-8.698

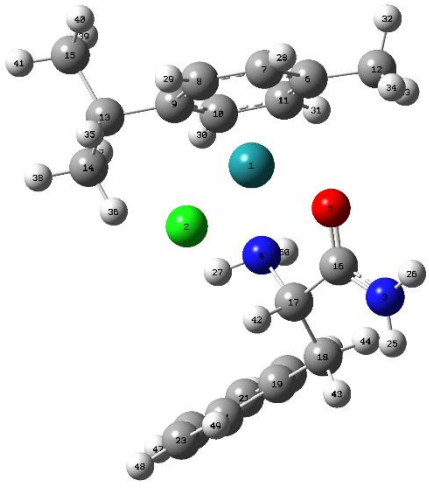

Figure 4.4. The PBE/TZ optimized geometry of [Ru(*S*)(η^{6}-p-cymene)Phenyl alanine amide]Cl^{+}

Table 4.3.principal bond lengths,angles and dihedrals of [Ru(η^6-indane) Phenyl alanine amide]Cl$^+$complex, and related errors.

Empirical bond length (A˚)		Calculated bond length (A˚) (methods/error)							
nomenclature	Bond length (A˚)	PBE /TZ	Error	TPSS /TZ	Error	BP86 /TZ	Error	B3LYP /TZ	Error
Ru-CM	1.65	1.679	0.029	1.682	0.032	1.651	0.001	1.731	0.08
Ru-Cl	2.423	2.398	-0.025	2.408	-0.015	2.407	-0.016	2.411	-0.012
Ru-N	2.142	2.178	0.036	2.173	0.031	2.173	0.031	2.182	0.04
Ru-O	2.109	2.146	0.037	2.126	0.017	2.153	0.044	2.158	0.049
Empirical bond angle (˚)		Calculated bond angle (˚) (methods/error)							
nomenclature	Bond angle (˚)	PBE /TZ	Error	TPSS /TZ	Error	BP86 /TZ	Error	B3LYP /TZ	Error
Cl-Ru-CM	130.0	128.840	-1.16	129.130	-0.87	130.037	0.037	128.572	-1.428
N-Ru-CM	132.8	135.060	2.26	135.742	2.942	135.113	2.313	136.770	3.97
O-Ru-CM	126.5	129.707	3.207	130.110	3.61	126.526	0.026	130.970	4.47
Cl-Ru-O	88.21	85.310	-2.9	84.841	-3.369	85.528	-2.682	84.311	-3.899
O-Ru-N	77.73	76.664	-0.166	77.248	-0.482	76.498	-1.232	75.722	-2.008
Cl-Ru-N	84.0	82.099	-1.901	80.037	-3.963	79.111	-4.889	80.089	-3.911
Empirical bond dihedral (˚)		Calculated bond dihedral (˚) (methods/error)							
nomenclature	Bond dihedral (˚)	PBE /TZ	Error	TPSS /TZ	Error	BP86 /TZ	Error	B3LYP /TZ	Error
N-C(6)-C(7)-O	-20	-1.865	18.135	3.553	23.553	29.496	49.496	27.376	47.376
C(20)-C(23)-Ru-O	-29	-22.437	6.563	-28.122	0.878	-13.760	15.24	4.411	33.411
C(19)-C(21)-Ru-N	30	41.708	11.708	37.817	7.817	51.337	21.337	77.697	47.697

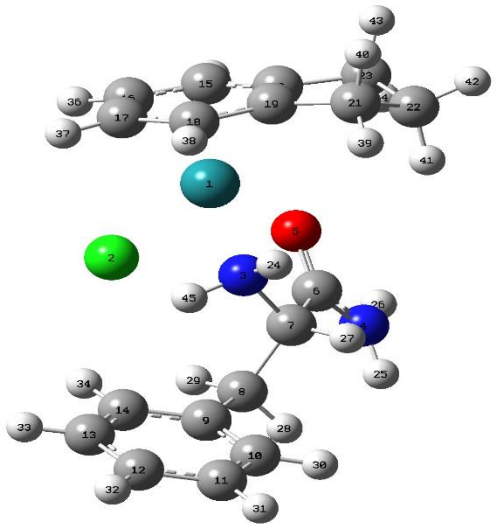

Figure 4.5. The PBE/TZ optimized geometry of [Ru(η^6-indane)Phenyl alanine amide]Cl$^+$

Table 4.4.principal bond lengths,angles and dihedrals of [Ru(η^6-indane) prolineamide]Cl$^+$ complex, and related errors.

Empirical bond length (A˚)		Calculated bond length (A˚) (methods/error)							
nomenclature	Bond length (A˚)	PBE /TZ	Error	TPSS /TZ	Error	BP86 /TZ	Error	B3LYP /TZ	Error
Ru-CM	1.67	1.681	0.011	1.686	0.016	1.694	0.024	1.732	0.062
Ru-Cl	2.418	2.404	-0.014	2.407	-0.011	2.408	-0.01	2.418	0.0
Ru-N	2.149	2.187	0.038	2.186	0.037	2.188	0.039	2.196	0.047
Ru-O	2.092	2.144	0.052	2.131	0.039	2.142	0.05	2.142	0.05
Empirical bond angle (˚)		Calculated bond angle (˚) (methods/error)							
nomenclature	Bond angle (˚)	PBE /TZ	Error	TPSS /TZ	Error	BP86 /TZ	Error	B3LYP /TZ	Error
Cl-Ru-CM	130.0	128.346	-1.654	128.216	-1.784	128.193	-1.807	127.748	-2.252
N-Ru-CM	134.1	137.297	3.197	137.390	3.29	137.342	3.242	137.449	3.349
O-Ru-CM	128.5	129.001	0.501	129.361	0.861	129.105	0.605	129.369	0.869
Cl-Ru-O	83.61	85.701	2.091	85.054	1.444	85.758	2.148	85.894	2.284
O-Ru-N	78.67	77.334	-1.336	77.664	-1.006	77.405	-1.265	76.989	-1.681
Cl-Ru-N	82.85	79.691	-3.159	79.791	-3.059	79.603	-3.247	79.961	-2.889
Empirical bond dihedral (˚)		Calculated bond dihedral (˚) (methods/error)							
nomenclature	Bond dihedral (˚)	PBE /TZ	Error	TPSS /TZ	Error	BP86 /TZ	Error	B3LYP /TZ	Error
N-C(6)-C(7)-O	0	9.311	9.311	8.229	8.229	8.999	8.999	7.394	7.394
C(17)-C(15)-Ru-O	-47	-35.414	11.586	-35.018	11.982	-35.473	11.527	-35.390	11.61
C(19)-C(14)-Ru-Cl	20	35.800	15.8	35.752	15.752	35.746	15.746	35.419	15.419

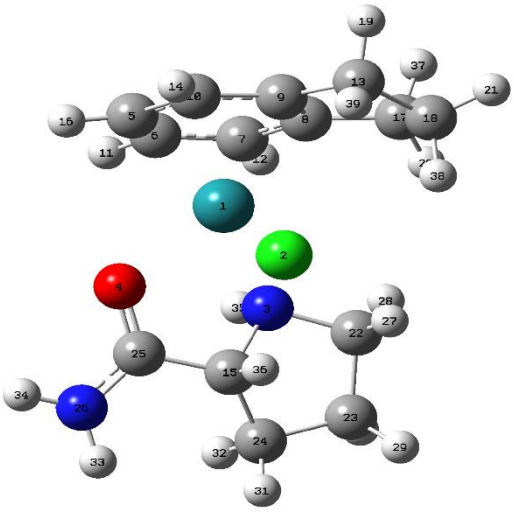

Figure 4.6. The PBE/TZ optimized geometry of [Ru(η^6-indane)Proline amide]Cl$^+$

Table 4.5.principal bond lengths,angles and dihedrals of [Ru(*R*)(η^6-p-cymene) Phenyl alanine amide]Cl$^+$complex, and related errors.

Empirical bond length (A˚)		Calculated bond length (A˚) (methods/error)							
nomenclature	Bond length (A˚)	M06 /TZ	Error	M06L /TZ	Error	wB97X /TZ	Error	wB97XD /TZ	Error
Ru-CM	1.64	1.678	0.038	1.643	0.003	1.683	0.043	1.681	0.041
Ru-Cl	2.394	2.402	0.008	2.419	0.025	2.404	0.01	2.400	0.006
Ru-N	2.130	2.191	0.061	2.208	0.017	2.178	0.048	2.164	0.034
Ru-O	2.095	2.183	0.088	2.217	0.122	2.161	0.066	2.158	0.063
Empirical bond angle (˚)		Calculated bond angle (˚) (methods/error)							
nomenclature	Bond angle (˚)	M06 /TZ	Error	M06L /TZ	Error	wB97X /TZ	Error	wB97XD /TZ	Error
Cl-Ru-CM	129.8	128.321	-1.479	128.203	-1.597	127.613	-2.187	128.015	-1.785
N-Ru-CM	134.4	136.019	1.619	135.326	0.926	135.980	1.58	134.448	0.048
O-Ru-CM	126.8	129.834	3.034	130.667	3.867	129.795	2.995	130.360	3.56
Cl-Ru-O	88.2	86.857	-1.343	87.582	-0.618	87.335	-0.865	87.120	-1.08
O-Ru-N	76.5	74.554	-1.946	73.365	-1.946	72.251	-4.249	75.124	-1.376
Cl-Ru-N	82.9	81.899	-1.001	82.202	-0.698	82.014	-0.886	82.959	0.059
Empirical bond dihedral (˚)		Calculated bond dihedral (˚) (methods/error)							
nomenclature	Bond dihedral (˚)	M06 /TZ	Error	M06L /TZ	Error	wB97X /TZ	Error	wB97XD /TZ	Error
N-C(16)-C(17)-O	19.7	18.687	-1.013	24.102	4.402	19.320	-0.38	18.827	-0.873
C(12)-C(9)-Ru-O	0	8.559	8.559	-0.475	-0.475	13.061	13.061	-1.880	-1.88
C(13)-C(6)-Ru-Cl	-34	-29.894	4.106	-38.897	-4.897	-25.601	8.399	-41.692	-7.692
C(13)-C(6)-Ru-N	52	53.541	1.541	45.814	-6.186	56.622	4.622	44.457	-7.543

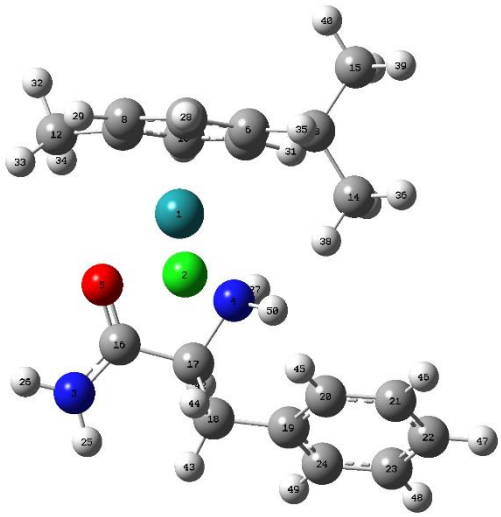

Figure 4.7. The wB97XD/TZ optimized geometry of [Ru(*R*)(η^6-p-cymene)Phenyl alanine amide]Cl$^+$

Table 4.6.principal bond lengths, angles and dihedrals of [Ru(*S*) (η6-p-cymene) Phenyl alanine amide] Cl^+complex, and related errors.

Empirical bond length (A˚)		Calculated bond length (A˚) (methods/error)							
nomenclature	Bond length (A˚)	M06 /TZ	Error	M06L /TZ	Error	wB97X /TZ	Error	wB97XD /TZ	Error
Ru-CM	1.660	1.676	0.016	1.644	-0.016	1.683	0.023	1.682	0.022
Ru-Cl	2.406	2.397	-0.009	2.417	0.011	2.404	-0.002	2.399	-0.007
Ru-N	2.140	2.199	0.059	2.210	0.07	2.178	0.038	2.168	0.028
Ru-O	2.146	2.179	0.033	2.191	0.045	2.151	0.005	2.149	0.003
Empirical bond angle (˚)		Calculated bond angle (˚) (methods/error)							
nomenclature	Bond angle (˚)	M06 /TZ	Error	M06L /TZ	Error	wB97X /TZ	Error	wB97XD /TZ	Error
Cl-Ru-CM	127.6	127.804	0.204	129.167	1.567	127.643	0.043	127.521	-0.079
N-Ru-CM	132.5	134.963	2.463	135.055	2.555	135.305	3.015	133.713	1.213
O-Ru-CM	132	130.644	-1.356	131.515	-0.485	130.178	-1.822	130.983	1.017
Cl-Ru-O	86.6	85.698	-0.902	84.685	-1.942	86.313	-0.287	85.840	-0.76
O-Ru-N	76.4	75.041	-1.359	74.827	-1.573	76.316	-0.048	76.028	-0.372
Cl-Ru-N	83.3	83.617	0.317	81.355	-1.945	82.258	-1.042	84.308	1.008
Empirical bond dihedral (˚)		Calculated bond dihedral (˚) (methods/error)							
nomenclature	Bond dihedral (˚)	M06 /TZ	Error	M06L /TZ	Error	wB97X /TZ	Error	wB97XD /TZ	Error
N-C(16)-C(17)-O	0.6	-3.874	-4.474	0.307	-0.293	-2.910	-3.51	-4.025	-4.625
C(12)-C(6)-Ru-O	2	-1.392	-3.392	-0.412	-2.412	-13.074	-15.074	-0.832	-2.832
C(13)-C(9)-Ru-Cl	38	39.103	1.103	39.612	1.612	26.404	-11.596	40.599	2.599
C(13)-C(9)-Ru-N	-48	-47.547	0.453	-44.678	3.222	-56.355	-8.355	-46.651	1.349

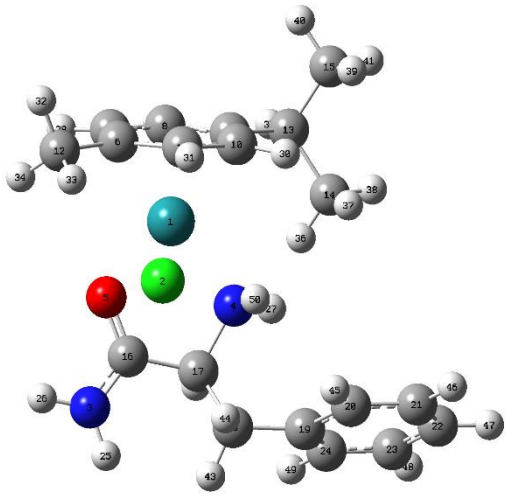

Figure 4.8. The wB97XD /TZ optimized geometry of [Ru(*S*)(η^6-p-cymene)Phenyl alanine amide]Cl^+

Table 4.7.principal bond lengths,angles and dihedrals of [Ru(η^6-indane) Phenyl alanine amide] Cl$^+$ complex, and related errors.

Empirical bond length (A˚)		Calculated bond length (A˚) (methods/error)							
nomenclature	Bond length (A˚)	M06 /TZ	Error	M06L /TZ	Error	wB97X /TZ	Error	wB97XD /TZ	Error
Ru-CM	1.65	1.677	0.027	1.645	-0.005	1.680	0.03	1.678	0.028
Ru-Cl	2.423	2.402	-0.021	2.422	-0.001	2.403	-0.02	2.401	-0.022
Ru-N	2.142	2.195	0.053	2.212	0.07	2.180	0.038	2.168	0.026
Ru-O	2.109	2.161	0.052	2.176	0.067	2.144	0.035	2.139	0.03
Empirical bond angle (˚)		Calculated bond angle (˚) (methods/error)							
nomenclature	Bond angle (˚)	M06 /TZ	Error	M06L /TZ	Error	wB97X /TZ	Error	wB97XD /TZ	Error
Cl-Ru-CM	130.0	129.257	-0.743	130.451	0.451	128.662	-1.338	128.938	-1.062
N-Ru-CM	132.8	135.220	2.42	136.072	3.272	135.247	2.447	134.075	1.275
O-Ru-CM	126.5	129.193	2.693	129.850	3.35	129.534	3.034	129.192	2.692
Cl-Ru-O	88.21	86.128	-2.082	84.678	-3.532	86.325	-1.885	86.762	-1.448
O-Ru-N	77.73	75.803	-1.927	75.423	-2.307	76.366	-1.364	76.516	-1.214
Cl-Ru-N	84.0	81.929	-2.071	79.779	-4.221	81.683	-2.317	82.764	-1.236
Empirical bond dihedral (˚)		Calculated bond dihedral (˚) (methods/error)							
nomenclature	Bond dihedral (˚)	M06 /TZ	Error	M06L /TZ	Error	wB97X /TZ	Error	wB97XD /TZ	Error
N-C(6)-C(7)-O	-20	-2.587	17.413	3.702	23.702	-0.680	19.32	-3.765	16.235
C(20)-C(23)-Ru-O	-29	-27.395	1.605	-28.569	0.431	-30.350	-1.35	-33.570	-4.57
C(19)-C(21)-Ru-N	30	35.082	5.082	34.691	4.691	33.105	3.105	29.292	-0.708

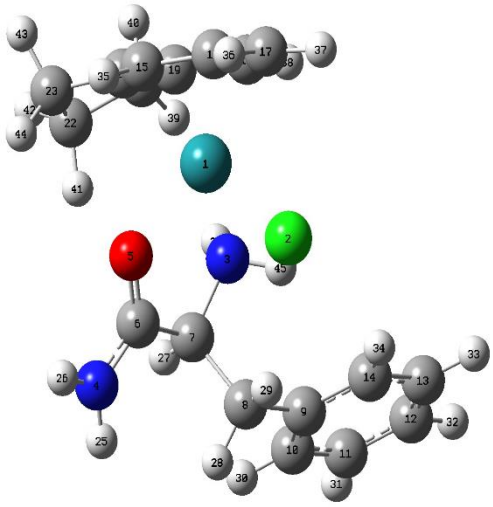

Figure 4.9. The wB97XD /TZ optimized geometry of [Ru(η^6-indane)Phenyl alanine amide]Cl$^+$

Table 4.8.principal bond lengths,angles and dihedrals of [Ru(η^6-indane) proline amide] Cl^+ complex, and related errors.

Empirical bond length (A˚)		Calculated bond length (A˚) (methods/error)							
nomenclature	Bond length (A˚)	M06 /TZ	Error	M06L /TZ	Error	wB97X /TZ	Error	wB97XD /TZ	Error
Ru-CM	1.67	1.680	0.01	1.647	-0.023	1.685	0.015	1.685	0.015
Ru-Cl	2.418	2.403	-0.015	2.420	0.002	2.404	0.014	2.403	-0.015
Ru-N	2.149	2.198	0.049	2.221	0.072	2.185	0.036	2.173	0.024
Ru-O	2.092	2.163	0.071	2.180	0.088	2.146	0.054	2.139	0.047
Empirical bond angle (˚)		Calculated bond angle (˚) (methods/error)							
nomenclature	Bond angle (˚)	M06 /TZ	Error	M06L /TZ	Error	wB97X /TZ	Error	wB97XD /TZ	Error
Cl-Ru-CM	130.0	128.044	-1.956	128.760	-1.24	127.852	-2.148	128.072	-1.928
N-Ru-CM	134.1	137.799	3.699	138.283	4.183	137.389	3.289	136.848	2.748
O-Ru-CM	128.5	129.512	1.012	129.611	1.111	129.584	1.048	129.451	0.951
Cl-Ru-O	83.61	85.236	1.626	84.118	0.508	85.385	1.775	85.562	1.952
O-Ru-N	78.67	76.053	-2.617	75.590	-3.08	76.746	-1.924	76.963	-1.707
Cl-Ru-N	82.85	80.312	-2.538	79.406	-3.444	80.325	-2.525	80.581	-2.269
Empirical bond dihedral (˚)		Calculated bond dihedral (˚) (methods/error)							
nomenclature	Bond dihedral (˚)	M06 /TZ	Error	M06L /TZ	Error	wB97X /TZ	Error	wB97XD /TZ	Error
N-C(6)-C(7)-O	0	7.815	7.815	7.377	7.377	7.983	7.983	7.099	7.099
C(17)-C(15)-Ru-O	-47	-33.203	13.797	-36.951	10.049	-37.778	9.222	-36.481	10.519
C(19)-C(14)-Ru-Cl	20	36.816	16.816	32.345	12.345	32.231	12.231	33.966	13.966

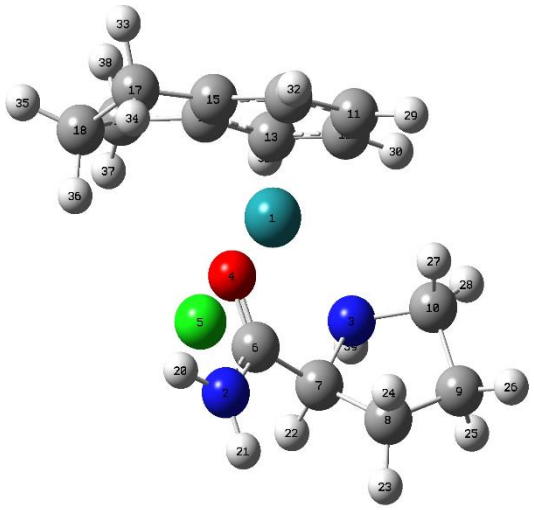

Figure 4.10. The wB97XD /TZ optimized geometry of [Ru(η^6-indane)Phenyl alanine amide]Cl^+

Table 4.9.principal bond lengths,angles and dihedrals of [Ru(*R*) (η6-p-cymene) Phenyl alanine amide] Cl^+complex, and related errors.

Empirical bond length (A˚)		Calculated bond length (A˚) (methods/error)							
nomenclature	Bond length (A˚)	PBE-D3 /TZ	Error	TPSS-D3 /TZ	Error	BP86-D3 /TZ	Error	B3LYP-D3 /TZ	Error
Ru-CM	1.64	1.668	0.028	1.671	0.031	1.676	0.036	1.709	0.069
Ru-Cl	2.394	2.395	0.001	2.397	0.003	2.397	0.003	2.405	0.011
Ru-N	2.130	2.160	0.03	2.158	0.028	2.153	0.023	2.162	0.032
Ru-O	2.095	2.173	0.078	2.155	0.06	2.168	0.073	2.161	0.066
Empirical bond angle (˚)		Calculated bond angle (˚) (methods/error)							
nomenclature	Bond angle (˚)	PBE-D3 /TZ	Error	TPSS-D3 /TZ	Error	BP86-D3 /TZ	Error	B3LYP-D3 /TZ	Error
Cl-Ru-CM	129.8	128.208	-1.592	127.973	-1.826	127.933	-1.867	127.581	-2.219
N-Ru-CM	134.4	134.304	-0.096	134.474	0.074	134.166	-0.234	134.636	0.236
O-Ru-CM	126.8	130.003	3.203	130.257	3.457	130.124	3.324	130.452	3.652
Cl-Ru-O	88.2	87.137	-1.063	86.964	-1.236	87.261	-0.939	87.298	-0.902
O-Ru-N	76.5	75.616	-0.884	75.838	-0.662	75.980	-0.52	75.598	-0.902
Cl-Ru-N	82.9	82.860	-0.004	82.647	-0.253	82.824	-0.076	82.658	-0.242
Empirical bond dihedral (˚)		Calculated bond dihedral (˚) (methods/error)							
nomenclature	Bond dihedral (˚)	PBE-D3 /TZ	Error	TPSS-D3 /TZ	Error	BP86-D3 /TZ	Error	B3LYP-D3 /TZ	Error
N-C(16)-C(17)-O	19.7	22.792	3.092	22.077	2.377	23.271	3.571	20.096	0.396
C(12)-C(9)-Ru-O	0	0.592	0.592	1.226	1.226	1.392	1.392	0.891	0.891
C(13)-C(6)-Ru-Cl	-34	-39.034	-5.034	-38.884	-4.884	-38.406	-4.406	-39.046	-5.046
C(13)-C(6)-Ru-N	52	46.488	-5.512	46.316	-5.684	46.846	-5.154	46.332	-5.668

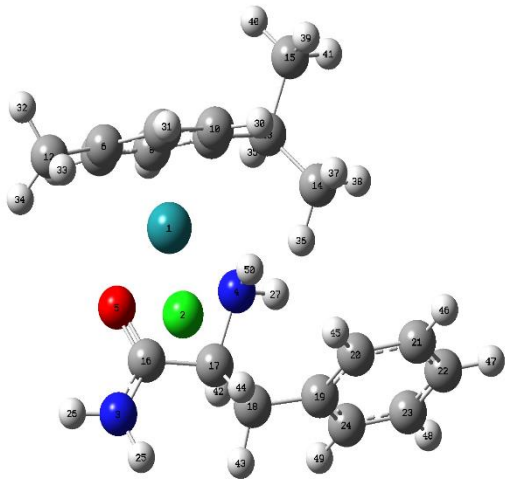

Figure 4.11. The PBE/GD3BJ/TZ optimized geometry of [Ru(*R*)(η^6-p-cymene)Phenyl alanine amide]Cl^+

Table 4.10.principal bond lengths, angles and dihedrals of [Ru(S) (η6-p-cymene) Phenyl alanine amide] Cl^{+}complex, and related errors.

Empirical bond length (A˚)		Calculated bond length (A˚) (methods/error)							
nomenclature	Bond length (A˚)	PBE-D3 /TZ	Error	TPSS-D3 /TZ	Error	BP86-D3 /TZ	Error	B3LYP-D3 /TZ	Error
Ru-CM	1.660	1.669	0.009	1.672	0.012	1.679	0.019	1.710	0.05
Ru-Cl	2.406	2.390	-0.016	2.394	-0.012	2.391	-0.015	2.405	0.015
Ru-N	2.140	2.165	0.025	2.160	0.02	2.157	0.017	2.165	0.025
Ru-O	2.146	2.158	0.012	2.137	-0.009	2.148	0.002	2.148	0.002
Empirical bond angle (˚)		Calculated bond angle (˚) (methods/error)							
nomenclature	Bond angle (˚)	PBE-D3 /TZ	Error	TPSS-D3 /TZ	Error	BP86-D3 /TZ	Error	B3LYP-D3 /TZ	Error
Cl-Ru-CM	127.6	128.163	0.563	128.403	0.803	128.169	0.569	127.332	-0.268
N-Ru-CM	132.5	133.975	1.475	134.181	1.681	133.659	1.159	134.230	1.73
O-Ru-CM	132	130.263	-1.737	130.636	-1.364	130.578	-1.422	130.573	-1.427
Cl-Ru-O	86.6	85.660	-0.94	85.012	-1.588	85.241	-1.359	86.061	-0.539
O-Ru-N	76.4	76.581	0.181	77.049	0.649	77.052	0.652	76.471	0.071
Cl-Ru-N	83.3	83.559	0.259	82.608	-0.692	83.501	0.201	83.799	0.499
Empirical bond dihedral (˚)		Calculated bond dihedral (˚) (methods/error)							
nomenclature	Bond dihedral (˚)	PBE-D3 /TZ	Error	TPSS-D3 /TZ	Error	BP86-D3 /TZ	Error	B3LYP-D3 /TZ	Error
N-C(16)-C(17)-O	0.6	-4.420	-5.02	-1.802	-2.402	-3.420	-4.02	-4.035	-4.635
C(12)-C(6)-Ru-O	2	-3.327	-5.327	-2.828	-4.828	-2.371	-4.371	-8.617	-10.617
C(13)-C(9)-Ru-Cl	38	37.326	-0.674	38.651	0.651	39.184	1.184	32.427	-5.573
C(13)-C(9)-Ru-N	-48	-48.823	-0.823	-46.708	1.292	-47.096	0.904	-53.071	-5.071

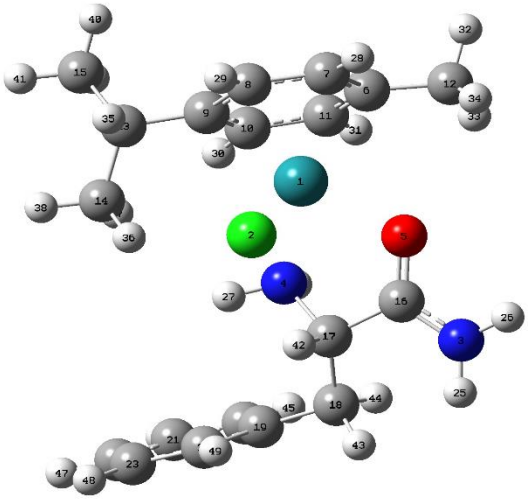

Figure 4.12. The PBE/GD3BJ/TZ optimized geometry of [Ru(*S*)(η^{6}-p-cymene)Phenyl alanine amide]Cl^{+}

Table 4.11.principal bond lengths,angles and dihedrals of [Ru(η^6-indane) Phenyl alanine amide]Cl$^+$complex, and related errors.

Empirical bond length (A˚)		Calculated bond length (A˚) (methods/error)							
nomenclature	Bond length (A˚)	PBE-D3 /TZ	Error	TPSS-D3 /TZ	Error	BP86-D3 /TZ	Error	B3LYP-D3 /TZ	Error
Ru-CM	1.65	1.670	0.02	1.671	0.021	1.676	0.026	1.711	0.061
Ru-Cl	2.423	2.395	-0.028	2.399	-0.024	2.397	-0.026	2.404	-0.019
Ru-N	2.142	2.164	0.022	2.159	0.017	2.156	0.014	2.166	0.024
Ru-O	2.109	2.140	0.031	2.125	0.016	2.135	0.026	2.135	0.026
Empirical bond angle (˚)		Calculated bond angle (˚) (methods/error)							
nomenclature	Bond angle (˚)	PBE-D3 /TZ	Error	TPSS-D3 /TZ	Error	BP86-D3 /TZ	Error	B3LYP-D3 /TZ	Error
Cl-Ru-CM	130.0	129.043	-0.957	129.193	-0.807	129.093	-0.907	128.572	-1.428
N-Ru-CM	132.8	134.089	1.289	134.383	1.583	133.750	0.95	136.770	3.97
O-Ru-CM	126.5	129.372	2.872	129.651	3.151	129.427	2.927	130.970	4.47
Cl-Ru-O	88.21	85.751	-2.459	85.238	-2.972	85.553	-2.657	84.311	-3.899
O-Ru-N	77.73	77.072	-0.658	77.468	-0.262	77.482	-0.248	75.722	-2.008
Cl-Ru-N	84.0	82.744	-1.256	81.867	-2.133	82.941	-1.059	80.089	-3.911
Empirical bond dihedral (˚)		Calculated bond dihedral (˚) (methods/error)							
nomenclature	Bond dihedral (˚)	PBE-D3 /TZ	Error	TPSS-D3 /TZ	Error	BP86-D3 /TZ	Error	B3LYP-D3 /TZ	Error
N-C(6)-C(7)-O	-20	-3.271	16.729	-1.398	18.602	-3.419	16.581	-4.272	15.728
Ru-C(20)-C(23)- O	-29	-29.943	-0.943	-30.198	-1.198	-31.418	-2.418	-29.093	-0.093
Ru-C(19)-C(21)- N	30	34.094	4.094	34.482	4.482	32.780	2.78	33.675	3.675

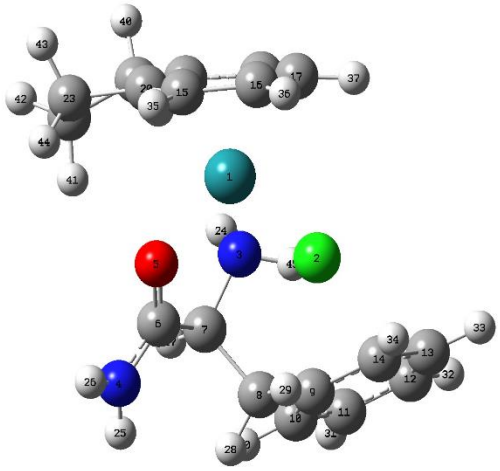

Figure 4.13. The PBE/GD3BJ/TZ optimized geometry of [Ru(η^6-indane)Phenyl alanine amide]Cl$^+$

Table 4.12.principal bond lengths,angles and dihedrals of [Ru(η^6-indane)proline amide]Cl$^+$ complex, and related errors.

Empirical bond length (A˚)		Calculated bond length (A˚) (methods/error)							
nomenclature	Bond length (A˚)	PBE-D3 /TZ	Error	TPSS-D3 /TZ	Error	BP86-D3 /TZ	Error	B3LYP-D3 /TZ	Error
Ru-CM	1.67	1.674	0.004	1.676	0.006	1.683	0.013	1.716	0.046
Ru-Cl	2.418	2.398	-0.02	2.400	-0.018	2.398	-0.02	2.407	-0.011
Ru-N	2.149	2.174	0.025	2.170	0.021	2.167	0.018	2.173	0.024
Ru-O	2.092	2.139	0.047	2.125	0.033	2.133	0.041	2.134	0.042
Empirical bond angle (˚)		Calculated bond angle (˚) (methods/error)							
nomenclature	Bond angle (˚)	PBE-D3 /TZ	Error	TPSS-D3 /TZ	Error	BP86-D3 /TZ	Error	B3LYP-D3 /TZ	Error
Cl-Ru-CM	130.0	128. 387	-1.613	128.297	-1.703	128.213	-1.787	127.796	-2.204
N-Ru-CM	134.1	137.127	3.027	137.138	3.038	137.079	2.979	137.130	3.03
O-Ru-CM	128.5	128.913	0.413	129.332	0.832	128.976	0.476	129.340	0.84
Cl-Ru-O	83.61	85.531	1.921	85.054	1.444	85.338	1.728	85.420	1.81
O-Ru-N	78.67	77.595	-1.075	77.664	-1.006	77.856	-0.814	77.385	-1.285
Cl-Ru-N	82.85	79.875	-2.975	79.791	-3.059	80.016	-2.834	80.403	-2.447
Empirical bond dihedral (˚) Calculated bond dihedral (˚) (methods/error)									
Empirical bond dihedral (˚)		Calculated bond dihedral (˚) (methods/error)							
nomenclature	Bond dihedral (˚)	PBE-D3 /TZ	Error	TPSS-D3 /TZ	Error	BP86-D3 /TZ	Error	B3LYP-D3 /TZ	Error
N-C(6)-C(7)-O	0	8.877	8.877	7.003	7.003	7.709	7.709	6.176	6.176
Ru-C(17)-C(15)- O	-47	-35.550	11.45	-36.039	10.961	-36.405	10.595	-37.011	9.989
Ru-C(19)-C(14)- Cl	20	35.065	15.065	33.793	13.793	33.578	13.578	32.590	12.590

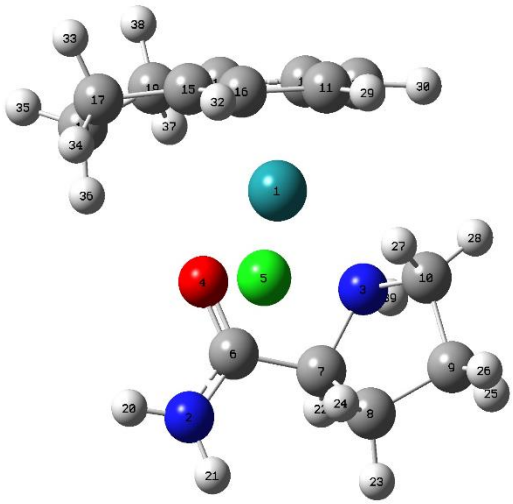

Figure 4.14. The PBE/GD3BJ/TZ optimized geometry of [Ru(η^6-indane)Phenyl alanine amide]Cl$^+$

Table 4.13.principal bond lengths,angles and dihedrals of [Ru(*R*)(η^6-p-cymene) Phenyl alanine amide] Cl$^+$ complex, and related errors.

Empirical bond length (A˚)		Calculated bond length (A˚) (methods/error)					
nomenclature	Bond length (A˚)	MP2 /TZ	Error	B2PLYP /TZ	Error	B2PLYPD /TZ	Error
Ru-CM	1.64	1.677	0.037	1.693	0.053	1.729	0.089
Ru-Cl	2.394	2.401	0.007	2.408	0.014	2.417	0.023
Ru-N	2.130	2.171	0.041	2.176	0.046	2.183	0.053
Ru-O	2.095	2.164	0.069	2.156	0.061	2.151	0.056
Empirical bond angle (˚)		Calculated bond angle (˚) (methods/error)					
nomenclature	Bond angle (˚)	MP2 /TZ	Error	B2PLYP /TZ	Error	B2PLYPD /TZ	Error
Cl-Ru-CM	129.8	128.478	-1.322	128.546	-1.254	128.030	-1.77
N-Ru-CM	134.4	135.469	1.069	135.589	1.189	135.894	1.494
O-Ru-CM	126.8	129.779	2.979	129.386	2.586	129.779	2.979
Cl-Ru-O	88.2	86.922	-1.278	86.474	-1.726	86.669	-1.531
O-Ru-N	76.5	75.851	-0.649	75.977	-0.523	75.585	-0.915
Cl-Ru-N	82.9	81.815	-1.127	81.773	-1.127	81.783	-1.117
Empirical bond dihedral (˚)		Calculated bond dihedral (˚) (methods/error)					
nomenclature	Bond dihedral (˚)	MP2 /TZ	Error	B2PLYP /TZ	Error	B2PLYPD /TZ	Error
N-C(16)-C(17)-O	19.7	20.028	0.328	18.262	-1.438	15.531	-4.497
C(12)-C(9)-Ru-O	0	9.288	9.288	18.741	18.741	17.111	17.111
C(13)-C(6)-Ru-Cl	-34	-29.120	4.88	-20.497	13.503	-21.671	12.329
C(13)-C(6)-Ru-N	52	54.066	2.066	60.633	8.633	60.015	8.015

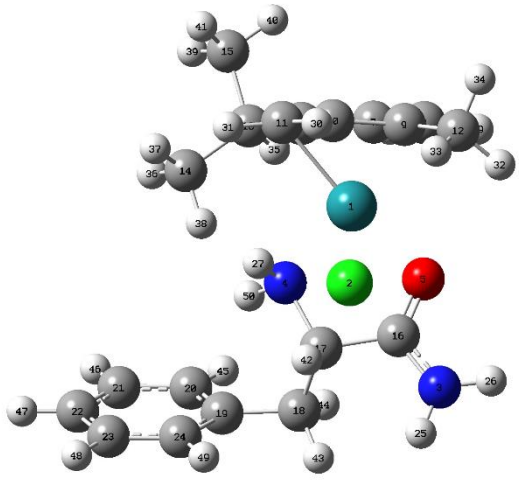

Figure 4.15. The MP2/TZ optimized geometry of [Ru(*R*)(η^6-p-cymene)Phenyl alanine amide]Cl$^+$

Table 4.14.principal bond lengths, angles and dihedrals of [Ru(S) (η6-p-cymene) Phenyl alanine amide] Cl^{+}complex, and related errors.

Empirical bond length (A˚)		Calculated bond length (A˚) (methods/error)					
nomenclature	Bond length (A˚)	MP2 /TZ	Error	B2PLYP /TZ	Error	B2PLYPD /TZ	Error
Ru-CM	1.660	1.607	-0.053	1.687	0.027	1.676	0.016
Ru-Cl	2.406	2.375	-0.031	2.407	0.001	2.399	-0.007
Ru-N	2.140	2.144	0.004	2.179	0.039	2.166	0.007
Ru-O	2.146	2.143	-0.003	2.148	0.002	2.153	0.026
Empirical bond angle (˚)		Calculated bond angle (˚) (methods/error)					
nomenclature	Bond angle (˚)	MP2 /TZ	Error	B2PLYP /TZ	Error	B2PLYPD /TZ	Error
Cl-Ru-CM	127.6	128.451	0.851	128.172	0.572	127.738	0.138
N-Ru-CM	132.5	134.297	1.797	135.363	2.863	134.173	1.673
O-Ru-CM	132	129.936	-2.064	129.852	-2.148	130.354	-1.646
Cl-Ru-O	86.6	84.938	-1.662	85.748	-0.852	85.880	-0.72
O-Ru-N	76.4	77.146	0.746	76.600	0.2	76.463	0.063
Cl-Ru-N	83.3	83.310	0.01	82.078	-1.222	83.753	0.453
Empirical bond dihedral (˚)		Calculated bond dihedral (˚) (methods/error)					
nomenclature	Bond dihedral (˚)	MP2 /TZ	Error	B2PLYP /TZ	Error	B2PLYPD /TZ	Error
N-C(16)-C(17)-O	0.6	-3.018	-3.618	-2.827	-3.427	-4.146	-4.746
C(12)-C(6)-Ru-O	2	-10.920	-12.92	-13.920	-15.920	-7.119	-9.119
C(13)-C(9)-Ru-Cl	38	31.086	-6.914	26.286	-11.714	34.125	-3.875
C(13)-C(9)-Ru-N	-48	-53.398	5.398	-56.491	8.491	-51.577	-3.577

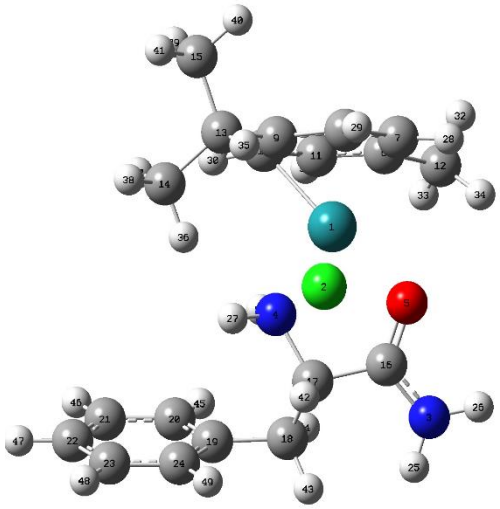

Figure 4.16. The MP2/TZ optimized geometry of [Ru(*S*)(η^{6}-p-cymene)Phenyl alanine amide]Cl^{+}

Table 4.15.principal bond lengths,angles and dihedrals of [Ru(η^6-indane) Phenyl alanine amide]Cl$^+$complex, and related errors.

Empirical bond length (A˚)		Calculated bond length (A˚) (methods/error)					
nomenclature	Bond length (A˚)	MP2 /TZ	Error	B2PLYP /TZ	Error	B2PLYPD /TZ	Error
Ru-CM	1.65	1.606	-0.044	1.686	0.036	1.676	0.026
Ru-Cl	2.423	2.377	-0.046	2.405	-0.018	2.400	-0.023
Ru-N	2.142	2.145	0.003	2.181	0.039	2.167	0.025
Ru-O	2.109	2.132	0.023	2.144	0.035	2.140	0.031

Empirical bond angle (˚)		Calculated bond angle (˚) (methods/error)					
nomenclature	Bond angle (˚)	MP2 /TZ	Error	B2PLYP /TZ	Error	B2PLYPD /TZ	Error
Cl-Ru-CM	130.0	129.421	-0.579	128.556	-1.444	128.909	-1.091
N-Ru-CM	132.8	134.206	1.406	135.301	2.501	134.235	1.435
O-Ru-CM	126.5	129.066	2.566	129.651	3.151	129.176	2.676
Cl-Ru-O	88.21	85.323	-2.887	85.706	-2.504	86.109	-2.101
O-Ru-N	77.73	77.309	-0.421	76.459	-1.271	76.808	-0.922
Cl-Ru-N	84.0	82.586	-1.414	82.063	-1.937	82.975	-1.025

Empirical bond dihedral (˚)		Calculated bond dihedral (˚) (methods/error)					
nomenclature	Bond dihedral (˚)	MP2 /TZ	Error	B2PLYP /TZ	Error	B2PLYPD /TZ	Error
N-C(6)-C(7)-O	-20	-0.683	19.317	-1.140	18.86	-3.401	16.599
C(20)-C(23)-Ru-O	-29	-28.090	0.91	-22.164	6.836	-27.877	1.123
C(19)-C(21)-Ru-N	30	36.631	6.631	41.427	11.427	35.237	5.237

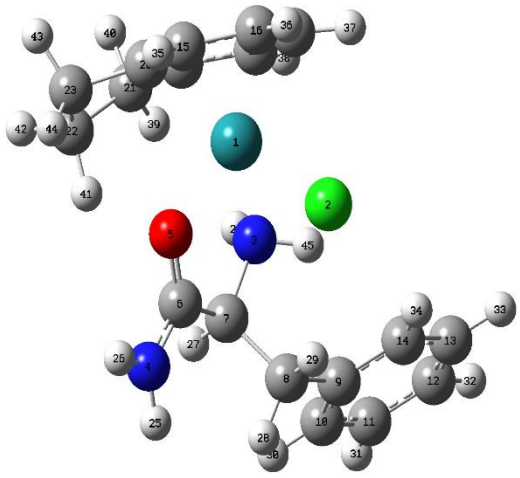

Figure 4.17. The MP2/TZ optimized geometry of [Ru(η^6-indane)Phenyl alanine amide]Cl$^+$

Table 4.16.principal bond lengths,angles and dihedrals of [Ru(η^6-indane)proline amide]Cl$^+$ complex, and related errors.

Empirical bond length (A˚)		Calculated bond length (A˚) (methods/error)					
nomenclature	Bond length (A˚)	MP2 /TZ	Error	B2PLYP /TZ	Error	B2PLYPD /TZ	Error
Ru-CM	1.67	1.610	-0.060	1.690	0.020	1.681	0.011
Ru-Cl	2.418	2.378	-0.040	2.409	-0.009	2.403	-0.015
Ru-N	2.149	2.153	0.004	2.187	0.038	2.173	0.024
Ru-O	2.092	2.130	0.038	2.143	0.051	2.138	0.046

Empirical bond angle (˚)		Calculated bond angle (˚) (methods/error)					
nomenclature	Bond angle (˚)	MP2 /TZ	Error	B2PLYP /TZ	Error	B2PLYPD /TZ	Error
Cl-Ru-CM	130.0	128.473	-1.527	128.023	-1.977	128.064	-1.936
N-Ru-CM	134.1	136.990	2.890	137.311	3.211	137.185	3.085
O-Ru-CM	128.5	129.017	0.517	129.381	0.881	129.268	0.768
Cl-Ru-O	83.61	84.732	1.122	85.433	1.823	85.156	1.546
O-Ru-N	78.67	77.543	-0.127	77.019	-1.651	77.305	-1.365
Cl-Ru-N	82.85	80.505	-2.345	80.093	-2.757	80.352	-2.498

Empirical bond dihedral (˚)		Calculated bond dihedral (˚) (methods/error)					
nomenclature	Bond dihedral (˚)	MP2 /TZ	Error	B2PLYP /TZ	Error	B2PLYPD /TZ	Error
N-C(6)-C(7)-O	0	5.331	5.331	6.771	6.771	5.643	5.643
C(17)-C(15)-Ru-O	-47	-34.254	12.746	-36.147	10.853	-35.943	11.057
C(19)-C(14)-Ru-Cl	20	36.145	16.145	34.589	14.589	33.968	13.968

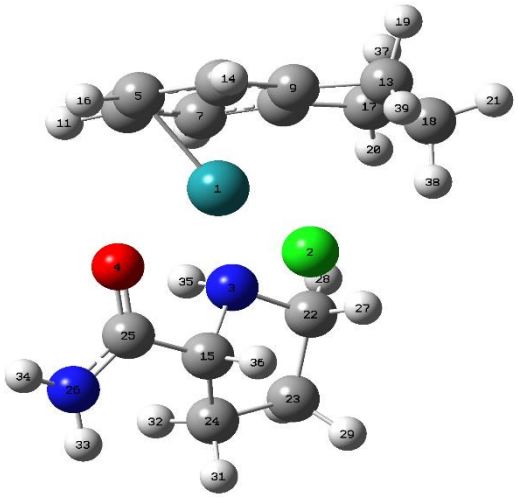

Figure 4.18. The MP2/TZ optimized geometry of [Ru(η^6-indane)Phenyl alanine amide]Cl$^+$

Figures (4.19– 4.21) present the error values of bond lengths, bond angles and dihedral angles for the considered functionals. The errors have been represented as the mean signed error (MSE) Eq. (4.1) and the mean unsigned error (MUE) Eq. (4.2).

$$MSE=\frac{\sum (yDFT-yexp)}{n} \qquad 4.1$$

$$MUE=\left|\frac{\sum (yDFT-yexp)}{n}\right| \qquad 4.2$$

yDFT are the DFT calculated values, yexp are obtained from structures reported in Ref [14]. and n is the number of values.

4.3.1.1. Bond distances

We examine the performance of the various DFT methods in reproducing the coordination center geometry. The results of this analysis are presented in Figure. 4.19. The most striking about these results is the extent to which B3LYP stands out as inferior to the rest of the functionals, with a clear tendency to overestimation of the metal–ligand distances (MSE and MUE equal to 0.041 Å and 0.043 Å, respectively, in Figure.4.19). On average M06L, M06, and B3LYP-GD3BJ overestimate also the bond distances (MSE and MUE equal to 0.034, 0.032, 0.029 Å and 0.039, 0.038, 0.033 Å, respectively, in Figure. 4.19). The other functionals perform rather similarly, the highest accuracy, as judged from the MSE/MUE, being obtained for PBE (MSE/MUE = 0.023 Å/0.028 Å), TPSS (MSE/MUE = 0.021 Å/0.026 Å) and BP86 (MSE/MUE = 0.025 Å/0.02 Å), closely followed by the dispersion-including wB97XD and wB97X. Finally, addition of the D3 version of Grimme's dispersion improves significantly the accuracy of PBE, BP86 and TPSS, decreasing the MSE/MUE by 0.007/0.004 Å (PBE-GD3BJ), 0.008/0.005 Å (TPSS-GD3BJ) and 0.009/0.006 Å (BP86-GD3BJ) (Figure.4.19).

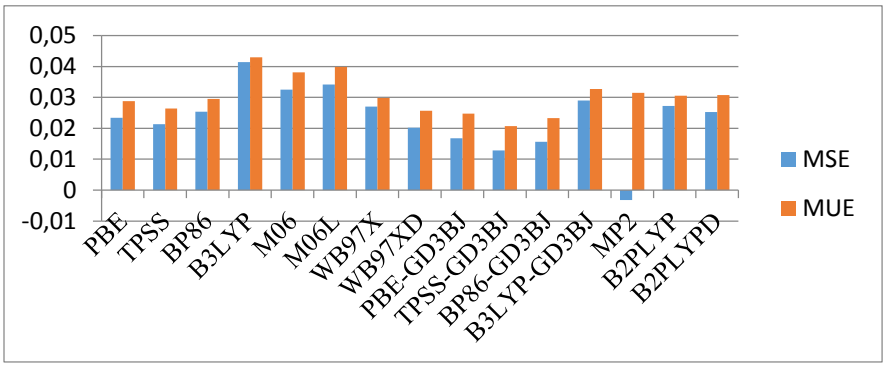

Figure. 4.19. Mean unsigned error (MUE) and mean signed error (MSE) for the bonded distances involving ruthenium of the DFT-optimized catalyst precursors relative to the corresponding X-ray structures.

4.3.1.2. Bond angles

Bond angles of the 4 diastereomeric half-sandwich Ru (II) cationic complexes containing amino amide ligands were investigated using the previous different functionals. Proposed angles were ∠Cl-Ru–O,∠ N-Ru–O, ∠N-Ru–Cl, ∠CM-Ru–Cl, ∠CM-Ru–O, and∠CM-Ru–N (Figure. 4.20). The bond angles show small dependency on the choice of the functional with a clear tendancy of overestimation, except M06 that, in opposite, shows an underestimation of the bond angles (MSE equal to -1.17°) in (Figure. 4.20). A very small discrepancy between all the functionals is observed. Results obtained for B2PLYPD and TPSS-GD3BJ are very similar and the results for MP2, WB97X, PBE-GD3BJ and BP86-GD3BJ are exactly equivalent.

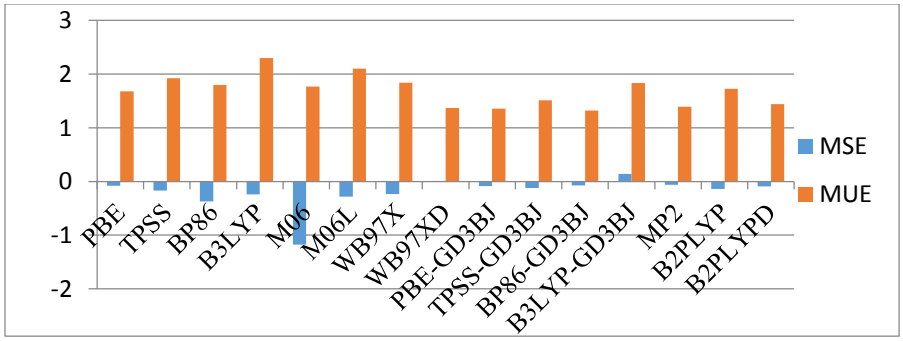

Figure. 4.20. Mean unsigned error (MUE) and mean signed error (MSE) for the bond angles involving ruthenium of the DFT-optimized catalyst precursors relative to the corresponding X-ray structures

4.3.1.3. Dihedral angles

For dihedral angles there is a very small discrepancy between all the functionals constructed to account dispersion and the density functionals with addition of the D3 version of Grimme's

dispersion. With the functionals not including dispersion, the highest accuracy, only a little worse that with the previous functionals, is obtained for PBE (MSE/MUE = 3.47°/9.33°) and TPSS (MSE/MUE =3.87°/8.46°), BP86 and B3LYP show the lowest accuracy in predicting the dihedral angles.

In summary, from a geometrical point of view, the best functionals seem to be the ones using the D3 Grimme's dispersion (PBE-GD3BJ, TPSS- GD3BJ, and BP86- GD3BJ).(Figure.4.21)

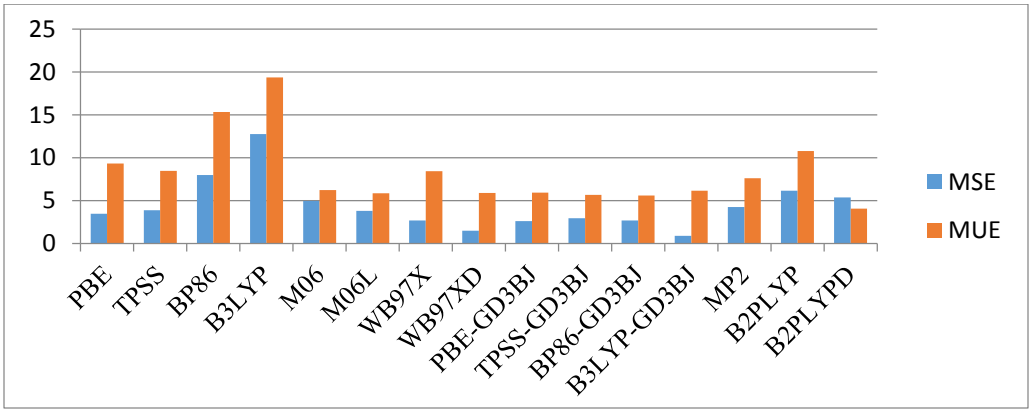

Figure.4.21. Mean unsigned error (MUE) and mean signed error (MSE) for the dihedral angles involving ruthenium of the DFT-optimized catalyst precursors relative to the corresponding X-ray structures

4.3.2. Energetics

4.3.2.1. Diastereoisomer energy difference

The energy difference of the two diastereomeric half-sandwich Ru (II) cationic complexes 1a ($Ru_{(S)}$) and 1b ($Ru_{(R)}$) containing the phenyl alanine amide ligand has been calculated using the fifteen density functionals and the basis set mentioned above.

The results are shown in Figure.4.22. PBE, B3LYP, TPSS, BP86 and B2PLYP lead to a small energy difference, the three latter not giving the same preferred isomer as all the other functionals. Besides, there is no significant difference between WB97XD, MP2 and B2PLYP on one hand and PBE-GD3BJ and TPSS-GD3BJ on the other hand, standard DFT (not including dispersion) is inferior to other methods accounting for dispersion in the predictions of energies.

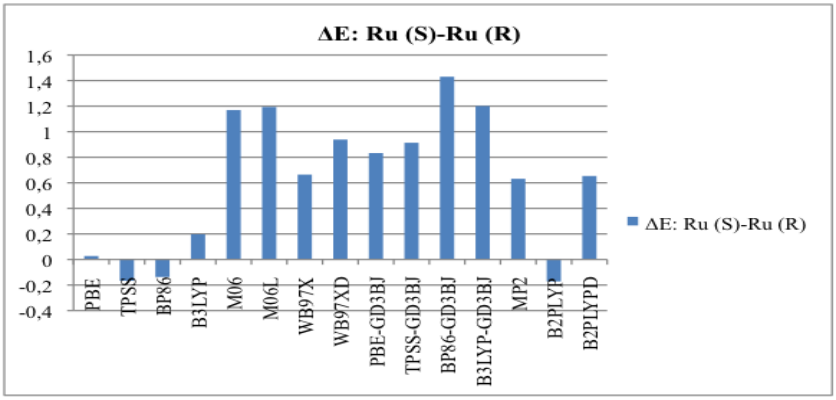

Figure.4.22. Difference of the energies in (kcal/mol) of the two diastereomeric half-sandwich Ru (II) cationic complexes 1a (Ru(S)) and 1b (Ru(R)) containing the phenyl alanine amide ligand

4.3.2.2. Activation energies

We have then tested the ability of the various functionals in predicting the enantioselectivity of a given ATH reaction. We have chosen the asymmetric transfer hydrogenation of acetophenone catalyzed by the Ru(p-cymene)(proline-amide) hydride complex. Experimentally, this reaction yields phenyl-ethanol with a conversion of 59% and an enantiomeric excess of 74%, as shown in Figure 4.23.

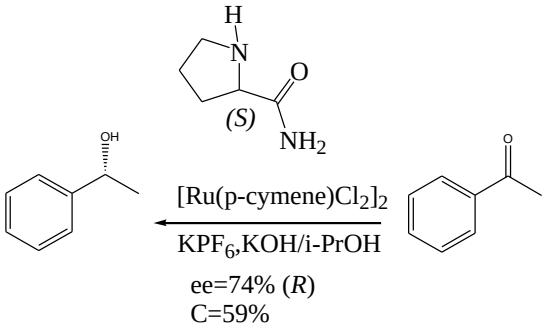

Figure. 4.23. Ru-catalyzed ATH of ketones with $[Ru(p\text{-cymene})Cl_2]_2$ and (L) proline amide

Firstly, two different mechanistic pathways were evaluated with the hybrid PBE0 functional: a concerted mechanism and a two-step mechanism through a ruthenium alkoxide intermediate . The optimized structures of the reactant, reaction intermediates, and transition states are collected in Figure 4.24.

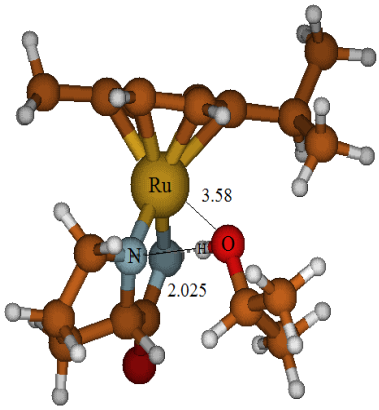

1c (-7.8) (-5)

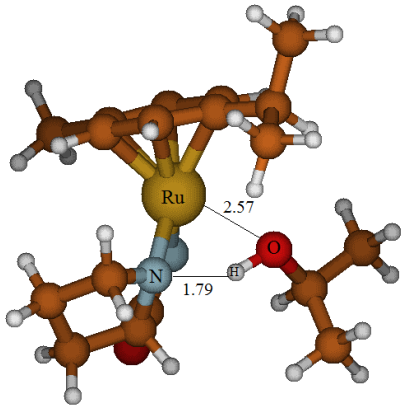

2c(TS) (-3.1) (1)

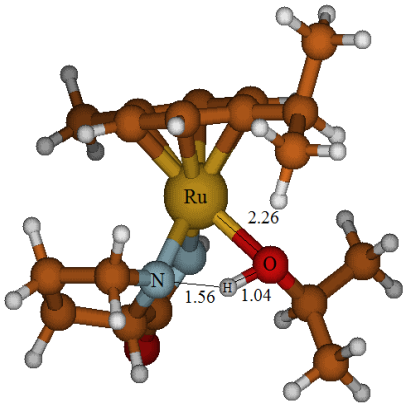

3c (-3.6) (0.01)

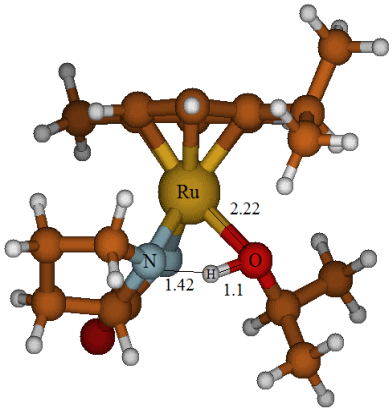

4c(TS) (-3.62) (0.3)

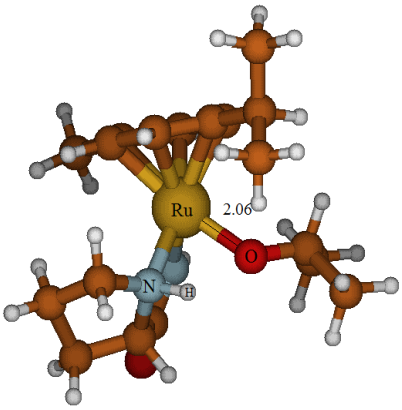

5c (-10.38) (-8)

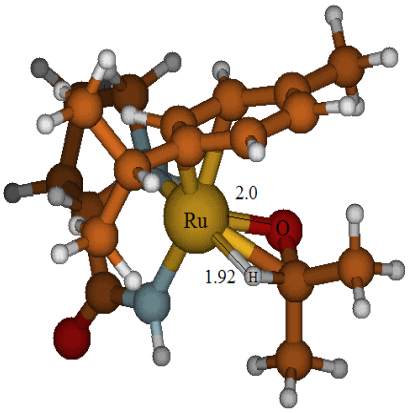

6c (28) (30)

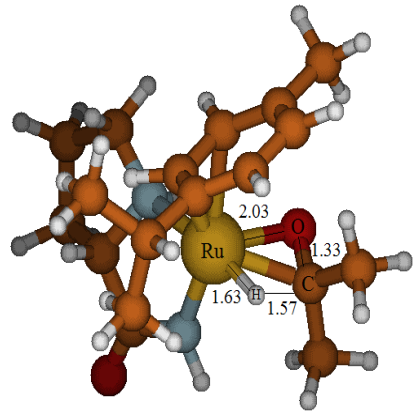

7c(TS) (31) (33)

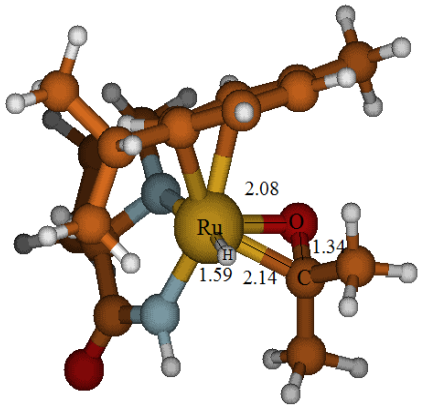

8c (26) (29)

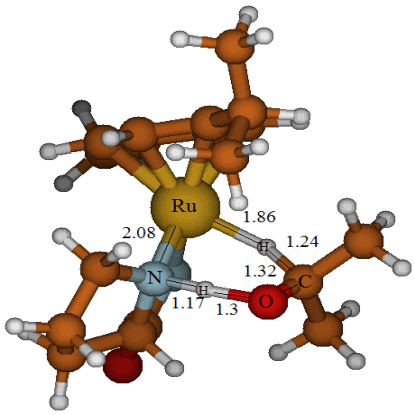

TS3S (6.8) (7)

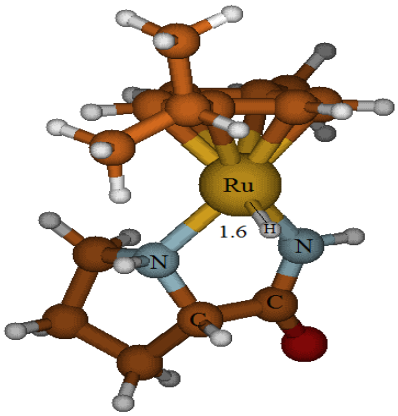

18e(S) (-0.34) (2.4)

Figure 4.24. The optimized structures of the reactants, reaction intermediates, and transition states for the two proposed mechanism energies in gas phase are in Kcal/mol^{-1} and relative to the separate reactants (16e+2-propanol). energies in gas phase in red, energies in 2-propanol in dark.

The energy profiles of the two mechanisms are depicted in Figure 4.25 .The two-step mechanism shows an energy barrier that is much higher than the concerted mechanism. Hence for the comparison of the functionals we have considered only the concerted mechanism.

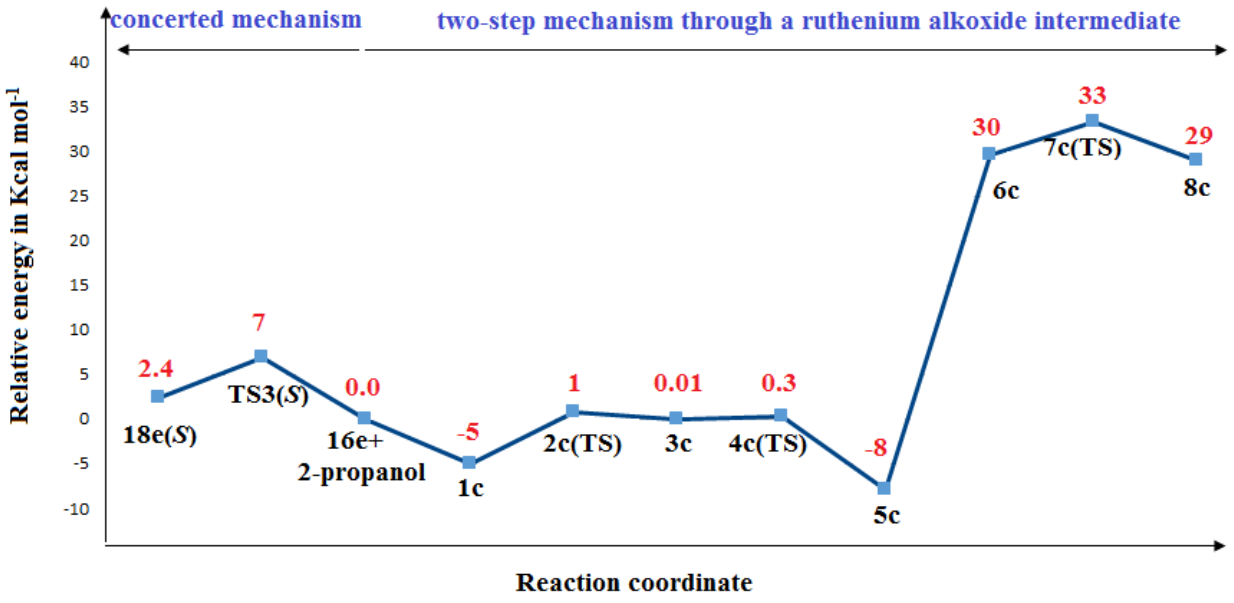

Figure 4.25. Overall energy profiles for The two-step mechanism and concerted mechanism in asymmetric hydrogenation reaction of acetophenone with *S* diastereoisomer of {(η6-arene)Ru[(κ²N,N) proline amide]Cl⁺}PF_6. Energies are in Kcal mol^{-1} and relative to the separate active catalyst (16e) and (+2-propanol)).

Hence, for the comparison of the functionals we have considered only the concerted mechanism.

The enantiomeric excess (ee) is given by

$$ee = \frac{k\text{favored} - kdisfavored}{kfavored + kdisfavored} \quad 4.3$$

Where $k_{favored}$ and $k_{disfavored}$ are the rate constants leading to the transition states for the favored and disfavored enantiomer, respectively. The rate constants k is then given by

$$k = A(T)e^{-\Delta G^{+}_{+}/RT} \quad 4.4$$

Where A (T) is the pre-exponential factor, assumed to be identical for both enantiomeric pathways, $\Delta G^{++}$is the Gibbs free energy of activation, R is the gas constant, and T is the temperature.
From eqs 4.3 and 4.4 we have

$$ee = \frac{e^{-\delta\Delta G^{+}_{+}/RT} - 1}{e^{-\delta\Delta G^{+}_{+}/RT} + 1} \quad 4.5$$

Where δΔG is given by :

$$\delta\Delta G^{+}_{+} = \Delta G^{+}_{+}{}_{favored} - \Delta G^{+}_{+}{}_{disfavored} \quad 4.6$$

As the starting materials leading to the two different enantiomers are identical, and therefore also have identical free energy, we can write the difference in Gibbs free activation energy, δΔG, just as the difference in transition state free energies, ΔG^{TS}.

$$\delta\Delta G^{+}_{+} = \Delta G^{TS} = G^{TS}_{favored} - G^{TS}_{disfavored} \quad 4.7$$

Combining eqs 4.5 and 4.7 gives

$$\Delta G^{TS} = RTln\left(\frac{1+ee}{1-ee}\right) \quad 4.8$$

In this reaction, experimental enantioselectivity equal 74 %,the stereo determining step is TS2

ΔG^{TS} experimental =1.987*303*ln (1+74/1-74) =1.14 kcal

Finally, the test set included 9 functionals PBE, TPSS, BP86, B3LYP, M06, PBE-GD3BJ, TPSS-GD3BJ, BP86-GD3BJ, and B3LYP-GD3BJ and three solvent models PCM [37], CPCM [38] and SMD [39]. The calculated free energy barriers for the stereo-determining step TS2 are collected in Figure. 4.26 The best overall performance is observed for (PBE-GD3BJ)/PCM.

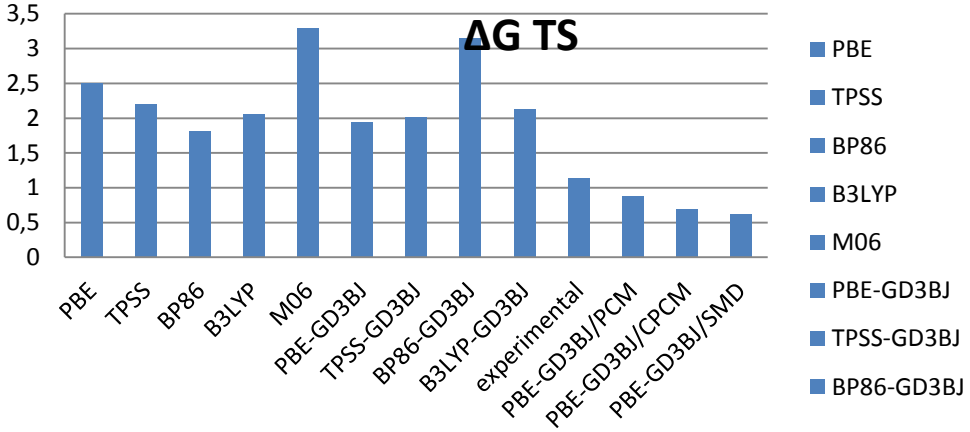

Figure. 4.26 free energy barriers for the stereo-determining step TS2 in Kcal/mol^{-1}

4.4. Conclusion

We have tested the performance of four popular density functional not including dispersion, PBE , BP86, B3LYP TPSS and four have been constructed to account for dispersion (wB97X, wB97XD, M06, and M06L) and foor functionals includes dispersion by addition of the D3 version of Grimme's dispersion with Beck-Johnson Damping functions [PBE-GD3BJ, TPSS-GD3BJ, BP86-GD3BJ, B3LYP-GD3BJ]. The second-order Moller-Plesset [MP2] method and the double hybrid functionals [B2PLYP, B2PLYPD] were also used in predicting the geometries of ruthenium(II) complexes. It is revealed that [PBE-GD3BJ, TPSS-GD3BJ, BP86-GD3BJ perform much better than the rest of functional.PBE-GD3BJ) functional gives good results both for the geometry and the energetics and is not too costly in terms of computation time. For the solvent system, we chosen PCM.

4.5. References

[1] I Ojima. Catalytic asymmetric synthesis, 3rd Edition, Wiley-VCH, Weinheim, **2010**.

[2] HU Blaser; C Malan; B Pugin; F Spindler; H Steiner; M Studer. *Adv. Synth. Catal*., **2003**, 345(1-2), 103-151.

[3] D Wangming; W Qingfu; Y. Zhengkun. *Chinese J .Cat.,* **2013**, 34(7), 1373-1377.

[4] YQ Xu; SL Yu; YY Li; ZR Dong; JX Gao. *Chinese Chem. Lett.,* **2013**, 24(6), 527-530.

[5] SA French; DDi Tommaso; A Zanotti-Gerosa; F Hancock; CRA Catlow. *Chem. Commun*., **2007**, 1(23), 2381–2383.

[6] DDi Tommaso; SA French; A Zanotti-Gerosa; F Hancock; EJ Palin; CRA Catlow. *Inorg. Chem*., **2008**, 47(7), 2674–2687.

[7] P Šot; M Kuzma; J Václavík; J Pecháček; J Přech; J Januščák; P Kačer. *Organometallics.,* **2012**, 31 (17), 6496–6499.

[8] *KH Hopmann. Int. J. Quantum Chem., **2015**, 115(18),* 1232–1249.

[9] A Dedieu.*Chem. Rev.*, **2000**, 100 (2), 543–600.

[10] D Balcells; E Clot; O Eisenstein. *Chem. Rev.*, **2010**, 110 (2), 749–823.

[11] M García-Melchor; AAC Braga; A Lledós; G Ujaque; F Maseras. *Acc. Chem. Res.*, **2013**, 46 (11), 2626–2634.

[12] CJ Cramer; DG Truhlar. *Phys Chem Chem Phys.*, **2009**, 11(46), 10757-10816.

[13] DDi Tommaso; SA French; CRA Catlow. *Journal of Molecular Structure: THEOCHEM*., **2007**, 812(1–3), 39-49.

[14] A Bacchi; M Balordi; P Pelagatti; C Pelizzi. *Journal of Organometallic Chemistry*., **2009,** 694 (19), 3281–3286.

[15] MJ Frisch; GW Trucks; HB Schlegel; GE Scuseria; MA Robb; JR Cheeseman; G Scalmani; V Barone; B Mennucci, GA Petersson; H Nakatsuji; M Caricato; X Li; HP Hratchian; AF

Izmaylov; J Bloino; G Zheng; JL Sonnenberg; M Hada; M Ehara; K Toyota ; R Fukuda; J Hasegawa; M Ishida; T Nakajima; Y Honda; O Kitao; H Nakai;T Vreven; JA JR Montgomery; JE Peralta; F Ogliaro; M Bearpark; JJ Heyd; E Brothers; KN Kudin; VN Staroverov; R Kobayashi; J Normand; K Raghavachari; A Rendell; JC Burant; SS Iyengar; J Tomasi; M Cossi; N Rega N; JM Millam; M Klene; JE Knox; JB Cross; V Bakken; C Adamo; J Jaramillo; R Gomperts; RE Stratmann; O Yazyev; AJ Austin; R Cammi; C Pomelli; JW Ochterski; RL Martin; K Morokuma; VG Zakrzewski; GA Voth; P Salvador; JJ Dannenberg; S Dapprich; AD Daniels; Ö Farkas; JB Foresman; JV Ortiz; J Cioslowski; FoxDJ **(2009)** *Gaussian 09 Revision D.01*. *Gaussian Inc., Wallingford.*

[16] JP Perdew; K Burke; M Ernzerhof. *Phys Rev Lett*., **1996**, 77(18-28),3865.

[17] AD Becke. *Phys Rev A*., **1988**, 38(6), 3098.

[18] JP Perdew. *Phys Rev* B., **1986**, 33(12), 8822.

[19] PJ Stephens; FJ Devlin; CF Chabalowski; MJ Frisch. *J Phys Chem*.,**1994**, 98(45),11623.

[20] C Lee; W Yang; RG Parr.*Phys. Rev. B*., **1988,** 37(2), 785.

[21] J Tao; JP Perdew; VN Staroverov; GE Scuseria; **2003**, *Phys Rev Lett* 91(14), 146401.

[22] JD Chai; M Head-Gordon. *J. Chem. Phys.*, **2008**, 128(8), 084106.

[23] JD Chai; M Head-Gordon. *Phys. Chem. Chem. Phys.*, **2008,** 10(44)**,** 6615-6620.

[24] Y Zhao; DG Truhlar. *J Chem Phys.*, **2006**, 125(19):194101.

[25] Y Zhao; DG Truhlar. *Acc Chem Res*., **2008**, 41(2), 157.

[26] Y Zhao; DG Truhlar. *Theor Chem Acc*., **2008**, 120(1), 215-241.

[27] S Grimme; S Ehrlich; L Goerigk. *J. Comp. Chem*., **2011**, 32(7), 1456-1465.

[28] C Møller; MS Plesset. *Phys Rev*., **1934**, 46(7), 618.

[29] S Grimme. *J Chem Phys*., **2006**, 124(3), 034108.

[30] S. Grimme, *J. Comp. Chem.*, **2006**, 27(15), 1787-1799.

[31] PC Hariharan; JA Pople. *Mol. Phys*., **1974**, 27(1), 209–214.

[32] VA Rassolov; MA Ratner; JA Pople; PC Redfern; LA Curtiss. *J. Comput. Chem.*, **2001**, 22(9), 976–984.

[33] PJ Hay; W. R Wadt. *J. Chem. Phys*., **1985**, 82(1), 270.

[34] P Pelagatti; M Carcelli; F Calbiani; C Cassi; L Elviri; C Pelizzi; U Rizzotti; D Rogolino ; Organometallics., **2005**, 24(24), 5836-5844.

[35] M Yamakawa; H Ito; R Noyori. *J. Am. Chem. Soc.*, **2000**, 122 (7), 1466-1478.

[36] R Noyori; M Yamakawa; S Hashiguchi. *J. Org. Chem.*, **2001**, 66(24), 7931-7944.

[37] G Scalmani; M. J. Frisch. *J. Chem. Phys.*, **2010**, 132(11), 114110.

[38] V Barone; M. Cossi. *J. Phys. Chem. A.*, **1998**, 102(11), 1995-2001.

[39] AV Marenich; CJ Cramer;DG Truhlar. *J. Phys. Chem. B.*, **2009**, 113 (18)6378-6396.

Chapter 5: Application II

Theoretical Study of the enantioselective reduction of prochiral ketones promoted by amino amide ruthenium Complexes

5.1. Introduction

The asymmetric hydrogenation of ketones by hydrogen transfer (ATH) is one of the largest applications of catalysis in synthetic and pharmaceutical industry [1] .Much effort has been devoted to design asymmetric transition-metal catalysts, able to yield high stereoselectivities [2] , For example, Noyori's ruthenium complexes containing arene and N-(p-toluenesulfonyl)-1,2-diphenylethylenediamine (TsDPEN) ligands are efficient catalysts for the asymmetric hydrogenation of ketones by H transfer [3]. Established catalytic systems for asymmetric hydrogenation are typically based on expensive chiral ligands such as diamines or amino alcohols. The replacement of these ligands with cheaper amino acids and their derivatives is an ongoing quest in academia and industry. T. Ohta et al. have reported the hydrogenation of ketones by H transfer catalyzed by Ru (II) coordinated with various aminoacids,The best enantiomeric excess was obtained using proline and the selectivity was explained by the high geometric constraint imposed onto the Ru–N–C– C(O)–N chelation ring [4]. In 2001, the group of Faller reported an in situ generated (p-Cymene) Ru(L-prolineamide)Cl_2 catalyst that gave excellent yields, 70-90% but with moderate enantiocontrol, 68-93%, in the hydrogenation of a variety of ketones at -24 C° [5]. These investigations have also shown that the enantiomeric purity of the product can be affected by electronic as well as steric effects of the substituents on the ketone substrate. However, the precatalyst formed from prolineamide and (p-Cymene$RuCl_2)_2$ appears to be a single diastereoisomer. At the same time, Chung described the first water-soluble ruthenium (II) catalyst coordinated by amides derived from (S)-proline that was active in reduction of aromatic ketones in an aqueous solution, with enantiomeric excesses up to 95.3 % [6]. Moreover, several groups reported the ATH reaction catalyzed by amide ligands, for which excellent enantioselectivities (95.5%) were reached with in situ formed Ru-precatalysts [7]. Recently, Çetinkaya et al. compared the proline amine ligands with amide analogues and also investigated the steric effect of aryl ring in the enantioselectivity. They found that the bulkiness of the aryl substituents on the ligand increased the enantioselectivity [8]. In 2009, A. Bacchi et al. reported that the phenylalanine amide (ligand 1), and the Proline amide (ligand 2) generate pre-catalysts with Ru (p-cymene) Cl_2 for the transfer hydrogenation of acetophenone in basic isopropanol [9] (see Figure 5.1). They evidenced a strong impact of the choice of the ligand on the conversation and the enantiomeric excess, the less active catalyst being the more selective one (ligand 1). In this article, we aim at rationalizing the impact of the ligand on the activity and the enantiomeric excess based on a Density Functional Theory (DFT) based study of the reaction mechanism [10].

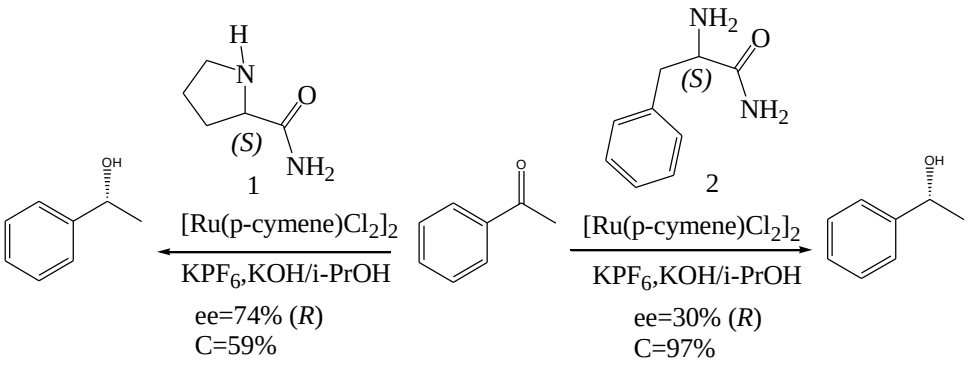

Figure 5.1. Ru-catalyzed ATH of ketones with [Ru (p-cymene)Cl_2]$_2$ and (L) proline amide or (L) phenyl alanine. ee is the enantiomeric excess and C the conversion obtained .

In previous works, we have shown that DFT calculations are a very useful tool for explaining mechanisms. Our results showed that important insights can be obtained with such a theoretical approach, particularly the origin of the reaction asymmetry. This can help experimentalists to design new catalysts that will ensure good enantioselectivity [11]. Several DFT studies have been already reported in the literature related to the hydrogenation of ketone and enamine catalyzed by homogeneous catalysts and demonstrated the potential impact of this approach [12]. R. Abbel et al. studied theoretically the hydrogenation of acetophenone by several $Ru(H)_2(PPh_3)_2$(diamine) complexes [13]. They showed that the relative position of the hydrides and of the phosphines is important, the trans hydrides-cis phosphines giving the highest selectivity. The very active and selective Noyori-type catalysts for the asymmetric hydrogenation of ketones contain a chelating, enantiopure diphosphine ligand and thus, necessarily have phosphorus donors that are mutually cis. Recently, F. Himo et al. employed DFT calculations to rationalize the enantioselectivity observed experimentally in ATH of aryl alkyl ketones with [RhCp*Cl_2] and hydroxamic acid-functionalized L-valine or hydroxamic acid-functionalized derived from the amino acid L-phenylalanine.

The plausible mechanism for the transfer hydrogenation of ketones promoted by amino amide based Ru catalysts was studied experimentally by the group of P. Pelagatti [14]. The high-resolution MS (ESI) experiments of precatalytic solutions, indicates that the catalytic process is governed by a bifunctional mechanism, analogous to that proposed by Noyori [15] and al and shown in Figure 5.2. The deprotonation of the pre-catalyst by two equivalent of a strong base such as KOH leads to a 16-electron intermediate where the amino-amido ligand is

deprotonated both on the amino and the amido function. Then, a ruthenium hydride (Ru-H) is formed together with the reprotonation of the amine (N-H), via TSa the reaction of this 16-electrons intermediate with the hydrogen donor (isopropanol). The key step is the simultaneous transfer of the hydritic H (Ru–H) and the protic H (N–H) to the C=O functional group via a six-membered transition state TSb (Figure 5.2). Last, the active 16-electrons intermediate is regenerated with the liberation of the chiral alcohol, closing the catalytic cycle.

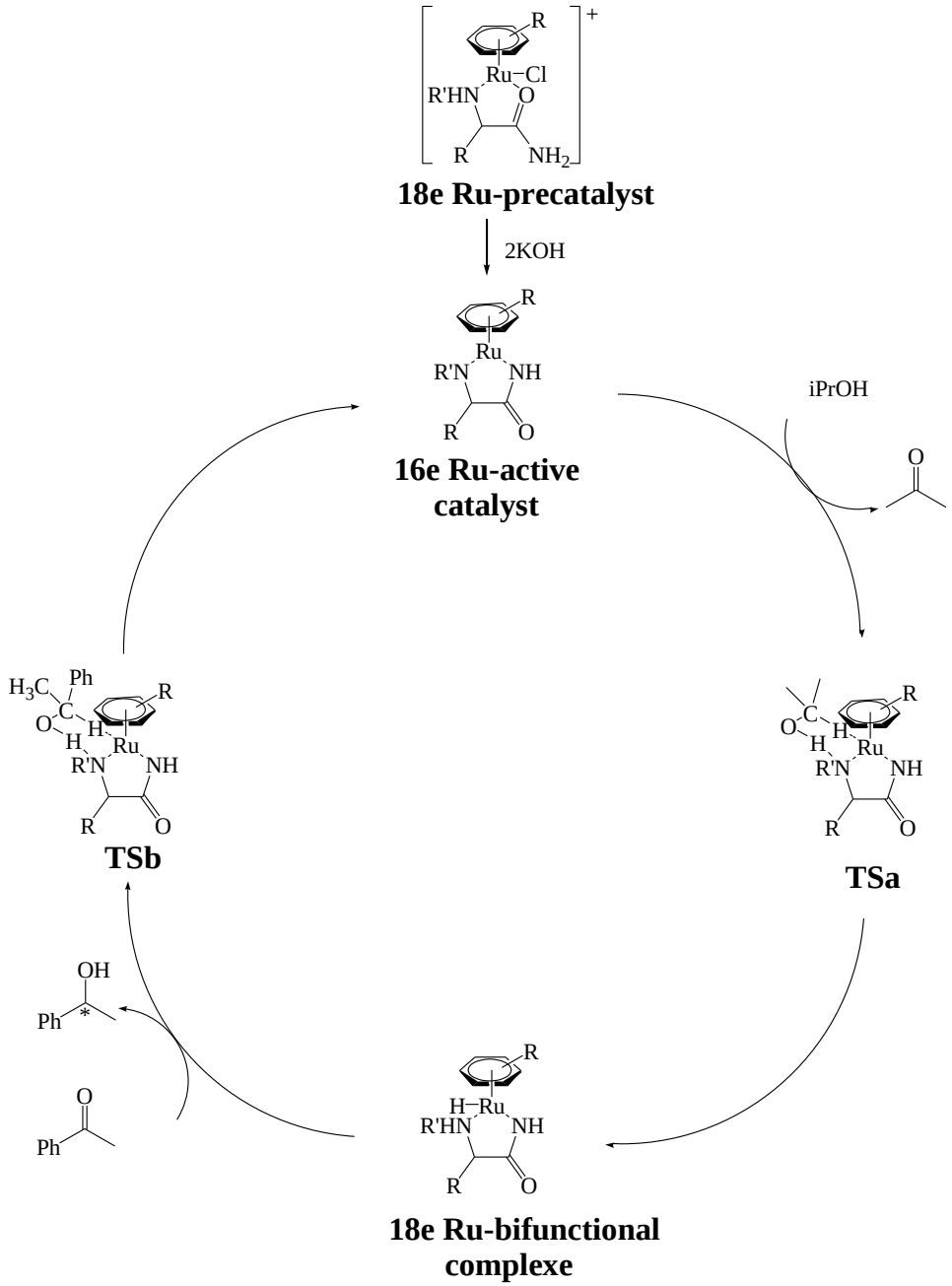

Figure 5.2. Plausible mechanism for transfer hydrogenation of acetophenone catalyzed by Ru (II) complexes containing amino amide ligands.

We based our approach on this plausible mechanism and compared the reaction profiles of the full cycle for both catalysts (ligand 1 and ligand 2 in Figure 5.1) by the means of DFT calculations.In particular, we aim at explaining the low selectivity in favor of the *R* isomer (ee=30%) obtained with ligand 2 (Phenylalanine amide) and the high conversion C=97% while the selectivity is higher (ee=74%) with ligand 1 (proline amide) affording also the *R* isomer but the conversion is low C =59% (Figure 5.2).

5.2. Computational Methods

All the calculations presented herein were carried out by means of density functional theory (DFT). After an extensive study of several functionals (see chapter 4), the PBE functional [16] was chosen, with addition of the D3 version of Grimme's dispersion with Beck-Johnson damping functions [17] . For the geometry optimization, the 6-31G (d,p) basis set was used for the C, N, O, and H elements [18] and the LANL2DZ [19] pseudopotential and basis set for ruthenium .The solvation energies were calculated as single-point corrections on the optimized structures using the polarizable continuum model method [20] , with dielectric constant e=19.264 for 2-propanol. We confirmed that all reactants and intermediates have no imaginary frequencies, and that each transition structure has one, and only one, imaginary frequency. Intrinsic reaction coordinate (IRC) calculations, at the same level of theory, were performed to ensure that the transition structures led to the expected reactants and products. All free energies were calculated at 298.15K and include the solvation free energies. All the calculations were performed by using the Gaussian 09 D01 program package [21].

5.3. Results and Discussion

The mechanistic discussion is divided into three sections following the three major steps of the reaction mechanism represented in Figure 2.To start with, we focus on the formation of the active catalysts Then, we discuss the results concerning the formation of the bifunctional ruthenium complex. Finally,we presents the results for the ATH and provides an explanation for the enantioselectivity observed in the catalytic system.

In this study, no simplification was made in any of the reactant molecules selected for the computational study. ATH of acetophenone was chosen for the theoretical calculations, employing [{$RuCl_2$ (para-cymene)}$_2$], proline amide or phenyl alanine amide as the ligand, and isopropyl alcohol (IPA) as the solvent and hydrogen source.

A. Bacchi et al. isolated the crystal structure of{ Ru[(η6-p-cymene)phenyl alanine amide]Cl}$^{+}$. This complex presents two independent diastereoisomeric cations with opposite absolute configuration on the metal. On the other hand, the {Ru[(η6- p-cymene) proline amide]Cl}$^{+}$ .is isolated as a pure Ru (*S*)- C(*S*) enantiomer in the solid state.In this study we undertaken the calculations with the Ru(*S*)-C(*S*) isomer of {Ru[(η6- arene) proline amide]Cl}$^{+}$ and the two diastereoisomeric cations Ru(*S*)-C(*S*) and Ru(*R*)-C(*S*) of {(η6-arene)Ru[(Ϗ^{2}N,N) phenyl alanine amide]Cl}$^{+}$.

5.3.1. Formation of the active catalyst

By treatment of the precatalyst {(η6-arene)Ru[(Ϗ^{2}O,N)LH$_2$]Cl}$^{+}$ with excess of KOH, the deprotonation of the amide function leads to the formation of the active catalyst {(η6-arene)Ru[(Ϗ^{2}N,N)L]}. The optimized structures of the precatalyst and the resulting active catalyst (16e) for the three complexes are collected in Figure 5.3. In order to have a more complete picture about the geometrie in M1 and M4 of (16e phenylalanine) see figure 5.4.

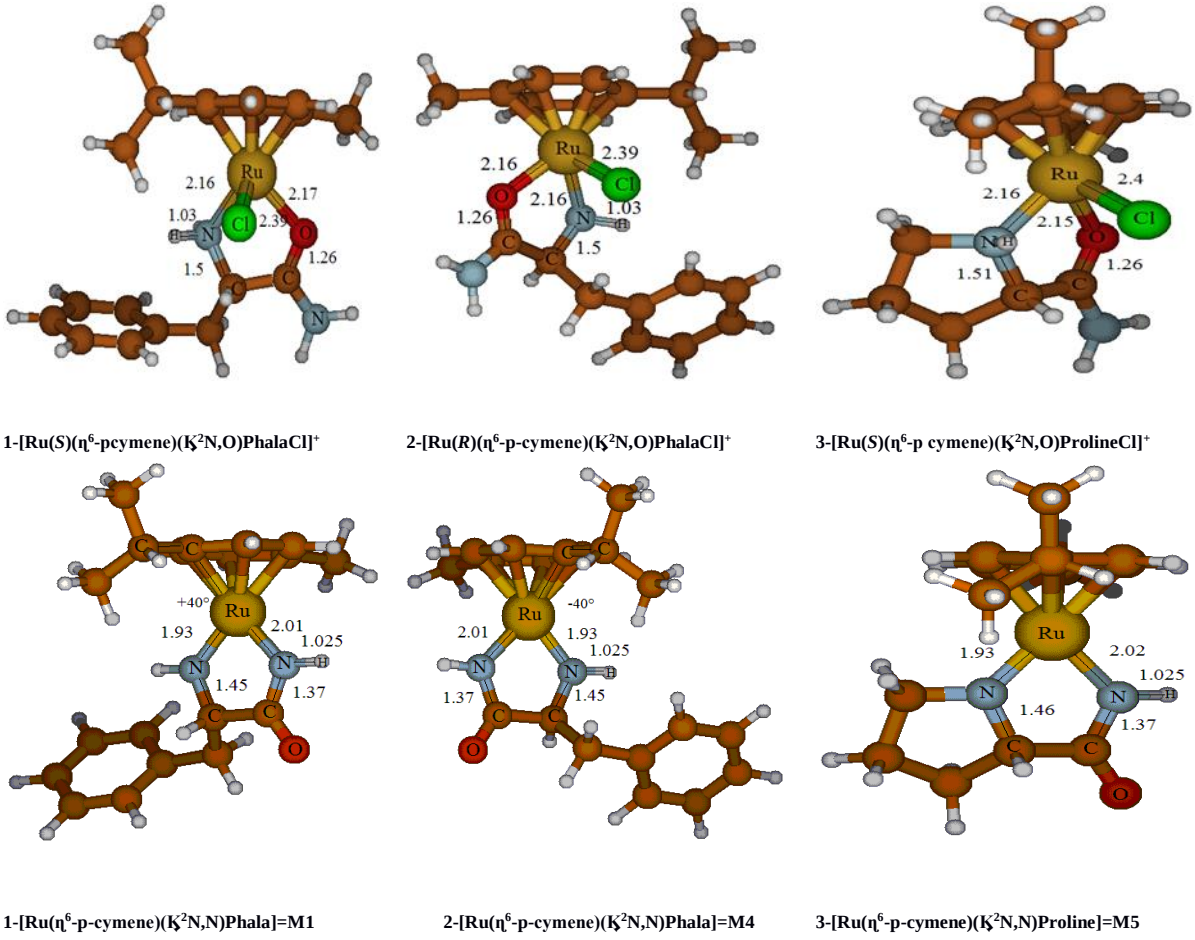

Figure 5.3. Optimized geometries at PBE-GD3BJ level. Top: starting complexes; bottom: active catalyst (16e). The main distances are indicated in Å.

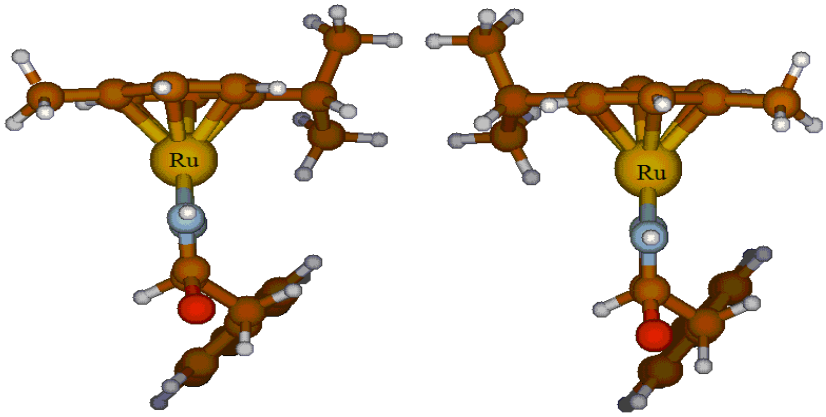

1-[Ru(η⁶-p-cymene)(Ƙ²N,N)Phala]=M4 **2-[Ru(η⁶-p-cymene)(Ƙ²N,N)Phala]=M1**

E= 0 Kcal **E= 0.36 Kcal**

Figure 5.4. (16e phenylalanine)

Since there is a small energy difference between the two conformer M4 and M1 (0.36 kcalmol^{-1}), the less stable diasteroisomer M4 could only be ruled out as a relevant participant in the reaction if the barrier for the rearrangement process M1 ↔ M4 was high. We search a barrier for this rearrangement (rotation of p-cymene), which is depicted in figure 5.5.

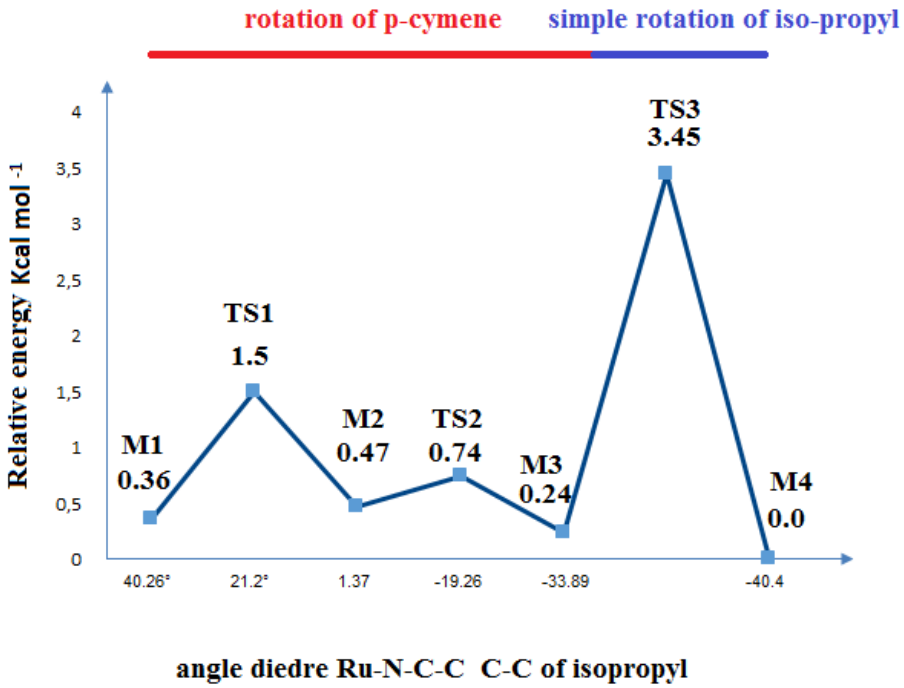

Figure 5.5. Relative barrier for rearrangement M1 ↔M4

by a low relative barrier In this rearrangement. Since the thermodynamic energy gap between M1 and M4 is just 0.36 kcalmol^{-1} , and the rotation of cymene process has a relatively low energy barrier, M1 could not be discarded and the participation of both isomers of [Ru(ɳ6-p-cymene)(Ķ^{2}N,N)Phala] in the ATH mechanism was studied. In other hand, we search a barrier of the rearrangement (rotation of p-cymene) in proline ligand this rearrangement is depicted in figure 5.6.

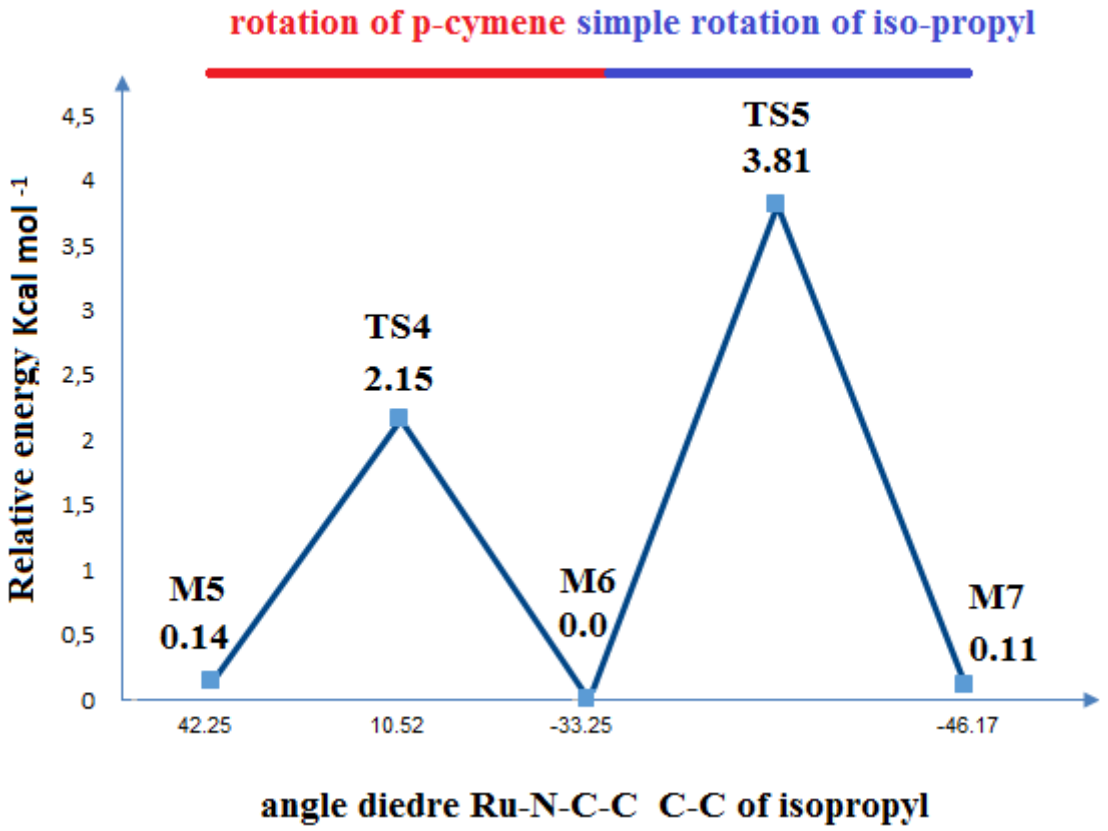

Figure 5.6. Relative barrier for rearrangement in proline ligand

By a low relative barrier In this rearrangement. Since the thermodynamic energy gap between the two isomer of active catalyst (proline 16e) M5 and M7 is just 0.03 kcalmol^{-1} , and the rotation of cymene process has a relatively low energy barrier, the other isomer could not be discarded and the participation of both isomers of [Ru(ɳ6-p-cymene)(Ķ^{2}N,N)Proline] in the ATH mechanism was unfortunately studied (see Appendix for the other isomer).

5.3.2. Formation of the bi-functional ruthenium complex

Our calculations showed that the H transfer from iso-propanol (IPA) through a *B*-hydride elimination step has an energy barrier that is much higher than the one obtained for the concerted hydrogen transfer mechanism (see chapter 4). This is consistent with the literature

[22]. Hence, the reaction takes place through a concerted six-membered cyclic transition state. In each complex, the active catalyst is able to dehydrogenate IPA from two different sides (*Si* and *Re* faces) to afford metal hydride diastereomers with Ru(*R*) and Ru(*S*) configurations and acetone, leading to a total of six .transition states and six hydrogenated catalysts (18e). The corresponding structures are collected in Figure 5.7 together with the corresponding activation free energies.

5.3.2.1. With the (N, N) Phenylalanine

Precatalyst *S* diastereoisomer of {(η6-arene) Ru [(Ƙ²N, N) phenyl alanine amide] Cl^+ PF_6}

TSa1(*S*) results from the approach of IPA to the *Re* face of the catalyst M1 (16e) and leads to hydrogenated catalyst (18e) (*S*) (Fig. 5.7). In TSa1(*S*), the free energy of TSa1(*S*) is calculated to lie 5.5 kcal/mol above that of the separate reactants (catalyst (16e) +2-propanol). TSa1(*R*) results from the approach of IPA to the *Si* face of the catalyst M1 (16e), and lies 6.2 kcal/mol above the free energy of the reactants and leads to the other configuration hydrogenated catalyst (18e) (*R*) (Fig. 5.7).

The reason for this preference is that

- In transition state TSa1(*S*) a stabilizing NH–p interaction between the phenyl group of the catalyst and the NH_2 unit of the catalyst.

- And in TSa1(*R*) the clashes of the methyl groups of IPA with the cymene ring of the catalyst; this is not present in the TSa1(*S*).

The free energy of the hydrogenated catalyst (18e) with *R* and *S* configuration lies -4.5 and -6.5 kcal/mol, respectively, below the free energy of separate reactants (catalyst (16e) +2-propanol). The hydrogenated catalyst (18e) *R* suffers from interactions between the Ru-N-C-C(O)-N chelation ring and the isopropyl group of cymene ring. The reaction is exergonic.

Precatalyst *R* diastereoisomer of {(η6-arene) Ru [(Ƙ²N, N) phenylalanine amide] Cl^+} PF_6

TSa2(*S*) results from the approach of IPA to the *Re* face of the catalyst M4 (16e) and leads to the hydrogenated catalyst (18e) (*S*) (Fig. 5.7). In TSa2(*S*), the free energy of TSa2(*S*) is

calculated to lie 7.1 kcal/mol above that of the separate reactants (catalyst (16e) +2-propanol). TSa2(*R*) results from the approach of IPA to the *Si* face of the catalyst M4 (16e), and lies 6.2 kcal/mol above the free energy of the reactants and leads to the other configuration hydrogenated catalyst (18e) (*R*) (Fig. 5.7). The reason for this preference is the presence in TSa2(*S*) of repulsive interactions between the methyl groups of IPA and the isopropyl group of cymene ring of the catalyst; they are not present in the TSa2(*R*).

The free energy of the hydrogenated catalyst (18e) *R* and *S* configuration lies -5.1 and -5.75 kcal/mol, respectively, below the free energy of separate reactants (catalyst (16e) +2-propanol). The hydrogenated catalyst (18e) *R* suffers from interactions between the isopropyl group of cymene ring and the aryl ring. The reaction is exergonic.

5.3.2.2. With the (N, N) proline amide

precatalyst *S* diastereoisomer of {Ru[(ɳ6- arene) proline amide]Cl}PF_6

TSa3(*S*) results from the approach of IPA to the *Re* face of the catalyst M5 (16e) and leads to hydrogenated catalyst (18e) (*S*) (Fig. 5.7).The free energy of TSa3(*S*) is calculated to lie 8.3 kcal/mol above that of the separate reactants (catalyst(16e)+2-propanol). TSa3(*R*) results from the approach of IPA to the Si face of the catalyst M5 (16e), and lies 12.3 kcal/mol above the free energy of the reactants and leads to the other configuration hydrogenated catalyst (18e) (*R*) (Fig. 5.7). The reason for this preference is that the approach of IPA in TSa3(*R*) pushes the cymene ring towards the proline cycle, which induces steric repulsions. This is not the case in TSa3(*S*).

The free energy of the hydrogenated catalyst (18e) with *R* and *S* configuration lies +0.25 and -5.1 kcal/mol, respectively, below the free energy of separate reactants (catalyst (16e) +2-propanol). The hydrogenated catalyst (18e) *R* suffers from interactions between the isopropyl group of cymene ring and the Ru-N-C-C(O)-N chelation ring. The reaction is exergonic for S but endergonic for R.

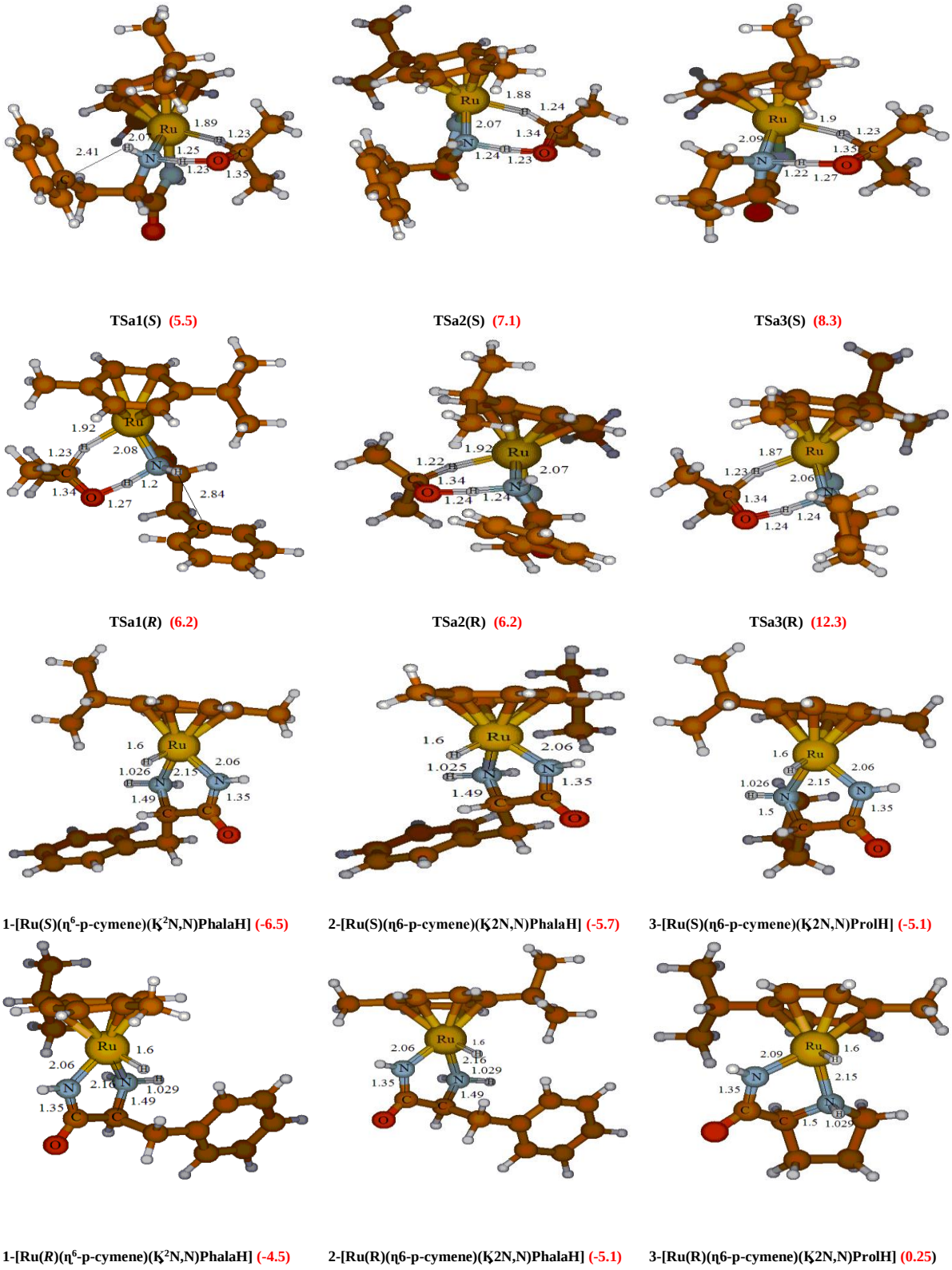

Figure 5.7. Optimized geometries of the PBE-GD3BJ level of transition states and of the hydrogenated catalyst (18e) for the concerted H-transfer from IPA to the 16e complex.

5.3.3. Asymmetric transfer hydrogenation of acetophenone

For each diastereoisomeric hydrogenated catalyst (18e) (*R* or *S*), the transfer of the metal hydride and of the amine proton can occur via two different pathways, which gives two diastereotopic transition state structures. The first pathway corresponds to the attack of the metal hydride at the *Re* face of acetophenone while the other pathway involves attack at the *Si* face of the ketone. This results in a total of four transition states TSb*RR*, TSb*RS*, TSb*SR*, and TSb*SS* for each precatalyst.. The optimized structures of these transition states for the three complexes are collected in Figure 5.8.

The complete energetic profiles for each case are represented in Figure 5.9, 5.10 and 5.11.

Precatalyst S diastereoisomer of {(η6-arene)Ru[(Ķ^{2}N,N) phenylalanine amide]Cl$^+$}PF_6

The hydrogenated catalyst (18e) *S* (-6.5) kcal/mol below reactants interacts with the C=O double bond of the prochiral acetophenone . The simultaneous transfer of the amine proton and the hydride to the ketone leads to the formation of *R*-phenylethanol or *S*-phenylethanol via the TSb1*SR* or TSb1*SS* that lie 4.9 and 6.1 kcal/mol respectively above the reactants. The hydrogenated catalyst (18e) *R* (-4.5 kcal/mol) interacts with the C=O double bond of acetophenone. The simultaneous transfer of the amine proton and hydride ligand to the ketone leads to the formation of *R*-phenylethanol or *S*-phenylethanol and takes place via TSb1*RR* and TSb1*RS* which lie 7.1 and 6.9 kcal/mol, respectively, above reactants.

The overall energy profiles of the asymmetric transfer hydrogenation of acetophenone catalyzed by the active catalyst derived from the Ru(*S*) C(*R*) phenyl alanine are displayed in Figure 5.9. As we have seen in the previous part, the intermediate 18e is more stable under its Ru(*S*) form that under its Ru(*R*) form. In addition, looking at the energy levels of the TS for the second step, we can see that those corresponding to hydrogenated catalyst (18e) *R* are higher, which suggests that the (18e) *S* is the main reactive channel. This channel gives preferentially the *R* isomer of phenylethanol via TSb*SR* with a difference in the barriers of 1.2 kcal/mol. The reason for this preference is that, in the transition state TSb1*SR* a stabilizing CH–p interaction exists between the phenyl group of acetophenone and the cymene ring of the catalyst. This is in line with the explanations provided by Noyori et al. for the ruthenium catalysts [23].

And a stabilizing NH–p interaction between the phenyl group of the catalyst and the NH_2 unit of the catalyst

Precatalyst *R* diastereoisomer of {(η6-arene) Ru [(Ƙ^{2}N, N) phenyl alanine amide] Cl^+} PF6

The hydrogenated catalyst (18e) *S* (-5.7 kcal/mol) interacts with the C=O double bond of acetophenone. The simultaneous transfer of the amine proton and hydride ligand to the ketone leads to the formation of *R*-phenylethanol or *S*-phenylethanol and takes place via TSb2*SR* and TSb2*SS* which lies 6.2 and 8.2 kcal/mol, respectively, above the reactants. The hydrogenated catalyst (18e) *R* (-5.1 kcal/mol) interacts with the C=O double bond of the acetophenone. The simultaneous transfer of the amine proton and hydride ligand to the ketone leads to the formation of *R*-phenylethanol or *S*-phenylethanol and takes place via TSb2*RR* and TS2b*RS* which lies 7.2 and 5.3 kcal/mol, respectively, above reactants.

The energy profiles of the asymmetric transfer hydrogenation of acetophenone catalyzed by the hydrogenated catalyst (18e) *S* and *R* are displayed in Figure 5.10. If we look at the energy levels of the TS, we can see that the lowest *S* product is formed from the hydrogenated catalyst (18e) *R* while the lowest R product is formed from the hydrogenated catalyst (18e) S.the lowest barrier is obtained for the formation of the *S* product,which is only 0.9 Kcal mol^{-1}

Experimentally, both diastereoisomers, Ru(*R*) C(*S*) and Ru(*S*) C(*S*), crystallize together and are probably present in the catalytic solutions and the low barriers in the rotation of cymene. Since they lead to the opposite 1-phenylethanol enantiomers, we need to consider both diastereoisomers together to compare our results with the experimental ones. By comparing Figures 5.9 and 5.10, the lowest TS leading to the *R* phenyl ethanol at 4.9 kcal/mol ,whereas the lowest TS leading to the *S* phenyl ethanol lies 5.3 kcal/mol , our calculations correctly reproduce the fact that the ligand phenylalanine affords modest ee values in favor of the *R* isomer. The energy difference between TSb1*SR* and TSb2*RS* (0.4 kcal/mol) leads to a preference of 30% for the latter, which can be related to the experimental value of ee (30%).

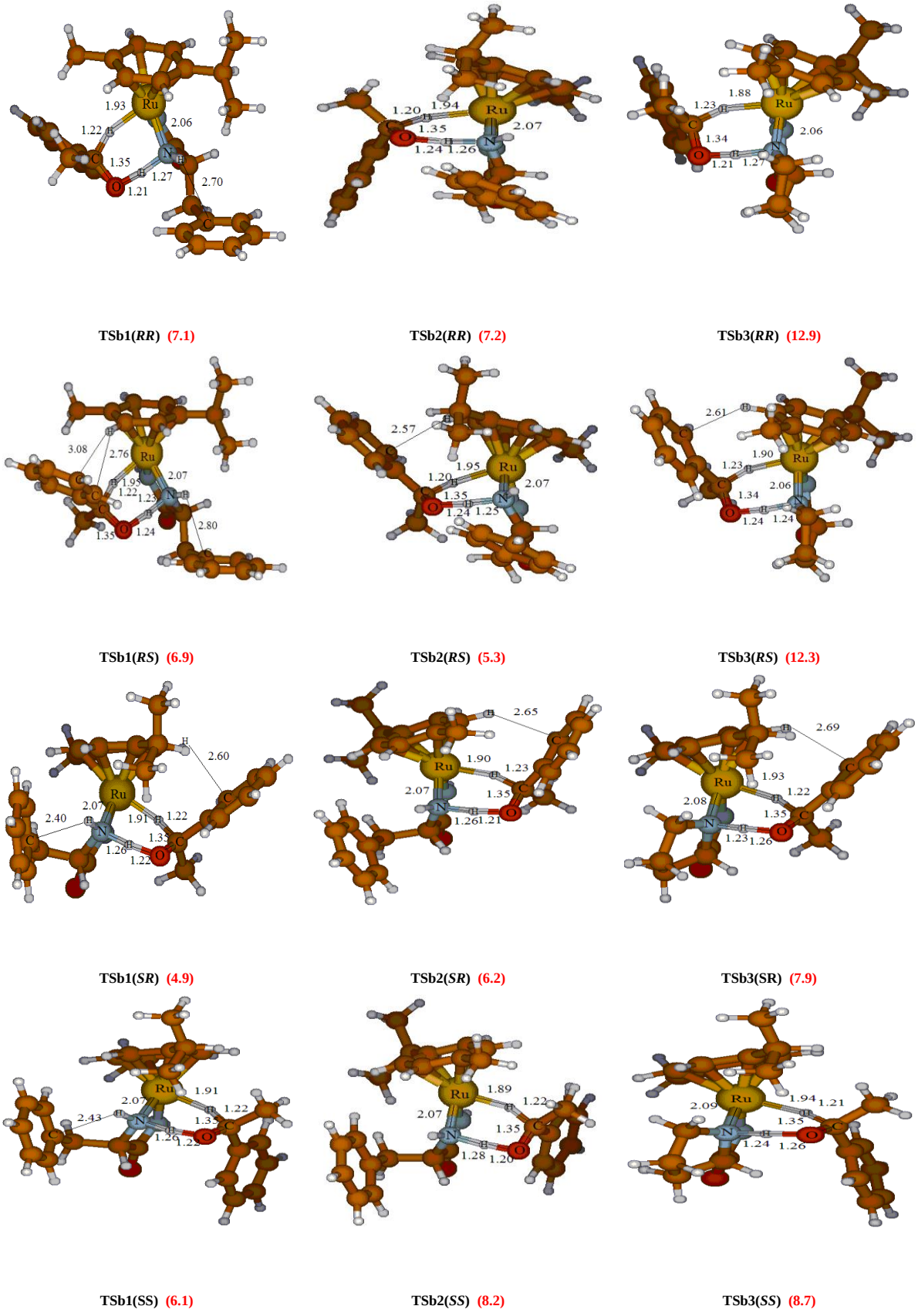

Figure 5.8. Optimized geometries of the PBE-GD3BJ level of transition states for the concerted H-transfer from 18e complex to acetophenone.

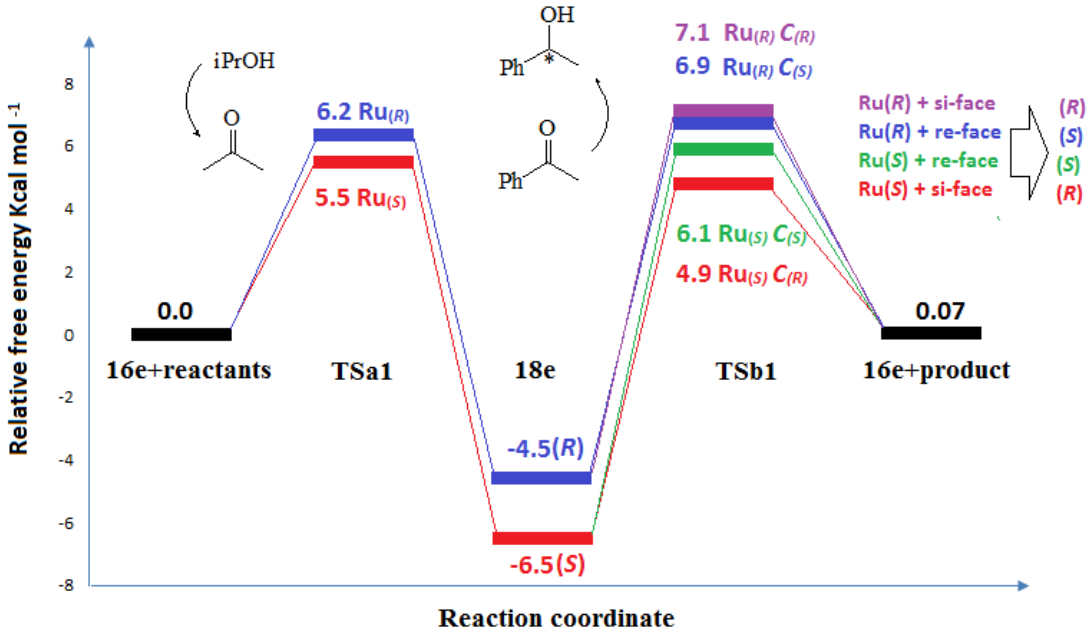

Figure 5.9. Overall free eneergy profiles for the asymmetric hydrogenation reaction of acetophenone with *S* diastereoisomer of {(η6-arene)Ru[(Ƙ^{2}N,N) phenyl alanine amide]Cl$^+$}PF$_6$. Free energies are in Kcal mol^{-1} and relative to the separate active catalyst (16e) and reactants (+2-propanol and acetophenone).

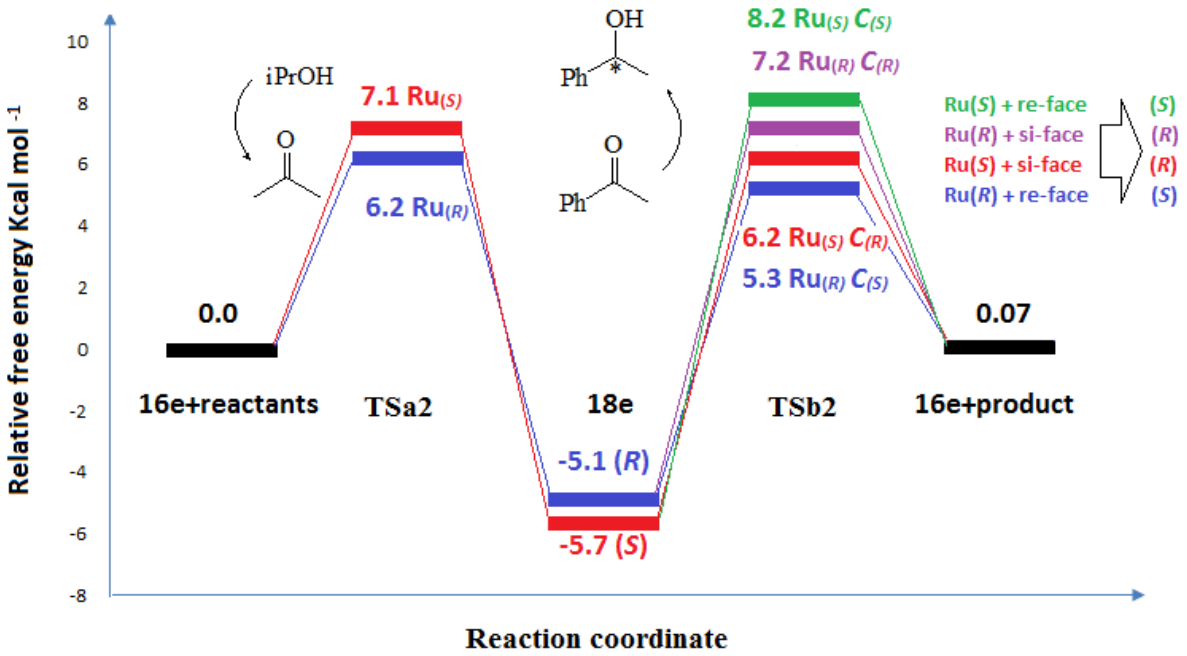

Figure 5.10. Overall free energy profiles for the asymmetric hydrogenation reaction of acetophenone with *R* diastereoisomer of {(η6-arene)Ru[(Ƙ^{2}N,N) phenyl alanine amide]Cl$^+$}PF$_6$. Free energies are in kcal mol^{-1} and relative to the separate reactants (16e+2-propanol).

Precatalyst *S* diasterisomer of {(η6-arene) Ru [(Ķ²N, N) proline amide] Cl^+} PF_6

The hydrogenated catalyst (18e) *S* (-5.1 kcal/mol) interacts with the C=O double bond of acetophenone. The simultaneous transfer of the amine proton and hydride ligand to the ketone leads to the formation of *R*-phenylethanol or *S*-phenylethanol and takes place via TSb3*SR* and TSb3*SS* which lies 7.9 and 8.7 kcal/mol, respectivly, above reactants. The hydrogenated catalyst (18e) *R* (0.25 kcal/mol) interacts with the C=O double bond of acetophenone. The simultaneous transfer of the amine proton and hydride ligand to the ketone leads to the formation of *R*-phenylethanol or *S*-phenylethanol and takes place via TSb3*RR* and TSb3*RS*, which lies 12.9 and 12.3 kcal/mol respectively above reactants. The energy profiles of asymmetric transfer hydrogenation of acetophenone catalyzed by *S* diastereoisomer of {(η6-arene)Ru[(Ķ²N,N) proline amide]Cl}$^+$ PF_6 is displayed in Figure 5.11.

If we look at the energy levels of TSb3*SS* and TSb3*SR*, we can see that TSb3*SR* lies 0.8 kcal/mol higher in energy than TSb3*SS*, which suggests that the H transfer leads to the *R* isomer of phenyl ethanol with a high selectivity. Like previously, this is due to the stabilizing CH–p interaction between the phenyl group of acetophenone and the cymene ring of the catalyst.

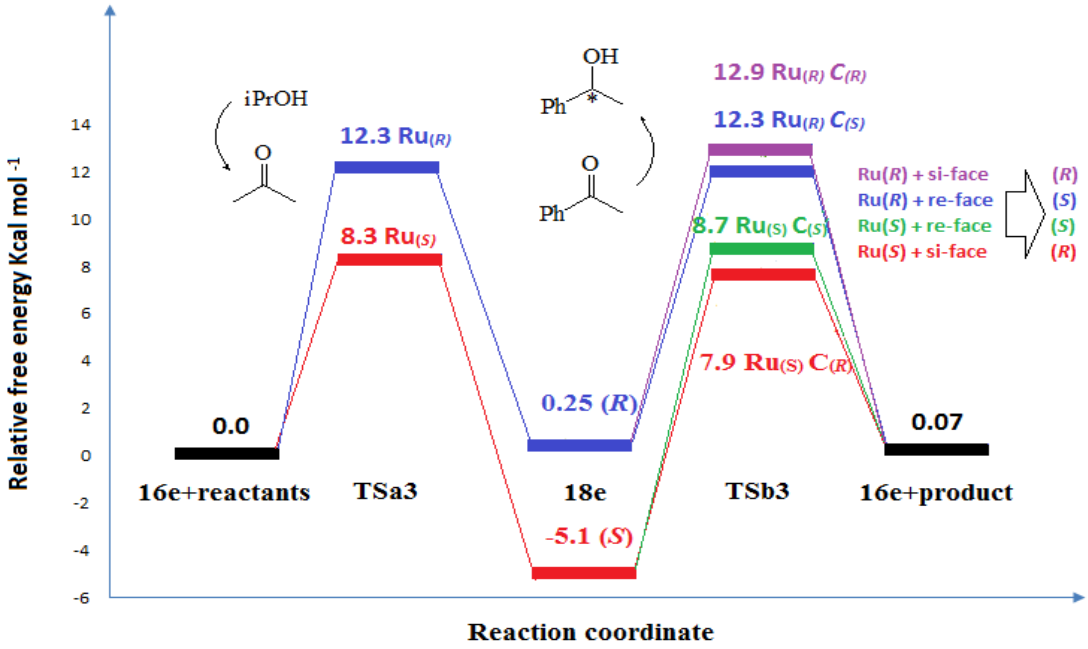

Figure 5.11. Overall free energy curves for the asymmetric hydrogenation reaction of acetophenone with *S* diasteromer of {(η6-arene)Ru[(Ķ²N,N) Proline amide]Cl^+}PF_6. Free energies are in kcal mol^{-1} and relative to the separate reactants (16e+2-propanol)

We need to consider both Precatalyst *S* and *R* diasterisomer of {(η6-arene) Ru [(Ƙ^{2}N, N) proline amide] Cl^+} PF_6 together to compare our results with the experimental ones. By comparing Figures 5.11 and 5.13 (see Appendix), the lowest TS leading to the *R* phenyl ethanol at 7.9 kcal/mol ,whereas the lowest TS leading to the *S* phenyl ethanol lies 8.7 kcal/mol ,These calculations correctly reproduce the fact that the ligand proline affords the *R*-phenylethanol with a high selectivity (experimentally ee=75%).

5.4. Conclusion

In the present study, the ruthenium-catalyzed asymmetric reduction of acetophenone was investigated by means of DFT calculations. Two amino acid-based ligands were considered. For the first one, ligand 1 (phenyl alanine amide), the full catalytic cycle was studied according to the well-established outer-sphere reaction mechanism. For the other ligand 2 (proline amide), which was shown experimentally to yield the high enantioselectivity. The DFT calculations reproduce the experimental selectivities for both ligands and also provide rationalization to the observations. For each ligand, a number of plausible configuration of the metal were considered and it was shown that both *R* and *S* configuration are energetically accessible and must be considered for the overall catalytic process.

The first step of the reaction, the hydrogenation of the metal center by 2-propanol, is possible from two sides of the catalyst metal–ligand chelate ring, resulting in the formation of two metal hydride diastereomers, with Ru(R) or Ru(S) configurations. In the second step, a stabilizing CH–p interaction between a cymene of the catalyst and the phenyl ring of the substrate exists on hydrogenation from either the *Re* or the *Si* face of the substrate with both ligands 1 and 2, which contributes to stereoselectivity. The balance between these two factors, that is, the energy difference between the metal hydride diastereomers, and the CH–p interaction, will ultimately determine the stereochemical outcome of the reaction.

5.5. References

[1] (a) Ojima I **(2010)** Catalytic asymmetric synthesis. Wiley-VCH, Weinheim; (b) H. U. Blaser, C. Malan, B. Pugin, F. Spindler, H. Steiner and M. Studer, *Adv. Synth. Catal.,* **2003**, 345, 103; (c) F. Naud, F. Spindler, C. J. Rueggeberg, A. T. Schmidt and H. U. Blaser, *Org. Process Res. Dev.*, **2007**, 11, 519. 4; (d) D. Wangming, W. Qingfu, Y. Zhengkun,*Chinese J. Cat.* 34 **(2013)** 1373-1377; (e) Y.-Q. Xu, S.-L. Yu, Y.-Y. Li, Z.-R. Dong, J.-X. Gao,*Chinese Chem. Lett.* 24 **(2013)** 527-530.

[2] (a) Palmer, M.; Wills, M. *Tetrahedron: Asymmetry* **1999**, 10, 2045. (b) Noyori, R.; Hashiguchi, S. *Acc. Chem. Res*. **1997**, 30, 97. (c) Zassinovich, G.; Mestroni, G.; Gladiali, S. *Chem. Rev.* **1992**, 92, 1051.

Ohkuma, T.; Ooka, H.; Hashiguchi, S.; Ikariya, T.; Noyori, R. *J. Am. Chem. Soc*. **1995**, 117, 2675.

[3] (a) T. Ohta, S. Nakahara, Y. Shigemura, K. Hattori, I. Furukawa, *Appl. Organomet. Chem.* 15 **(2001)** 699–709. (b) Ohta, T.; Nakahara, S.; Shigemura, Y.; Hattori, K.; Furukawa, I. *Chem. Lett.* **1998**, 491.

[4] J.W. Faller, A.R. Lavoie, *Organometallics* 20 **(2001)** 5245–5247.

[5] a) H. Y. Rhyoo, H. J. Park, Y. K. Chung, *Chem. Commun*. **2001**, 2064–2065; b) H. Y. Rhyoo, Y. A. Yoon, H. J. Park, W. H. Suh, Y. K. Chung, *Tetrahedron Lett.* **2002**, 43, 269–272

[6] a) S. Zeror, J. Collin, J.-C. Fiaud, L.A. Zouioueche, *J. Mol. Catal. A: Chemical* 256 **(2006)** 85-89; b) S. Zeror, J. Collin, J.-C. Fiaud and L. A. Zouioueche, *Adv. Synth. Catal.*, **2008**, 350, (1), 197; (c) Z. Zhou, L. Wu *Catalysis Communications* 9 **(2008)** 2539–2542 ; (d) J. Mao, J. Guo, *Chirality* 22 **(2010)** 173-181; (e) M. Boukachabia, S. Zeror, J. Collin, J.-C. Fiaud, L.A. Zouioueche, *Tetrahedron Lett*. 52 **(2011)** 1485-1489 (f) K. Ahlford, H. Adolfsson *Catalysis Communications* 12 **(2011)** 1118–1121

[7] SerpilDenizaltı, DenizMercan, BetülŞen, AytaçGürhanGökçe, BekirÇetinkaya, *Journal of Organometallic Chemistry* 59 **(2014)** 6287-6295.

[8] Alessia Bacchi, Marcella Balordi, Paolo Pelagatti , Corrado Pelizzi Dipartimento, *Journal of Organometallic Chemistry* 694 **(2009)** 3281–3286.

[9] (a) V. Guiral, F. Delbecq, P. Sautet, *Organometallics* **2000**, 19, 1589. (b) V. Guiral, F. Delbecq, P. Sautet, *Organometallics* **2001**, 20, 2207. (c) F. Delbecq, V. Guiral, P. Sautet *Eur. J. Org. Chem.* **2003**, 2092-2097

[10] (a) J. M. Brown and R. J. Deeth, *Angew. Chem.,* Int. Ed., **2009**, 48, 4476– 4479. (b) F. Maseras and D. Balcells, *New J. Chem*., **2007**, 31, 333–343. (c) D. Di Tommaso, S. A. French, A. Zanotti-Gerosa, F. Hancock, E. J. Palin and C.R.A.Catlow*, Inorg. Chem.*, **2008**, 47, 2674–2687. (d) S. A. French, D. Di Tommaso, A. Zanotti-Gerosa, F. Hancock and C. R. A. Catlow, *Chem. Commun*., **2007**, 2381–2383. (e) Hsin-Yi Tiffany Chen, Devis Di Tommaso, Graeme Hogarth and C. Richard A. Catlow *Dalton Trans*., **2012**, 41, 1867–1877 (f) H.-Y. T. Chen, D. Di Tommaso, G. Hogarth and C. R. A. Catlow, *Catal. Lett*., **2011**, 141, 1761–1766. (g) Václavík, J.; Šot, P.; Vilhanová, B.; Pecháček, J.; Kuzma, M.; Kačer, P. *Molecules* **2013**, 18 (6), 6804–6828. (h) Šot, P.; Kuzma, M.; Václavík, J.; Pecháček, J.; Přech, J.; Januščák, J.; Kačer, P. *Organometallics* **2012**, 31 (17), 6496–6499. (i) Šot, P.; Vilhanová, B.; Pecháček, J.; Václavík, J.; Zápal, J.; Kuzma, M.; Kačer, P. *Tetrahedron: Asymmetry* **2014**, 25 (18-19), 1346–1351.(j) for recent review see K. H., Hopmann *Int. J. Quantum Chem*. **2015**, DOI: 10.1002/qua.24882

[11] Abbel, Robert,Abdur-Rashid, Kamaluddin Faatz, Michael Hadzovic, Alen Lough, Alan J Morris, Robert H *J. Am. Chem. Soc* **2005**,127,1870-1882

[12] Paolo Pelagatti, Mauro Carcelli, Francesca Calbiani, Claudio Cassi, Lisa Elviri, Corrado Pelizzi, Umberto Rizzotti, and Dominga Rogolino, *Organometallics* **2005**, 24, 5836-5844.

[13] (a) R. Noyori, M. Yamakawa, S, Hashiguchi, *J. Org. Chem.* **2001**, 66, 7931. (b) M. Yamakawa, H. Ito, R. Noyori, *J. Am. Chem. Soc.* **2000**, 122, 1466.

[14] J.P. Perdew, K. Burke, M. Ernzerhof, *Phys. Rev. Lett.* 77 **(1996)** 3865.

[15] S. Grimme, S. Ehrlich and L. Goerigk, *J. Comp. Chem*. 32 **(2011)** 1456-65.

[16](a) P. C. Hariharan, J. A. Pople, *Mol. Phys*. **1974**, 27, 209–214; (b) V. A. Rassolov, M. A. Ratner, J. A. Pople, P. C. Redfern, L. A. Curtiss, *J. Comput. Chem*. **2001**, 22, 976–984.

[17] Hay, P. J.; Wadt, W. R. *J. Chem. Phys*. **1985**, 82, 270

[18] G. Scalmani and M. J. Frisch, *J. Chem. Phys*., 132 **(2010)** 114110

[19] Frisch MJ, Trucks GW, Schlegel HB, Scuseria GE, Robb MA, Cheeseman JR, Scalmani G, Barone V, Mennucci B, Petersson GA, Nakatsuji H, Caricato M, Li X, Hratchian HP, Izmaylov AF, Bloino J, Zheng G, Sonnenberg JL, Hada M, Ehara M, Toy- ota K, Fukuda R, Hasegawa J, Ishida M, Nakajima T, Honda Y, Kitao O, Nakai H, Vreven T, Montgomery JA Jr, Peralta JE, Ogliaro F, Bearpark M, Heyd JJ,Brothers E, KudinKN,Staroverov VN, Kobayashi R, Normand J,Raghavachari K,Rendell A, Burant JC, Iyengar SS, Tomasi J, Cossi M, Rega N, Millam JM, Klene M, Knox JE, Cross JB, Bakken V, Adamo C, Jaramillo J, Gomperts R, Stratmann RE, Yazyev O, AustinAJ, Cammi R, Pomelli C, Ochterski JW, Martin

RL, Morokuma K, Zakrzewski VG, Voth GA, Salvador P, Dannenberg JJ, Dapprich S, Daniels AD, Farkas Ö, Foresman JB, Ortiz JV, Cioslowski J, FoxDJ **(2009)** *Gaussian 09 Revision D.01*. *Gaussian Inc., Wallingford.*

[20] (a) M. Yamakawa, H. Ito, R. Noyori, *J. Am. Chem. Soc.* **2000**, 122, 1466; (b) D. A. Alonso, P. Brandt, S. J. M. Nordin, P. G. Andersson, *J. Am. Chem. Soc.* **1999**, 121, 9580; (c) P. Brandt, P. Roth, P. G. Andersson, *J. Org. Chem*. **2004**, 69, 4885;.

[21] (a) M. Yamakawa, I. Yamada, R. Noyori, *Angew. Chem*. **2001**, 113, 2900; *Angew. Chem.* Int. Ed. **2001**, 40, 2818; (b) R. Noyori, M. Yamakawa, S. Hashiguchi, *J. Org. Chem*. **2001**, 66, 7931;

[22] (a) M. Yamakawa, H. Ito, R. Noyori, *J. Am. Chem. Soc.* **2000**, 122, 1466; (b) D. A. Alonso, P. Brandt, S. J. M. Nordin, P. G. Andersson, *J. Am. Chem. Soc.* **1999**, 121, 9580; (c) P. Brandt, P. Roth, P. G. Andersson, *J. Org. Chem*. **2004**, 69, 4885;.

[23] (a) M. Yamakawa, I. Yamada, R. Noyori, *Angew. Chem.* **2001**, 113, 2900; Angew. Chem. Int. Ed. 2001, 40, 2818; (b) R. Noyori, M. Yamakawa, S. Ha- shiguchi, *J. Org. Chem*. **2001**, 66, 7931;

Chapter 6: Application III

DFT modeling of the enantiomeric excess for Asymmetric transfer hydrogenation reaction of prochiral ketones in water promoted by chiral proline (amide/amine) ruthenium (II) complexes

6.1. Introduction

Asymmetric transfer hydrogenation of ketones is an important transformation in the production of many fine chemical compounds at both laboratory and industrial level [1-2].Therefore, many studies have been undertaken to develop new highly selective catalyst [3-4]. Noyori et al [5-6]. Showed that a ruthenium complex containing monotosylated 1, 2-diamines could serve as efficient catalyst for the ATH of ketones.

Amino acids are inexpensive chiral materials that have been used for the synthesis of optically active transition metal complexes [7-9]. In 2001, the group of Faller reported a in situ generated (*p*-cymene) Ru (L-proline amide) Cl_2 catalyst that gave excellent yields, 70-90%, with moderate enantiocontrol, 68-93%, in hydrogenations of a variety of ketones at -24 C° [10]. In the same year, Chung reported the first example of the asymmetric hydrogen-transfer reductions of aromatic ketones in an aqueous solution, with enantiomeric excesses up to 95.3 % using an functionalized proline amide as ligand [11]. Zeror and others, have constructed active and selective ATH-catalysts based on the use of proline amides [12-14].

Based on literature reports [15-17], a plausible mechanism for the ATH of ketones in aqueous media can follow an outer-sphere pathway analogous to that proposed by Noyori and al [18-19] figure 6.1.

Percatalyst Ru-proline amide is generated *in situ* from [Ru (p-cymene) $cl_2]_2$ and proline amide in water and then it reacts with HCOOHNa forming formato complex 2 the reduction prooceeds via the formato intermediate 2, followed by decarboxylation to give Ru-hydride intermediate 3, The key step is the simultaneous transfer of the hydritic H (Ru–H) and the protic H (N–H) to the C=O functional group via a six-membered transition state 4 TS. Last, the active intermediate 5 is regenerated with the liberation of the chiral alcohol, closing the catalytic cycle.

Recently, Serpil Denizaltı et al [20]. Compared the proline amine ligands with amide analogues in asymmetric transfer hydrogenation reaction of prochiral ketones in water figure 6.2, in this work we have rationalize the enantioselectivity observed experimentally using Density functional theory.

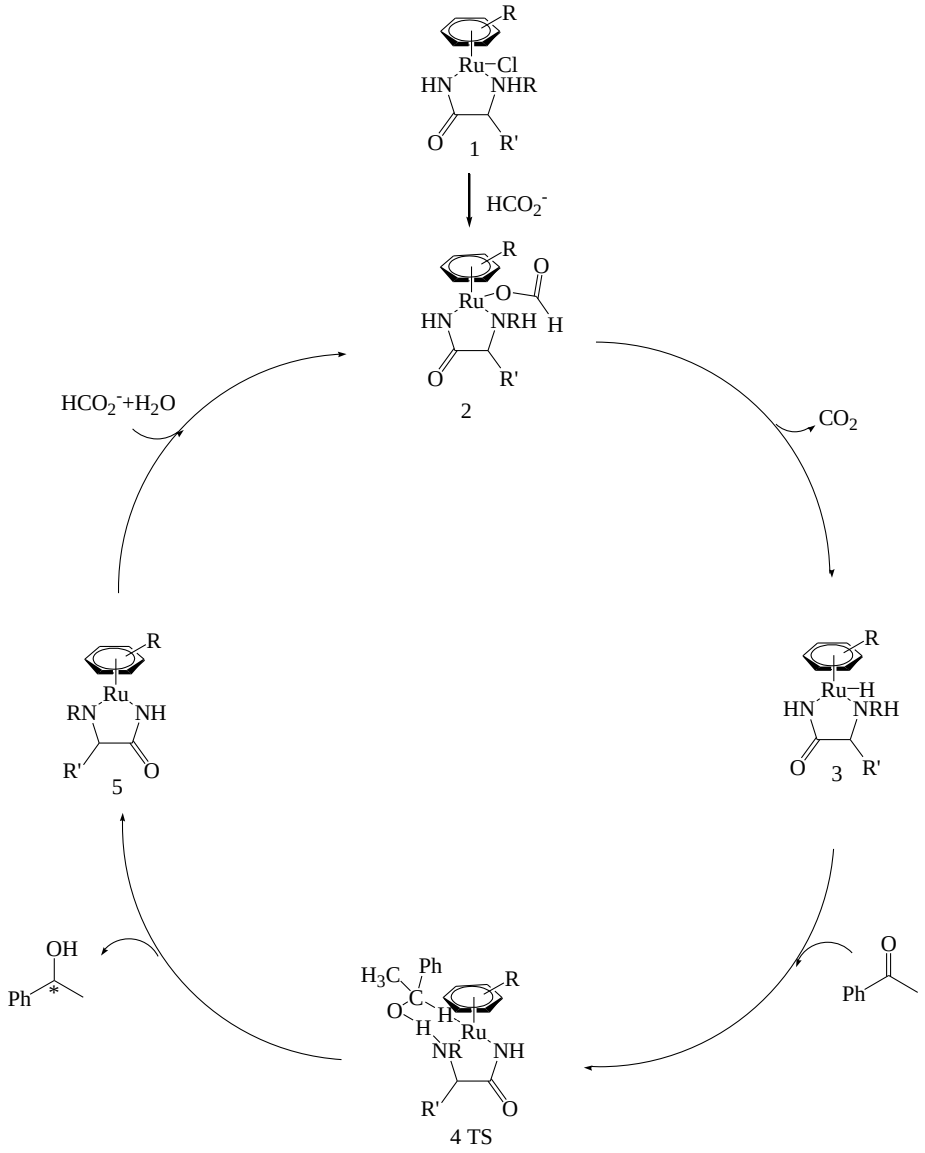

Figure 6.1. Plausible mechanism for transfer hydrogenation of acetophenone catalyzed by Ru (II) complexes containing amino amide ligands in aqueous media.

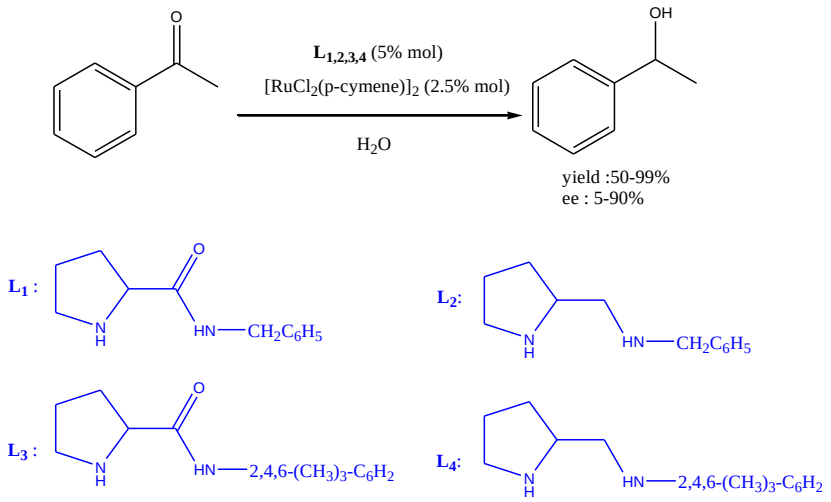

Figure 6.2. Ru-catalyzed ATH of ketones with [Ru (p-cymene)Cl_2]$_2$ and ($L_{1,3}$) proline amide or ($L_{2,4}$) proline amine. ee is the enantiomeric excess.

6.2. Experimental section

6.2.1. Computational Details

All calculations were performed at the density functional theory (DFT) level, using the PBE [21] functional by addition of the D3 version of Grimme's dispersion with Beck-Johnson Damping functions [22] as implemented in the Gaussian 09 D01 software package [23]. For all atoms except ruthenium, the 6-31G (d,p) basis set was used [24-25]; ruthenium was treated with the LANL2DZ basis set and effective core potential (ECP) [26].geometries for the transition state were located either by QST2 or by QST3 procedures, or by the guess based on the structure of the previously found TS.Vibrational frequency calculations were then performed at the optimized geometry of transition structure. We confirmed that all transition structure has one, and only one, imaginary frequency. The intrinsic reaction coordinate (IRC) calculations, at the same level of theory, were performed to ensure that the transition structures led to the expected reactants and products.The reported energies are Gibbs free energies, which include zero-point vibrational corrections, thermal corrections at 298 K and solvation free energies. The solvation energies were calculated as single point corrections on the optimized structures using the conductor-like polarizable continuum model method [27], with dielectric constant ε=78.3553 for water.

6.3. Results and discussion:

In acetophenone hydrogenation catalyzed by chiral proline (amide/amine) ruthenium (II) complexes, the hydride transfer can occur via two different pathways, each having a diastereotopic transition state. One pathway corresponds to the attack of the hydride at the *Re* face of acetophenone while the other pathway involves an attack at the *Si* face.

According to eqn (1) and the Arrhenius equation, we could obtain eqn (2) to calculate the ee values (ee Calculated).

$$ee = \frac{R-S}{R+S} \quad 6.1$$

$$ee_{calculated} = \frac{e^{\Delta\Delta Ga/RT}-1}{e^{\Delta\Delta Ga/RT}+1} \quad 6.2$$

6.3.1. Stereoselectivity with Ligand 1, 2 (proline amide/amine)

TS1(*S*) results from the approach of Ru-hydride intermediate to the *Re* face of the acetophenone and leads to (active catalyst + phenylethanol). In TS1(*S*), the free energy of TS1(*S*) is calculated to lie +8.4 kcal/mol above that of the separate reactants (Ru-hydride + acetophenone). TS1(*R*) results from the approach of Ru-hydride intermediate to the *Si* face of the acetophenone, and lies +7.9 kcal/mol above the free energy of the reactants and leads to the other configuration of phenylethanol + active catalyst. The optimized structures of these transition states are collected in Figure 6.3.

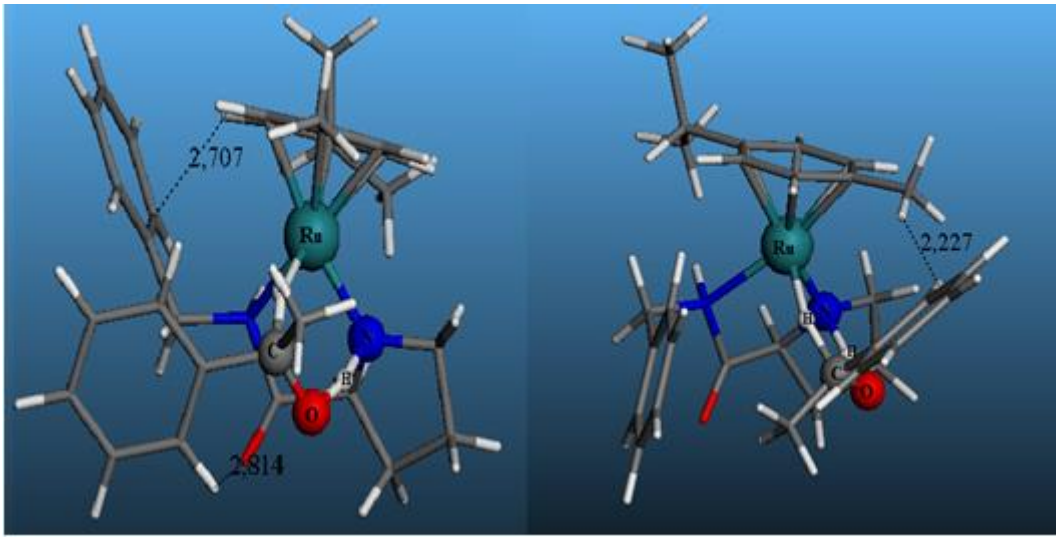

TS1(*R*) **TS1(*S*)**

+7,9 **+8,4**

ee experimental= 28%

ee calculated= 35%

Figure 6.3. Optimized geometries of the PBE-GD3BJ level of transition states with ligand 1. free energies are in kcal mol^{-1} and relative to the separate reactants.

The reason for this preference is that

- In transition state TS1(*R*) a stabilizing NH–p interaction between the phenyl group of the catalyst and the cymene of the catalyst.
- And in TS1(*S*) the clashes of the methyl groups of cymene with the phenyl ring of the acetophenone; this is not present in the TS1(*R*).

Optimized structures of transition states with ligand 2 (proline amine) are collected in Figure 6.4.

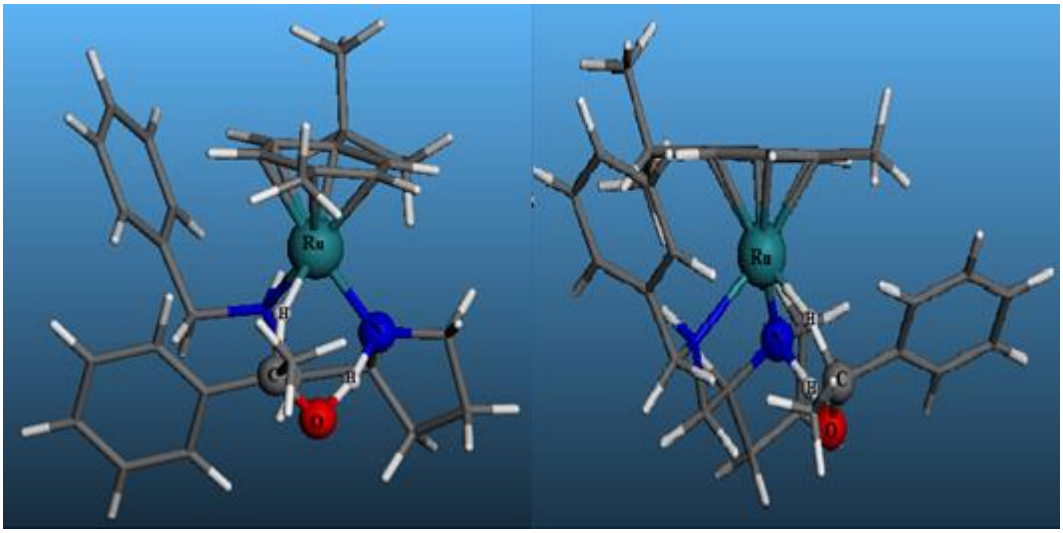

TS2(*R*) **TS2(*S*)**

+8.5 **+8,75**

ee experimental= 14%

ee calculated= 18%

Figure 6.4. Optimized geometries of the PBE-GD3BJ level of transition states with ligand 2. free energies are in kcal mol^{-1} and relative to the separate reactants.

The calculations correctly reproduce the fact that this ligand affords the *R* form of the product. TS2(*R*)

Is 0.25 kcal mol^{-1} lower than TS2(*S*) wich corresponds quite well with the experimental findings. Both of these transition states have the advantageous stabilizing CH–p electrostatic interaction between the Cymene of the catalyst and the phenyl ring of the catalyst. However, in the case of TS1(*R*) there is an additional similar attractive interaction between the oxygen and the hydrogen of the acetophenone (see Figure 3), which causes the energy of this TS to be lower and, thus, determines the selectivity. These results, in particular the fact that the calculations reproduce and rationalize the stereoselectivity of ligand 1 and 2.

6.3.2. Stereoselectivity with Ligand 3, 4 (proline amide/amine)

TS3(*S*) results from the approach of Ru-hydride intermediate to the *Re* face of the acetophenone and leads to (active catalyst + phenylethanol). In TS3(*S*), the free energy of TS3(*S*) is calculated to lie +8.3 kcal/mol above that of the separate reactants (Ru-hydride + acetophenone). TS3(*R*) results from the approach of Ru-hydride intermediate to the *Si* face of the acetophenone, and lies +7.9 kcal/mol above the free energy of the reactants and leads to the other configuration of phenylethanol+ active catalyst. The optimized structures of these transition states are collected in Figure 6.5.

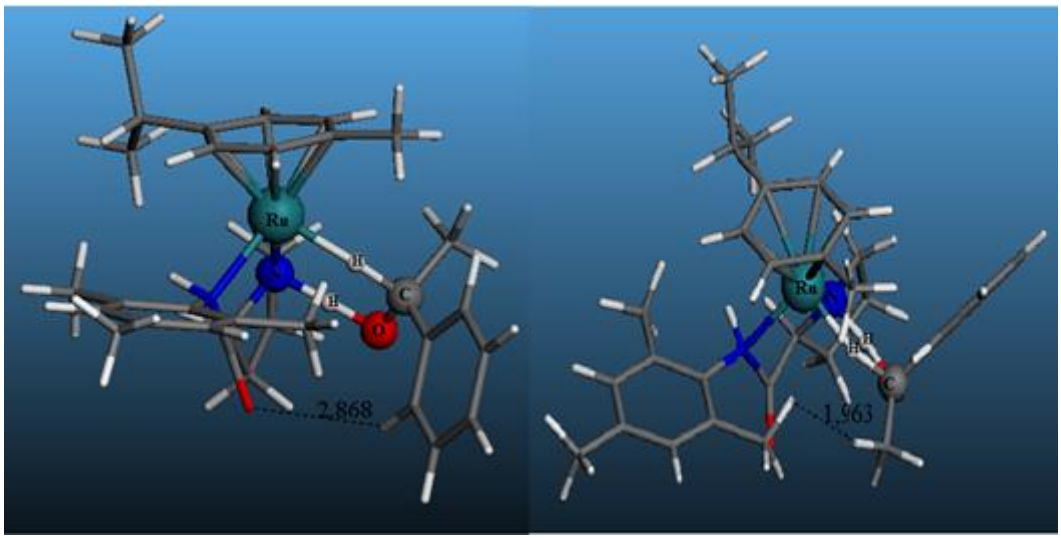

TS3(*R*) **TS3(*S*)**

+9,6 **+11,3**

ee experimental= 80%

ee calculated= 89%

Figure 6.5. Optimized geometries of the PBE-GD3BJ level of transition states with ligand 1. free energies are in kcal mol^{-1} and relative to the separate reactants.

The reason for this preference is that

- In transition state TS3(*R*) a stabilizing interaction between the oxygen of the catalyst and the hydrogen of the acetophenone.
- And in TS3(*S*) the clashes of the methyl groups of acetophenone with the phenyl ring of the catalyst; this is not present in the TS3(*R*).

Optimized structures of transition states with ligand 4 (proline amine) are collected in Figure 6.6.

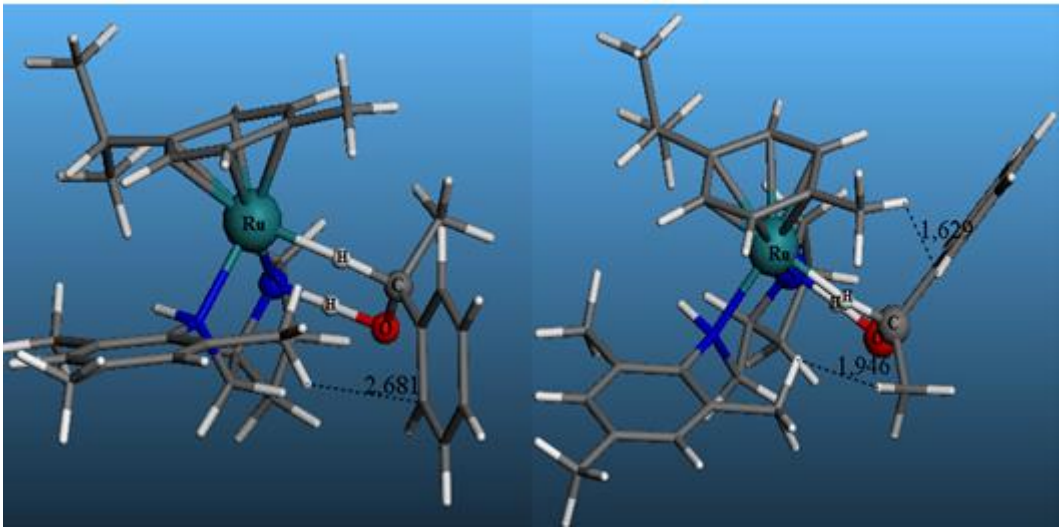

TS4(*R*) **TS4(*S*)**

+9,2 **+10,5**

ee experimental= 71%

ee calculated= 74%

Figure 6.6. Optimized geometries of the PBE-GD3BJ level of transition states with ligand 2. free energies are in kcal mol-1 and relative to the separate reactants.

Concerning the pro-(R) pathways, free energy barrier for the H transfer, TS4(*S*), is 10.5 kcalmol^{-1}. This value is the one corresponding to the approach of Ru-hydride intermediate to the *Re* face of the acetophenone. On the other hand, free energy barrier for the pro-(S) pathways, TS4(*R*), is 9.2 kcalmol^{-1} and corresponds to the approach of Ru-hydride intermediate to the *Re* face of the acetophenone. Since the difference between these free energy barrier values is 1.6 kcalmol^{-1}, the theoretical calculations predict a 71% ee of the (*R*)-product, which is consistent with the experimental results.Therefore, our theoretical model seems to be appropriate for explaining the stereoselectivity of this transfer-hydrogenation process.

6.4. Conclusion

A theoretical investigation of the factors that affect the enantioselective outcome of ruthenium (II) proline (amide/amine) catalysed transfer hydrogenation allowed the determination of a ligand structure-enantioselectivity relationship. It was shown that the chiral proline amide ligands gave better enantiomeric excess as compared with the corresponding amine derivatives

and the bulk of the aryl substituents on the ligand increased the enantioselectivity, all the synthetically useful high selectivities are successfully predicted. In addition, our results showed that important insights can be obtained with such a theoretical approach, particularly the origin of enantioselectivity. This can help experimentalists to design new active catalysts.

6.5. References

[1] Andersson PG, Munslow IJ. *Modern Reduction Methods;* Wiley-VCH: Weinheim, Germany, **2008**.

[2] Ojima I. *Catalytic asymmetric synthesis*; Wiley-VCH, Weinheim, **2010**.

[3] Palmer M, Wills M. *Tetrahedron Asymmetry* **1999**; 11: 2045-2061.

[4] Zassinovich G, Mestroni G, Gladiali S. *Chem Rev* **1992**; 5: 1051-1069.

[5] Ohkuma T, Ooka H, Hashiguchi S, Ikariya T, Noyori R. *J Am Chem Soc* **1995**; 9: 2675-2676

[6] Yamakawa M, Yamada I, Noyori R. *Angew Chem* **2001**; 15: 2900-2903;

[7] Ohta T, Nakahara S, Shigemura Y, Hattori K, Furukawa I. *Appl Organomet Chem* **2001**; 8: 699–709.

[8] Ohta T, Nakahara S, Shigemura Y, Hattori K, Furukawa I. *Chem Lett* **1998**; 6: 491-492.

[9] Ahlford K, Adolfsson H. *Catalysis Communications* **2011** ; 12:1118–1121.

[10] Faller JW, Lavoie AR. *Organometallics* **2001** ; 24 : 5245–5247.

[11] Rhyoo HY, Park HJ, Chung YK. *Chem Commun* **2001**; 20: 2064–2065.

[12] a) Zeror S, Collin J, Fiaud JC, Zouioueche LA. *J Mol Catal A: Chemical* **2006**;1-2:85-89.

b) Zeror S, Collin J, Fiaud JC, Zouioueche LA. *Adv Synth Catal* **2008**; 1: 197-204.

[13] Zhou Z, Wu L. *Catalysis Communications* **2008**; 15:2539–2542.

[14] Mao J, Guo J. *Chirality* **2010**; 10: 173-181;

[15] Wu X, Liu J, Tommaso DDI, Iggo J, Catlow CRA, Bacsa J, Xiao J. *chem J* **2008**; 25: 7699-7715.

[16] Jung YS, Marcus RA. *J Am Chem Soc* **2007**; 17: 5492-5502.

[17] Dub PA, Ikariya T. *J Am Chem Soc* **2013**; 26: 2604-2619.

[18] Noyori R, Yamakawa M, Hashiguchi S. *J Org Chem* **2001**; 24: 7931-7944.

[19] Yamakawa M, Ito H, Noyori R. *J Am Chem Soc* **2000**; 7: 1466-1478.

[20] Denizaltı S, Mercan D, Sen B, Gokçe AG, Çetinkaya B. *Journal of Organometallic Chemistry* **2015**; 1: 62-66.

[21] Perdew JP, Burke K, Ernzerhof M. *Phys Rev Lett* **1996**; 18-28 : 3865.

[22] Grimme S, Ehrlich S, Goerigk L. *J Comp Chem* **2011**; 7:1456-1465.

[23] Gaussian 09, Revision D.01, Frisch MJ, Trucks GW, Schlegel HB, Scuseria GE, Robb MA, Cheeseman JR, Scalmani G, Barone V, Mennucci B, Petersson GA, Nakatsuji H, Caricato MliX, Hratchian HP, Izmaylov AF, Bloino J, Zheng G, Sonnenberg JL, Hada M, Ehara M, Toyota K, Fukuda R, Hasegawa J, Ishida M, Nakajima T, Honda Y, Kitao O, Nakai H, Vreven T, Montgomery JAJr, Peralta JE, Ogliaro F, Bearpark M, Heyd JJ, Brothers E, Kudin KN,

Staroverov VN, Kobayashi R, Normand J, Raghavachari K, Rendell A, Burant JC, Iyengar SS, Tomasi J, Cossi M, Rega N, Millam JM, Klene M, Knox JE, Cross JB, Bakken V, Adamo C, Jaramillo J, Gomperts R, Stratmann RE, Yazyev O, Austin AJ, Cammi R, Pomelli C, Ochterski JW, Martin RL, Morokuma K, Zakrzewski VG, Voth GA, Salvador P, Dannenberg JJ, Dapprich S, Daniels AD, Farkas Ö, Foresman JB, Ortiz JV, Cioslowski J, Fox DJ. *Gaussian, Inc., Wallingford CT*, **2009**.

[24] Hariharan PC, Pople JA, *Mol. Phys* **1974**; 1: 209–214.

[25] Rassolov VA, Ratner MA, Pople GA, Redfern PC, Curtiss LA. *J Comput Chem* **2001**; 9: 976–984.

[26] Hay PJ, Wadt WR. *J Chem Phys* **1985**; 1:270.

[27] Scalmani G, Frisch MJ. *J Chem Phys* **2010**; 11: 114110.

Chapter 7

General Conclusion

6.1. General Conclusion

During the thesis work, We have tested the performance of four popular density functional not including dispersion, PBE , BP86, B3LYP TPSS and four have been constructed to account for dispersion (wB97X, wB97XD, M06, and M06L) and foor functionals includes dispersion by addition of the D3 version of Grimme's dispersion with Beck-Johnson Damping functions [PBE-GD3BJ, TPSS-GD3BJ, BP86-GD3BJ, B3LYP-GD3BJ]. The second-order Moller-Plesset [MP2] method and the double hybrid functionals [B2PLYP, B2PLYPD] were also used in predicting the geometries of ruthenium (II) complexes. It is revealed that [PBE-GD3BJ, TPSS-GD3BJ, BP86-GD3BJ] perform much better than the rest of functional.(PBE-GD3BJ) functional gives good results both for the geometry and the energetics and is not too costly in terms of computation time. For the solvent system, we chosen PCM.

Then, the ruthenium-catalyzed asymmetric reduction of acetophenone was investigated by means of DFT calculations. Two amino acid-based ligands were considered. For the first one, ligand 1 (phenyl alanine amide), the full catalytic cycle was studied according to the well-established outer-sphere reaction mechanism. For the other ligand 2 (proline amide), which was shown experimentally to yield the high enantioselectivity. The DFT calculations reproduce the experimental selectivities for both ligands and also provide rationalization to the observations. For each ligand, a number of plausible configuration of the metal were considered and it was shown that both *R* and *S* configuration are energetically accessible and must be considered for the overall catalytic process.

The first step of the reaction, the hydrogenation of the metal center by 2-propanol, is possible from two sides of the catalyst metal–ligand chelate ring, resulting in the formation of two metal hydride diastereomers, with Ru(R) or Ru(S) configurations. In the second step, a stabilizing CH–π interaction between a cymene of the catalyst and the phenyl ring of the substrate exists on hydrogenation from either the *Re* or the *Si* face of the substrate with both ligands 1 and 2, which contributes to stereoselectivity. The balance between these two factors, that is, the energy difference between the metal hydride diastereomers, and the CH–π interaction, will ultimately determine the stereochemical outcome of the reaction.

A theoretical investigation of the factors that affect the enantioselective outcome of ruthenium (II) proline (amide/amine) catalysed transfer hydrogenation allowed the determination of a ligand structure-enantioselectivity relationship. It was shown that the chiral proline amide ligands gave better enantiomeric excess as compared with the corresponding amine derivatives and the bulk of the aryl substituents on the ligand increased the enantioselectivity, all the

synthetically useful high selectivities are successfully predicted. In addition, our results showed that important insights can be obtained with such a theoretical approach, particularly the origin of enantioselectivity. This can help experimentalists to design new active catalysts.

Appendix

The other isomers of [Ru (η6-p-cymene) (Ķ²N, N) Proline]:

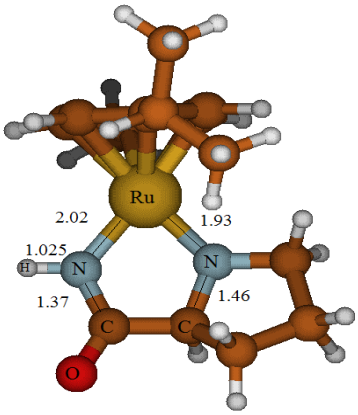

4-[Ru(η⁶-p-cymene)(Ķ²N,N)Proline]=M7

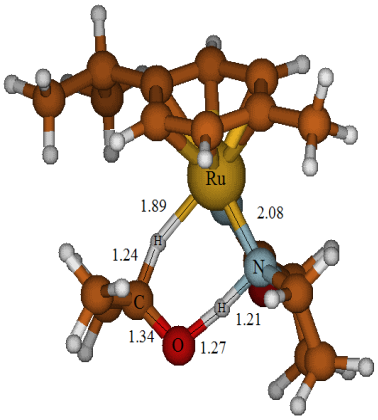

TSa4(*S*) (11.2)

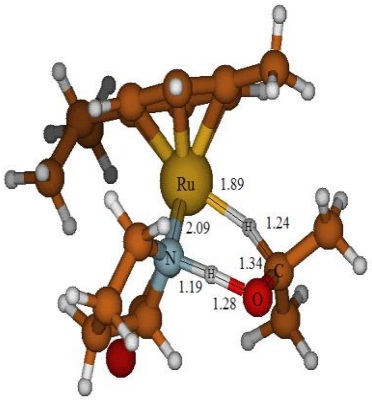

TSa4(*R*) (14.3)

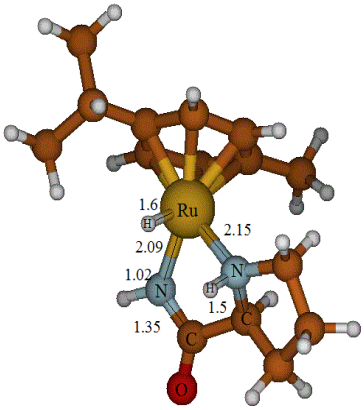

4-[Ru(*R*)(η⁶-p-cymene)(Ķ²N,N)ProlH] (0.7)

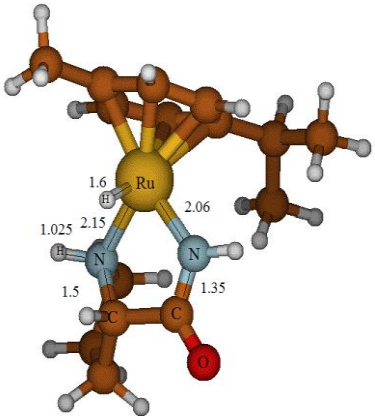

4-[Ru(*S*)(η⁶-p-cymene)(Ķ²N,N)ProlH] (-2.2)

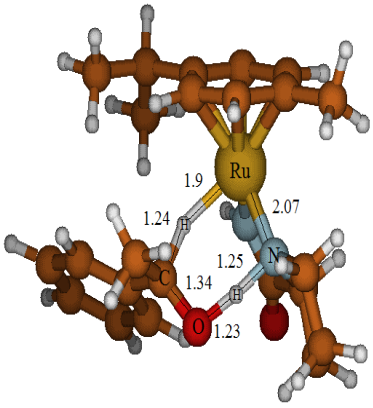

TSb4(*RR*) (15)

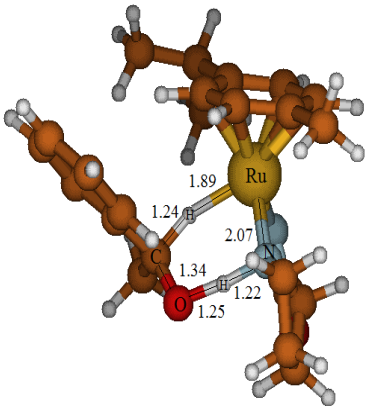

TSb4(*RS*) (14.6)

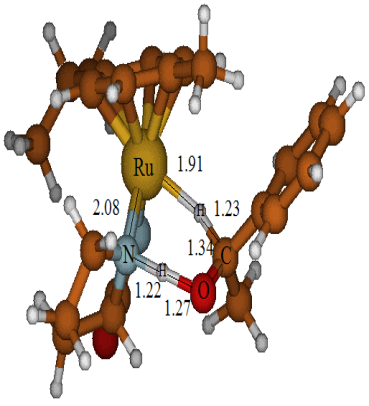

TSb4(*SS*) (12)

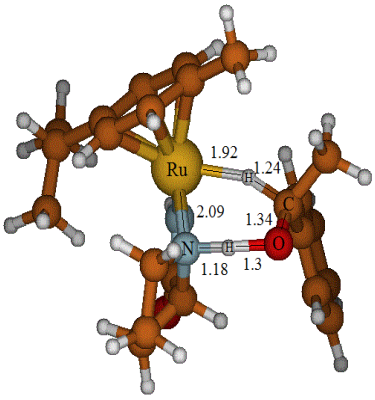

TSb4(*SR*) (10.4)

Figure 5.12. Optimized geometries of the PBE-GD3BJ of reactants ,products and transition states of the other isomer of [Ru(η6-p-cymene)(Ķ²N,N)Proline].

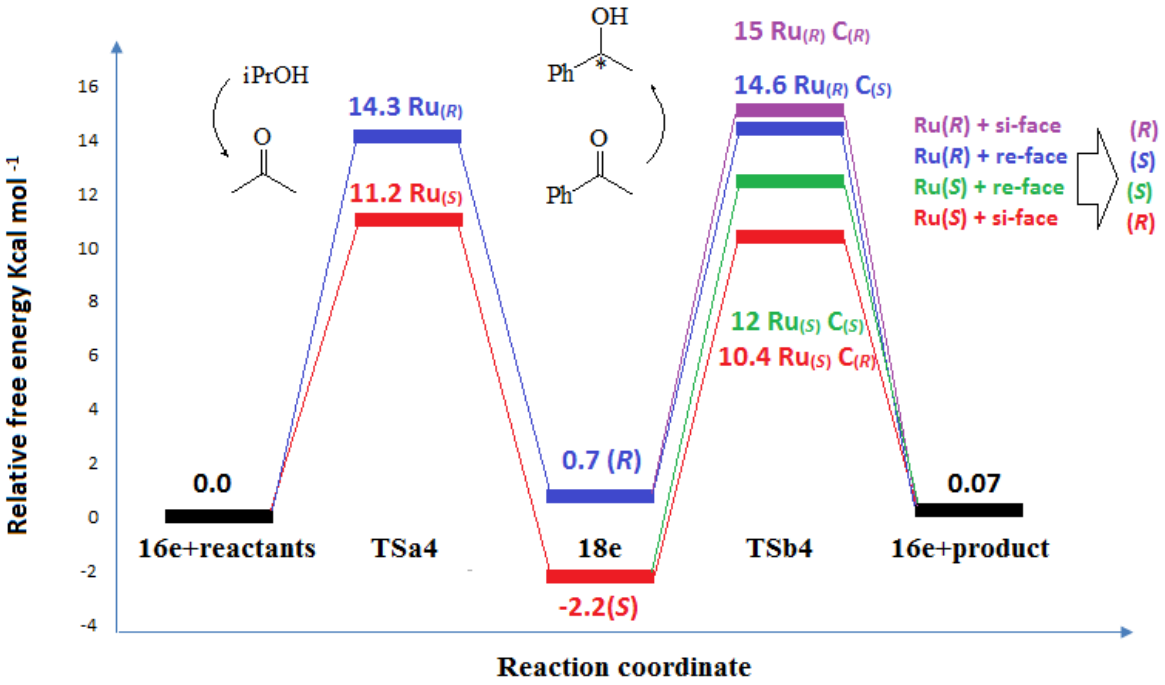

Figure 5.13 Overall free energy curves for the asymmetric hydrogenation reaction of acetophenone with other isomer of [Ru(*R*)(η6-p-cymene)(Ķ^{2}N,N)Proline]. Free energies are in kcal mol^{-1} and relative to the separate reactants (16e+2-propanol)

ISSN: 0975-8585

Research Journal of Pharmaceutical, Biological and Chemical Sciences

DFT Modeling of the Enantiomeric Excess in Asymmetric Transfer Hydrogenation Reaction of Prochiral Ketones in Water Promoted by Chiral Proline (Amide/Amine) Ruthenium (II) Complexes.

Yazid Meftah[1, 2], Youcef Boumedjane[1], Samira Maou[3], and Nadia Nebbache[3]*.

[1]Group de chimie théorique et pharmaceutique, laboratoire LMCE, Université de Biskra, B.P.145, R.P. 07000, Biskra, Algérie
[2]Centre de recherche scientifique et technique en analyses physico-chimiques (C.R.AP.C), BP 248, Alger RP 16004, Alger, Algérie
[3]Laboratoire de chimie appliquée, Université de Biskra, B.P.145, R.P. 07000, Biskra, Algérie

ABSTRACT

Recently, a proline amide/amine derived amino acid has been experimentally employed as an effective chiral catalytic precursor in the ruthenium-mediated asymmetric reduction of prochiral ketones in water to produce the corresponding secondary alcohols, which provides the products in 80% ee. In this paper, We show that transition state modeling according to the outer-sphere reaction mechanism at the PBE-GD3BJ/LANL2DZ/6-31G (d,p) level of theory can accurately model enantioselectivity for various proline-catalyzed asymmetric transfer hydrogenation.

Keywords: asymmetric transfer hydrogenation, ruthenium, DFT, Dispersion, enantioselectivity.

***Corresponding author*: nadia_nebbache@yahoo.fr**

ISSN: 0975-8585

INTRODUCTION

Asymmetric transfer hydrogenation of ketones is an important transformation in the production of many fine chemical compounds at both laboratory and industrial level [1-2].Therefore, many studies have been undertaken to develop new highly selective catalyst [3-4]. Noyori et al [5-6] Showed that a ruthenium complex containing monotosylated 1, 2-diamines could serve as efficient catalyst for the ATH of ketones.

Amino acids are inexpensive chiral materials that have been used for the synthesis of optically active transition metal complexes [7-9]. In 2001, the group of Faller reported a in situ generated (*p*-cymene) Ru (L-proline amide) Cl_2 catalyst that gave excellent yields, 70-90%, with moderate enantiocontrol, 68-93%, in hydrogenations of a variety of ketones at -24 C° [10]. In the same year, Chung reported the first example of the asymmetric hydrogen-transfer reductions of aromatic ketones in an aqueous solution, with enantiomeric excesses up to 95.3 % using a functionalized proline amide as ligand [11]. Zeror and others have constructed active and selective ATH-catalysts based on the use of proline amides [12-14].

Based on literature reports [15-17], a plausible mechanism for the ATH of ketones in aqueous media can follow an outer-sphere pathway analogous to that proposed by Noyori and al [18-19] fig1.

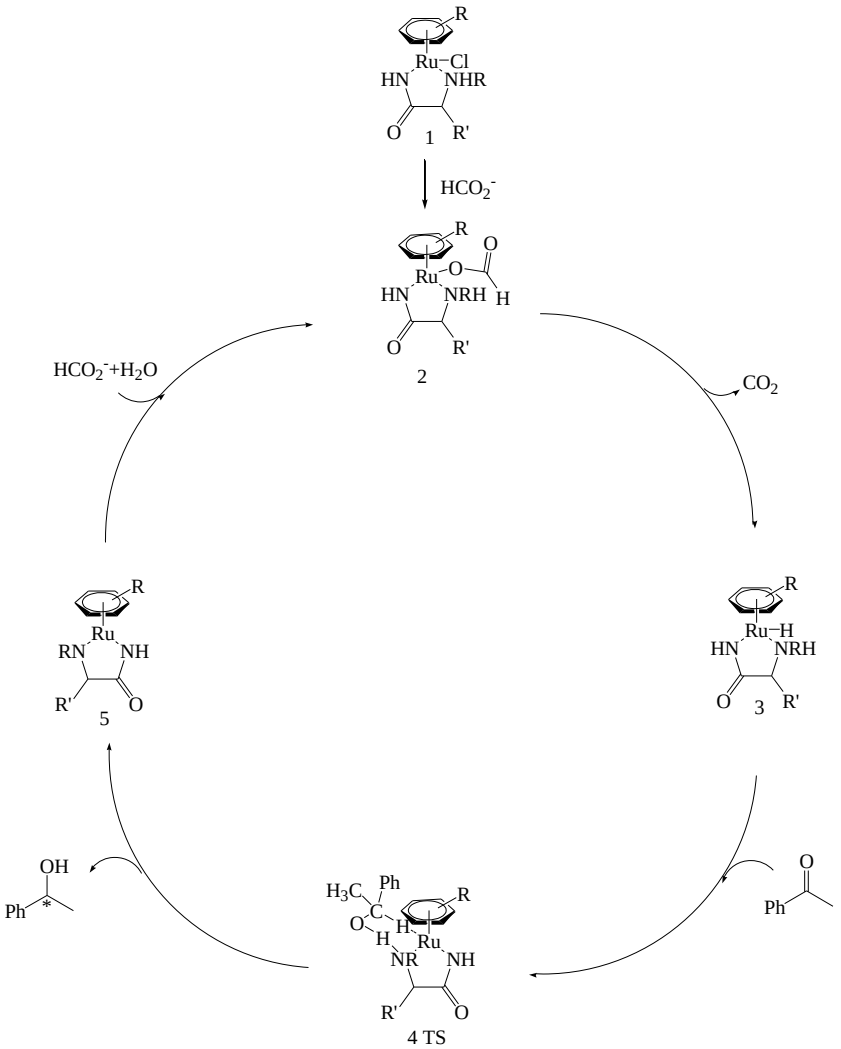

Figure 1: Plausible mechanism for transfer hydrogenation of acetophenone catalyzed by Ru (II) complexes containing amino amide ligands in aqueous media.

Percatalyst Ru-proline amide is generated *in situ* from [Ru (p-cymene) $cl_2]_2$ and proline amide in water and then it reacts with HCOOHNa forming formato complex 2 the reduction prooceeds via the formato intermediate 2, followed by decarboxylation to give Ru-hydride intermediate 3, The key step is the

ISSN: 0975-8585

simultaneous transfer of the hydritic H (Ru–H) and the protic H (N–H) to the C=O functional group via a six-membered transition state 4 TS. Last, the active intermediate 5 is regenerated with the liberation of the chiral alcohol, closing the catalytic cycle.

Recently, Serpil Denizaltı et al. [20] compared the proline amine ligands with amide analogues in asymmetric transfer hydrogenation reaction of prochiral ketones in water (figure 2). In this work we have rationalized the enantioselectivity observed experimentally using Density functional theory.

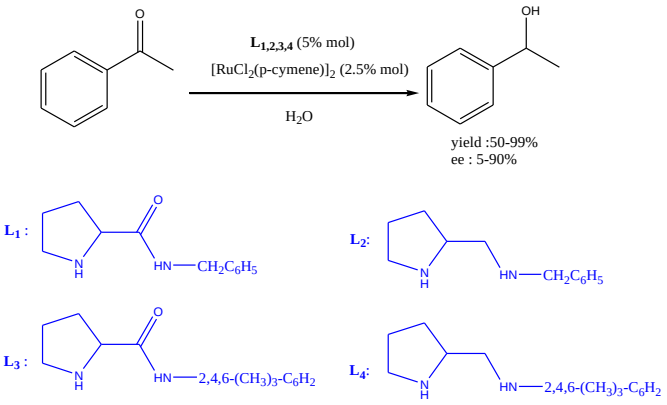

Figure 2: Ru-catalyzed ATH of ketones with [Ru (p-cymene)Cl_2]$_2$ and ($L_{1,3}$) proline amide or ($L_{2,4}$) proline amine. ee is the enantiomeric excess.

EXPERIMENTAL SECTION

Computational details

All calculations were performed at the density functional theory (DFT) level, using the PBE [21] functional by addition of the D3 version of Grimme's dispersion with Beck-Johnson Damping functions [22] as implemented in the Gaussian 09 D01 software package [23]. For all atoms except ruthenium, the 6-31G (d,p) basis set was used [24-25]; ruthenium was treated with the LANL2DZ basis set and effective core potential (ECP) [26].geometries for the transition state were located either by QST2 or by QST3 procedures, or by the guess based on the structure of the previously found TS. Vibrational frequency calculations were then performed at the optimized geometry of transition structure. We confirmed that all transition structures have one, and only one, imaginary frequency. The intrinsic reaction coordinate (IRC) calculations, at the same level of theory, were performed to ensure that the transition structures led to the expected reactants and products. The reported energies are Gibbs free energies, which include zero-point vibrational corrections, thermal corrections at 298 K and solvation free energies. The solvation energies were calculated as single point corrections on the optimized structures using the conductor-like polarizable continuum model method [27], with dielectric constant ε=78.3553 for water.

RESULTS AND DISCUSSION

In acetophenone hydrogenation catalyzed by chiral proline (amide/amine) ruthenium (II) complexes, the hydride transfer can occur via two different pathways, each having a diastereotopic transition state. One pathway corresponds to the attack of the hydride at the *Re* face of acetophenone while the other pathway involves an attack at the *Si* face.

According to eqn (1) and the Arrhenius equation, we could obtain eqn (2) to calculate the ee values (ee Calculated).

$$ee = \frac{R-S}{R+S} \qquad (1)$$

$$ee_{\text{calculated}} = \frac{e^{\Delta\Delta Ga/RT}-1}{e^{\Delta\Delta Ga/RT}+1} \qquad (2)$$

ISSN: 0975-8585

Stereoselectivity with Ligand 1, 2 (proline amide/amine)

TS1(*S*) results from the approach of Ru-hydride intermediate to the *Re* face of the acetophenone and leads to (active catalyst + phenylethanol). In TS1(*S*), the free energy of TS1(*S*) is calculated to lie +8.4 kcal/mol above that of the separate reactants (Ru-hydride + acetophenone). TS1(*R*) results from the approach of Ru-hydride intermediate to the *Si* face of the acetophenone and lies +7.9 kcal/mol above the free energy of the reactants and leads to the other configuration of phenylethanol + active catalyst. The optimized structures of these transition states are collected in Figure 3.

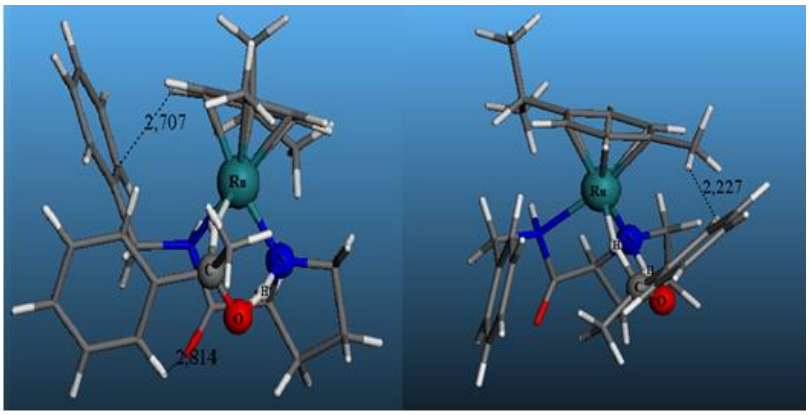

TS1(*R*) **TS1(*S*)**
+7,9 **+8,4**

ee experimental= 28%
ee calculated= 35%

Figure 3: Optimized geometries of the PBE-GD3BJ level of transition states with ligand 1. free energies are in kcal mol^{-1} and relative to the separate reactants.

The reason for this preference is that

- In transition state TS1(*R*) a stabilizing NH–p interaction between the phenyl group of the catalyst and the cymene of the catalyst.
- And in TS1(*S*) the clashes of the methyl groups of cymene with the phenyl ring of the acetophenone; this is not present in the TS1(*R*).

Optimized structures of transition states with ligand 2 (proline amine) are collected in Figure 4.

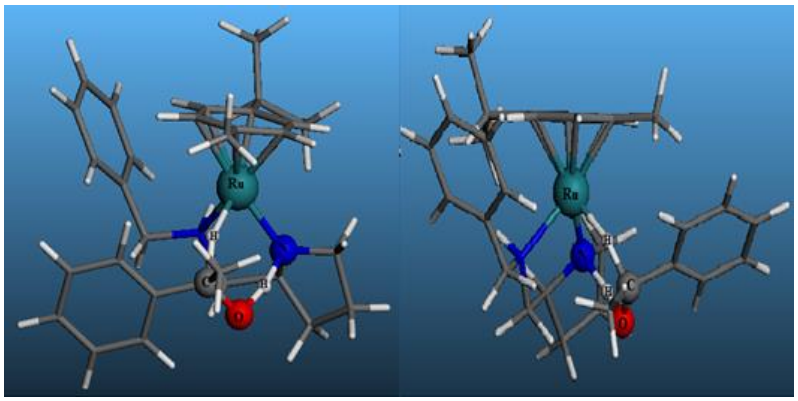

TS2(*R*) **TS2(*S*)**
+8.5 **+8,75**

ee experimental= 14%
ee calculated= 18%

Figure 4: Optimized geometries of the PBE-GD3BJ level of transition states with ligand 2. free energies are in kcal mol^{-1} and relative to the separate reactants.

The calculations correctly reproduce the fact that this ligand affords the *R* form of the product. TS2(*R*)

Is 0.25 kcal mol^{-1} lower than TS2(*S*) wich corresponds quite well with the experimental findings. Both of these transition states have the advantageous stabilizing CH–p electrostatic interaction between the Cymene of the catalyst and the phenyl ring of the catalyst. However, in the case of TS1(*R*) there is an additional similar attractive interaction between the oxygen and the hydrogen of the acetophenone (see Figure 3), which causes the energy of this TS to be lower and, thus, determines the selectivity. These results, in particular the fact that the calculations reproduce and rationalize the stereoselectivity of ligand 1 and 2.

Stereoselectivity with Ligand 3, 4 (proline amide/amine)

TS3(*S*) results from the approach of Ru-hydride intermediate to the *Re* face of the acetophenone and leads to (active catalyst + phenylethanol). In TS3(*S*), the free energy of TS3(*S*) is calculated to lie +11.3 kcal/mol above that of the separate reactants (Ru-hydride + acetophenone). TS3(*R*) results from the approach of Ru-hydride intermediate to the *Si* face of the acetophenone, and lies +9.6 kcal/mol above the free energy of the reactants and leads to the other configuration of phenylethanol+ active catalyst. The optimized structures of these transition states are collected in Figure 5.

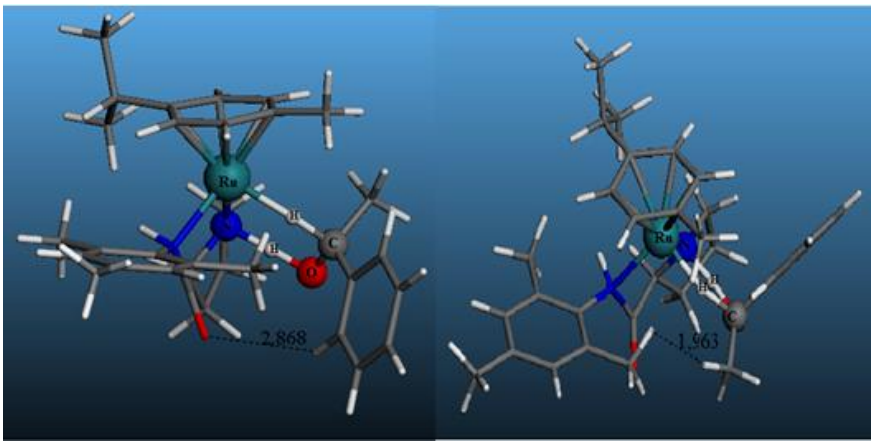

TS3(*R*) **TS3(*S*)**
+9,6 **+11,3**

ee experimental= 80%
ee calculated= 89%

Figure 5: Optimized geometries of the PBE-GD3BJ level of transition states with ligand 1. free energies are in kcal mol^{-1} and relative to the separate reactants.

The reason for this preference is that

- In transition state TS3(*R*) a stabilizing interaction between the oxygen of the catalyst and the hydrogen of the acetophenone.
- And in TS3(*S*) the clashes of the methyl groups of acetophenone with the phenyl ring of the catalyst; this is not present in the TS3(*R*).

Optimized structures of transition states with ligand 4 (proline amine) are collected in Figure 6.

Concerning the pro-(R) pathways, free energy barrier for the H transfer, TS4(*S*), is 10.9 $kcalmol^{-1}$. This value is the one corresponding to the approach of Ru-hydride intermediate to the *Re* face of the acetophenone. On the other hand, free energy barrier for the pro-(S) pathways, TS4(*R*), is 9.2 $kcalmol^{-1}$ and corresponds to the approach of Ru-hydride intermediate to the *Re* face of the acetophenone. Since the difference between these free energy barrier values is 1.7 $kcalmol^{-1}$, the theoretical calculations predict a 74% ee of the (*R*)-product, which is consistent with the experimental results.Therefore, our theoretical model seems to be appropriate for explaining the stereoselectivity of this transfer-hydrogenation process.

ISSN: 0975-8585

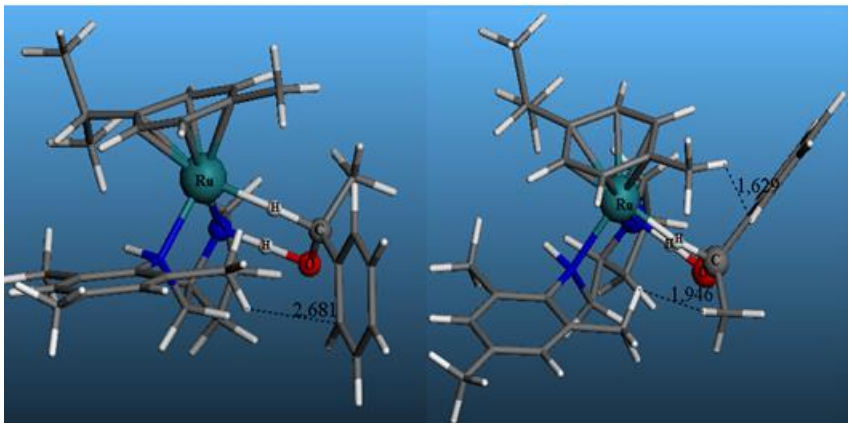

TS4(*R*) **TS4(*S*)**

+9,2 **+10,9**

ee experimental= 71%
ee calculated= 74%

Figure 6: Optimized geometries of the PBE-GD3BJ level of transition states with ligand 2. free energies are in kcal mol-1 and relative to the separate reactants.

CONCLUSION

A theoretical investigation of the factors that affect the enantioselective outcome of ruthenium (II) proline (amide/amine) catalysed transfer hydrogenation allowed the determination of a ligand structure-enantioselectivity relationship. It was shown that the chiral proline amide ligands gave better enantiomeric excess as compared with the corresponding amine derivatives and the bulk of the aryl substituents on the ligand increased the enantioselectivity, all the synthetically useful high selectivities are successfully predicted. In addition, our results showed that important insights can be obtained with such a theoretical approach, particularly the origin of enantioselectivity. This can help experimentalists to design new active catalysts.

ACKNOWLEDGEMENTS

The authors are very thankful to the « Université de Lyon, CNRS, Ecole Normale Supérieure de Lyon, 46 Allée d'Italie, 69364 Lyon, Cedex 07, France and Pole modélisation numérique (PSMN) in Ecole Normale Supérieure de Lyon for offering the computing facilities and helpful discussion with the scientists.

REFERENCES

[1] Andersson PG, Munslow IJ. Modern Reduction Methods; Wiley-VCH: Weinheim, Germany, 2008.
[2] Ojima I. Catalytic asymmetric synthesis; Wiley-VCH, Weinheim, 2010.
[3] Palmer M, Wills M. Tetrahedron Asymmetry 1999; 11: 2045-2061.
[4] Zassinovich G, Mestroni G, Gladiali S. Chem Rev 1992; 5: 1051-1069.
[5] Ohkuma T, Ooka H, Hashiguchi S, Ikariya T, Noyori R. J Am Chem Soc 1995; 9: 2675-2676
[6] Yamakawa M, Yamada I, Noyori R. Angew Chem 2001; 15: 2900-2903;
[7] Ohta T, Nakahara S, Shigemura Y, Hattori K, Furukawa I. Appl Organomet Chem 2001; 8: 699–709.
[8] Ohta T, Nakahara S, Shigemura Y, Hattori K, Furukawa I. Chem Lett 1998; 6: 491-492.
[9] Ahlford K, Adolfsson H. Catalysis Communications 2011; 12:1118–1121.
[10] Faller JW, Lavoie AR. Organometallics 2001 ; 24 : 5245–5247.
[11] Rhyoo HY, Park HJ, Chung YK. Chem Commun 2001; 20: 2064–2065.
[12] a) Zeror S, Collin J, Fiaud JC, Zouioueche LA. J Mol Catal A: Chemical 2006;1-2:85-89. b) Zeror S, Collin J, Fiaud JC, Zouioueche LA. Adv Synth Catal 2008; 1: 197-204.
[13] Zhou Z, Wu L. Catalysis Communications 2008; 15:2539–2542.
[14] Mao J, Guo J. Chirality 2010; 10: 173-181;
[15] Wu X, Liu J, Tommaso DDI, Iggo J, Catlow CRA, Bacsa J, Xiao J. chem J 2008; 25: 7699-7715.
[16] Jung YS, Marcus RA. J Am Chem Soc 2007; 17: 5492-5502.
[17] Dub PA, Ikariya T. J Am Chem Soc 2013; 26: 2604-2619.

[18] Noyori R, Yamakawa M, Hashiguchi S. J Org Chem 2001; 24: 7931-7944.
[19] Yamakawa M, Ito H, Noyori R. J Am Chem Soc 2000; 7: 1466-1478.
[20] Denizaltı S, Mercan D, Sen B, Gokçe AG, Çetinkaya B. Journal of Organometallic Chemistry 2015; 1: 62-66.
[21] Perdew JP, Burke K, Ernzerhof M. Phys Rev Lett 1996; 18-28: 3865.
[22] Grimme S, Ehrlich S, Goerigk L. J Comp Chem 2011; 7:1456-1465.
[23] Gaussian 09, Revision D.01, Frisch MJ, Trucks GW, Schlegel HB, Scuseria GE, Robb MA, Cheeseman JR, Scalmani G, Barone V, Mennucci B, Petersson GA, Nakatsuji H, Caricato MliX, Hratchian HP, Izmaylov AF, Bloino J, Zheng G, Sonnenberg JL, Hada M, Ehara M, Toyota K, Fukuda R, Hasegawa J, Ishida M, Nakajima T, Honda Y, Kitao O, Nakai H, Vreven T, Montgomery JAJr, Peralta JE, Ogliaro F, Bearpark M, Heyd JJ, Brothers E, Kudin KN, Staroverov VN, Kobayashi R, Normand J, Raghavachari K, Rendell A, Burant JC, Iyengar SS, Tomasi J, Cossi M, Rega N, Millam JM, Klene M, Knox JE, Cross JB, Bakken V, Adamo C, Jaramillo J, Gomperts R, Stratmann RE, Yazyev O, Austin AJ, Cammi R, Pomelli C, Ochterski JW, Martin RL, Morokuma K, Zakrzewski VG, Voth GA, Salvador P, Dannenberg JJ, Dapprich S, Daniels AD, Farkas Ö, Foresman JB, Ortiz JV, Cioslowski J, Fox DJ. Gaussian, Inc., Wallingford CT, 2009.
[24] Hariharan PC, Pople JA, Mol. Phys 1974; 1: 209–214.
[25] Rassolov VA, Ratner MA, Pople GA, Redfern PC, Curtiss LA. J Comput Chem 2001; 9: 976–984.
[26] Hay PJ, Wadt WR. J Chem Phys 1985; 1:270.
[27] Scalmani G, Frisch MJ. J Chem Phys 2010; 11: 114110.